arXiv:0902.0651v2 [astro-ph.HE] 4 Mar 2009

Noname manuscript No.
(will be inserted by the editor)

X-ray Absorption and Reflection in Active Galactic Nuclei

T.J.Turner · L.Miller

Received: date / Accepted: date

Abstract X-ray spectroscopy offers an opportunity to study the complex mixture of emitting and absorbing components in the circumnuclear regions of active galactic nuclei (AGN), and to learn about the accretion process that fuels AGN and the feedback of material to their host galaxies. We describe the spectral signatures that may be studied and review the X-ray spectra and spectral variability of active galaxies, concentrating on progress from recent *Chandra*, *XMM-Newton* and *Suzaku* data for local type 1 AGN. We describe the evidence for absorption covering a wide range of column densities, ionization and dynamics, and discuss the growing evidence for partial-covering absorption from data at energies $\gtrsim 10\,\mathrm{keV}$. Such absorption can also explain the observed X-ray spectral curvature and variability in AGN at lower energies and is likely an important factor in shaping the observed properties of this class of source. Consideration of self-consistent models for local AGN indicates that X-ray spectra likely comprise a combination of absorption and reflection effects from material originating within a few light days of the black hole as well as on larger scales. It is likely that AGN X-ray spectra may be strongly affected by the presence of disk-wind outflows that are expected in systems with high accretion rates, and we describe models that attempt to predict the effects of radiative transfer through such winds, and discuss the prospects for new data to test and address these ideas.

Keywords Galaxies: active · X-rays: galaxies

T.J.Turner
Dept. of Physics, University of Maryland Baltimore County, 1000 Hilltop Circle, Baltimore, MD 21250, USA
Tel: +1-410-455-1978
Fax: +1-410-455-1072
E-mail: tjturner@umbc.edu

L.Miller
Dept. of Physics, University of Oxford, Denys Wilkinson Building, Keble Road, Oxford OX1 3RH, UK

1 Introduction

Measurements of gas and stellar kinematics have shown that most galaxies harbor a black hole at their center (Kormendy and Richstone 1995; Magorrian et al. 1998; Ferrarese and Merritt 2000). The black holes in these galaxies are dubbed 'supermassive', with masses in the range $10^6 - 10^9\,\mathrm{M}_\odot$. The mass of the central black hole scales with galaxy bulge properties such as its velocity dispersion (Gebhardt et al. 2000; Tremaine et al. 2002), its luminosity (Marconi and Hunt 2003) and its stellar density profile (Graham et al. 2001), and so the formation of the galaxy and the nuclear supermassive black hole must be linked. In active galactic nuclei (AGN), radiation from the nuclear region is detected that is thought to be released from material accreting onto the black hole. Studying AGN offers the opportunity to understand the coevolution of galaxies and black holes, as accretion must be linked to growth of the black hole (Soltan 1982). The masses of black holes in active galaxies may also be estimated using "reverberation mapping" (Peterson 1993; Kaspi et al. 2000; Peterson and Wandel 2000; Peterson et al. 2004) giving results consistent with masses derived from stellar kinematics and luminosities (Wandel 2002; Onken et al. 2004) and with the black hole masses required to explain the linewidths of the photoionized broad-line regions in AGN (Wandel et al. 1999). The majority of nuclear black holes in the local Universe are evident only through their gravitational influence and either have no detectable signatures of accretion or are only weakly active (e.g. Heckman et al. 2004). The AGN phenomenon is observed over a wide range of intrinsic luminosity from dwarf Seyfert galaxies to quasars ($L_{\rm bol} \sim 10^{40} - 10^{47}$erg s^{-1}) and shows strong cosmological evolution, with a greater density of the most luminous AGN at earlier cosmic epochs (e.g. Boyle et al. 2000). However, the way in which black holes grow, and the conditions that cause active nuclei to switch off, are still being debated.

With the advent of X-ray observing satellites it was established (Elvis et al. 1978) that X-ray emission is a common property of active galaxies and that the X-ray flux comprises a significant fraction (about $5-40\%$: Ward et al. 1987) of the bolometric emission from such objects. Observation of rapid (down to ks) variability in the X-ray flux of local Seyfert galaxies constrained the X-ray emission to be small and thus likely to arise very close to the active nucleus (e.g. Lawrence et al. 1985; Pounds et al. 1986) [1] The origin of X-rays from close to the central black hole means that X-ray data offer a chance to study the immediate environs of supermassive black holes and the poorly understood accretion process that fuels them. Although the X-ray emission region is too small to image with current instrumentation, timing analysis and spectroscopy offer ways to probe these regions indirectly. In addition to tracing spectral signatures of the gas inflow and outflow at the heart of these accreting systems, X-ray data carry signatures of reprocessing in material within a few hundred gravitational radii and the potential for detecting measurable signatures from the accretion disk at even smaller radii.

At optical wavelengths AGN are usually classified as either "type 1", showing broad optical/UV emission lines, or "type 2", showing only narrow lines (see Osterbrock and Ferland 2006). The "standard model" supposes that in type 2 AGN the broad line region (BLR) exists but is highly extinguished, and it is usually supposed that the extinguishing region

---

[1] From the light travel-time across a source, in the absence of relativistic effects, a characteristic timescale of 1 ks corresponds to an upper limit to its size $D \lesssim 200 M_6^{-1}$, expressed in units of the gravitational radius $\mathrm{r_g} = \mathrm{G}M/\mathrm{c}^2$, where M_6 is the mass of a black hole in units of $10^6\,\mathrm{M}_\odot$.

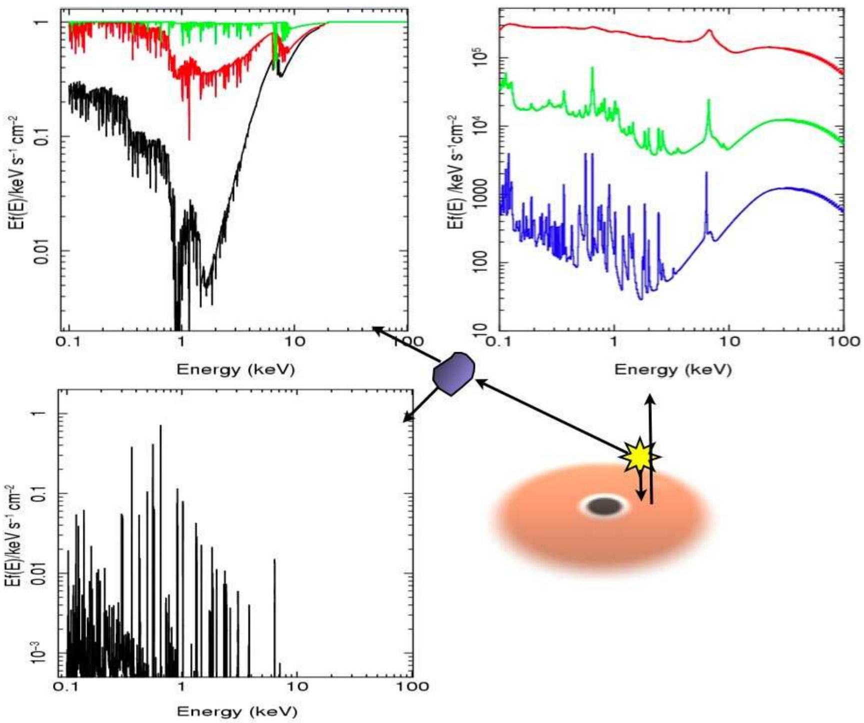

Fig. 1 A schematic of the accretion disk-black hole system. The region producing the primary X-ray continuum is denoted by a yellow star (this may be a "hotspot" or series of hotspots or an extended coronal region). The figure shows one sight-line where continuum reflection is seen and another where an absorption signature is imprinted onto the continuum. The top left panel shows the transmitted spectrum through gas with $N_H = 5 \times 10^{23} cm^{-2}$, log $\xi = 2$(black), 3(red) and 4(green), where ξ is the ionization parameter in units of erg cm s^{-1} (see section 2.2). The absorption model was generated from XSTAR 2.1ln8 with turbulent velocity 200 km s^{-1} and density $n = 10^{12} cm^{-3}$. Line re-emission should also be observed from the absorbing clouds; the emission spectrum from the log $\xi = 2$ cloud is shown in the lower left panel. The top right panel shows reflection from the ionized surface of the accretion disk seen face-on. The model is from the REFLIONX public model table of Ross and Fabian (2005) and shown for log $\xi = 2$(blue), 3(green) and 4(red), shifted in normalization for clarity (and therefore in arbitrary units). The primary continuum, which in practice dilutes the reflection spectrum, is not shown. Both models assumed solar abundances and a power-law continuum with photon index $\Gamma = 2$.

forms a torus around the central region. (e.g. Antonucci 1993). One expectation of the unified model, where the primary difference between types is the orientation with respect to the observer, is that any phenomena that are observed in type 2 AGN should also be present in type 1 AGN, perhaps modified by a differing viewing angle. This concept has been extended to the X-ray regime, where AGN whose X-ray emission is absorbed by intervening material are known as type 2, and those without significant absorption being evident are known as type 1. Although in general there is often a good correspondence between optical and X-ray classifications (e.g. Bassani et al. 1999), this agreement is by no means perfect (e.g. Panessa and Bassani 2002).

Within this broad classification there are intermediate types with detectable but weak broad-line components on their optical/UV emission lines (Osterbrock and Ferland 2006), designated by, e.g. "type 1.5". Osterbrock and Pogge (1985) also identified a class of "narrow-line Seyfert 1" galaxies that have many of the properties of type 1 AGN but with rather narrow Balmer lines. This class may comprise AGN accreting close to their Eddington limits (Leighly 1999; Turner et al. 1999) and as such are particularly interesting if we wish to study emission from accretion disks. At the other end of the scale, a high fraction of nearby galaxies have "Low Ionisation Nuclear Emission Regions" (LINERs: Heckman 1980): the accretion in these objects may be in the form of a radiatively inefficient flow (e.g. Ho 1999, 2008, and see section 2.1).

In this review we shall discuss physical processes at work in the X-ray regime and the progress that has been made over the last few decades. We will highlight the most recent observational results and critically address the degree to which we can constrain conditions in the environs of active nuclei using current X-ray instruments. As we are focusing on determining fundamentals of the accretion process we will limit this review to the properties of bright nearby Seyfert type 1 AGN for which the most detailed observational data are available, and whose timescales for variability are short enough for us to study the full range of their behavior. One of the original motivations for the unified scheme was to explain the radio properties of radio-luminous AGN (Urry and Padovani 1995). It is known that radio-loud AGN are stronger X-ray sources, with X-ray emission possibly being associated with a nuclear radio jet (Zamorani et al. 1981) and in this review we shall discuss X-ray emission only from radio-quiet AGN (although we should remember that all types of AGN have some level of nuclear radio emission).

2 X-ray continuum production and reprocessing

2.1 Continuum production

Accretion onto the central black hole has become the accepted model for AGN, as it is otherwise difficult to produce the observed radiation intensity over such a wide range of the electromagnetic spectrum. Accreting gas has angular momentum and we expect this material to form an accretion disk. When the gravitational potential energy lost by material moving inwards is released locally and efficiently through viscous dissipation, the gas becomes much cooler than the local virial temperature and forms a disk whose vertical thickness is much smaller than the radius, the so-called "thin disk" of Shakura and Syunyaev (1973). The disk emission is a composite of black-body radiation with a range of temperatures that depends on the range of emitting radii and the mass of the central black hole. For very low accretion rates an advection-dominated accretion flow (ADAF) may develop (e.g. Narayan and Yi 1994; Abramowicz et al. 1995), and as cooling by advection is inefficient the thermal energy in the disk is high and it becomes relatively thick in the vertical direction. These flows may be at work in low luminosity AGN such as LINERs.

Constraints on accretion can be obtained from consideration of some basic observable quantities. The observed X-ray background radiation and the integrated QSO luminosity are consistent with the expected integrated emission from the luminous accretion phase of AGN, given the estimated local mass density of black holes, if around 10 percent of accreted rest energy has been radiated (Yu and Tremaine 2002;

Marconi et al. 2004). This leads to an expectation that most of the energy output from AGN occurs within a few gravitational radii of the black hole (Fabian 2008), but we note here that this does not necessarily mean that the X-ray emission we *see* comes to us directly from close to the black hole. Whether or not we see any X-ray emission from the accretion disk at such small radii depends on the accretion disk extending close to the black hole and on there being sufficiently concentrated illuminating radiation to generate significant reflection and on there being no subsequent reprocessing of radiation by material further out. The estimate of this mean "radiative efficiency" from the X-ray background also depends critically on the range of redshifts over which the dominant growth occurs: this is constrained by the observed AGN luminosity function but we must be sure that the luminosity function in some waveband adequately reflects the black hole growth at each epoch.

In the case of thin accretion disks around supermassive black holes the intensity peak of the radiation is in the UV regime (Shakura and Syunyaev 1973). To obtain X-ray emission, it is thought that UV photons from the innermost edge of the accretion disk serve as 'seed photons' for multiple inverse Compton scatterings by a population of hot or relativistic electrons existing in a coronal region sandwiching the disk (Haardt and Maraschi 1991, 1993; Zdziarski et al. 1994). The origin of the Comptonizing electrons is at present uncertain but the coronal heating may be related to magnetic dissipation processes, or the corona may be populated with electron-positron pairs produced by photon-photon collisions (see, e.g., Fabian 1994 and references therein).

The Comptonizing electrons may have a thermal, non-thermal or mixed electron population. In this basic picture the observed X-ray continuum represents the Comptonized spectrum whose shape depends upon the parameters of the electron population (e.g. Haardt and Maraschi 1991; Titarchuk and Hua 1997). For example, the temperature of a thermal population can be parameterized as $\Theta_{\rm e} = {\rm k}T_{\rm e}/{\rm m_e c}^2$, and the energy-dependent optical depth to Compton scattering, $\tau_{\rm e}$. The coronal spectrum can be well approximated by a power-law for a region of parameter-space up to a cut-off energy $E_{\rm c} \sim {\rm k}T_{\rm e}$. Ignoring geometric details, measurement of the continuum slope and the cut-off energy could, in principle, constrain the physical parameters of the corona, and combining this with the observed luminosity one could estimate the luminosity of the seed photons and learn something about the accretion flow. Unfortunately, in practice the primary continuum is difficult to isolate in available observational data. In contrast to the spectra of accretion disks in AGN that peak in the UV band, those in Galactic Black Hole binary systems have a higher peak temperature, such that the Wien tail of the disk emission imposes a signature in the X-ray band that can be difficult to disentangle from the other spectral components.

The AGN corona is thought to exist on size scales less than a few tens of gravitational radii from the black hole (section 7.1.2), so the X-ray continuum could experience reprocessing in gas extending from very close to the black hole outwards. X-ray continuum photons produced in the corona would emerge quasi-isotropically (depending on the corona optical depth and shape), some of these escape along sight lines to the observer and could pick up an imprint of material along the line-of-sight, some X-ray photons may illuminate the accretion disk and reflect from the surface of the disk before reaching the observer (Figure 1). The observed spectrum is then the sum of primary continuum and reprocessed X-rays. While frustratingly making the true continuum difficult to uncover, these imprints of reprocessing are themselves valuable diagnostics of accreting systems, and we now discuss the details and diagnostic potential of those signatures.

2.2 X-ray reprocessing in the Compton-thin regime

In the $0.1 - 10\,\mathrm{keV}$ band, energetic X-ray photons can excite or ionize inner-shell electrons of atoms from C to Ni, with K-shell processes dominating. Early (proportional counter and other) observations of X-ray absorption in AGN concentrated on deriving gas parameters from the broad "curvature" (the systematic variation in apparent power-law slope with photon energy) produced by superposition of bound-free edges presumed from neutral gas, whose effects were most noticeable in the soft X-ray band. Initial treatment of ionized gas derived column densities and ionization-states from fits to K edges of O VII and O VIII. As data quality improved, and more detailed spectral features became detectable, the employment of photoionization models was justified, although most models necessarily make simplifying assumptions of geometry and distribution of matter. Common features of many models are the assumption of a slab of gas of constant density, photoionized by a central continuum source whose spectral form is usually specified as an input parameter. The gas is often assumed to be in thermal equilibrium with the thermal and ionization structure determined at some finite number of points in radial steps away from the central continuum. Photoionization codes that have been widely used to fit X-ray spectra include ION (Netzer 1993), CLOUDY (Ferland et al. 1998), XSTAR (Kallman and Bautista 2001) (with XSTAR 21ln onwards including the important inner shell transitions for Fe, Kallman et al. 2004), SPEX (Kaastra et al. 2003), TITAN (Collin et al. 2004) and MOCASSIN (Ercolano et al. 2008).

In photoionized gas the ionization state is determined by the form of the ionizing spectrum and a quantity that measures the ratio of ionizing photon density to proton density known as the *ionization parameter* (e.g. Osterbrock and Ferland 2006) In this review we use the ξ form of ionization parameter where $\xi = L/nr^2$ and L is the ionizing luminosity integrated from 1-1000 Ryd, n is the proton density and r the distance of the material from the central black hole (Tarter et al. 1969)[2] We adopt units for ξ of $\mathrm{erg\,cm\,s^{-1}}$. A convenient expression of the amount of gas in the line-of-sight is the equivalent column density of hydrogen atoms, $\mathrm{N_H}$ atoms $\mathrm{cm^{-2}}$, with solar abundances of other elements often assumed, although ionic columns, i.e. column densities of just one species, are also widely used. In high-ionization gas, hydrogen does not contribute significantly to the opacity, which is dominated by photoelectric absorption by heavier ions.

In addition to bound-free edges, resonance transitions can produce significant absorption signatures. The importance of resonance absorption lines in the X-ray regime was first discussed by Matt (1994), who noted that if material is in an ionization-state for which resonant absorption can occur (i.e. for Kα, those having an L shell vacancy, H-like to F-like ions) then in the optically-thin regime the Fe Kα absorption line equivalent width (EW) would be $\mathrm{EW} \simeq 20 A_{\mathrm{Fe}} (\mathrm{N_H}/10^{22}\mathrm{cm^{-2}})\,\mathrm{eV}$, where A_{Fe} is the iron abundance relative to the interstellar value, indicating that Fe Kα absorption should be highly significant in X-ray spectra of ionized gas (see also Nicastro et al. 1999 and Bianchi et al. 2005). Indeed, a few years after the publication of that paper, with the advent of a new generation of X-ray grating instruments, resonance absorption lines started to be detected in X-ray spectra of AGN (Kaastra et al. 2000; Sako et al. 2001; Kaspi et al. 2002, Figure 3). Krolik and Kriss (1995) discussed how the resonance line features would contribute to the X-ray spectral shape, such that they would seriously compromise correct identification of simple single edges fit in CCD quality spectra and also affect the observed fluxes and profiles of any emission lines close enough in energy to be unresolved in X-ray spectra.

---

[2] The ionization parameter is also commonly defined as a dimensionless quantity U (Osterbrock and Ferland 2006), widely used in UV astronomy: additional variants on the ionization parameter are U_x and U_{ox} that are distinguished by the range over which the illuminating ionizing luminosity is integrated (0.1-10.0 keV and 0.54-10.0 keV, respectively, see e.g. Netzer 1996; George et al. 1998). The conversion between the most commonly used ionization parameters is shown by George et al. (1998) for several assumed ionizing spectra. For analysis of multi-phase plasmas in pressure equilibrium a parameter Ξ defined in terms of pressure rather than density may be preferred (Krolik et al. 1981; Nayakshin et al. 2000).

Absorbing gas is also expected to produce line emission. In particular, Kα lines may be emitted by fluorescence, that is, relaxation after a K-shell photoionization, with a high fraction of photoionizations ultimately producing a Kα photon (Osterbrock and Ferland 2006). The strength of an emitted fluorescence line is governed by the probabilities of radiative de-excitation compared to auto-ionization (known as the Auger effect for this case of relaxation from a state with an inner-shell vacancy) and to two-photon emission. The probability of producing a Kα photon per ionization is known as the (Kα) fluorescence yield. Because fluorescence yield increases strongly with atomic number approximately as Z^4, and because Fe has a high abundance, Fe line emission is prominent in X-ray spectra of AGN.

Krolik and Kallman (1987) estimate that the luminosity of the Fe Kα fluorescence emission line is approximately

$$L_{\mathrm{K}\alpha} \simeq \frac{E_{\mathrm{K}\alpha}}{2+\Gamma} \langle Y \rangle \frac{\Delta\Omega}{4\pi} L_0 \langle \tau_0 \rangle$$

in the optically-thin limit and assuming a power-law illuminating continuum of photon index Γ, and where $E_{\mathrm{K}\alpha}$ is the energy of the Kα emission line, $\langle Y \rangle$ is the fluorescence yield averaged over ionization states, L_0 is the continuum luminosity per unit energy interval at the K edge and $\langle \tau_0 \rangle$ is the photoionization optical depth at the K edge averaged over the solid angle subtended by the absorber at the source. The above relation is an upper limit on the line strength because scattering and re-absorption of the fluorescence photons have been neglected. A consequence of Fe ions having high fluorescence yield is that we expect to see a direct correspondence between detection of bound-free edges (such as the Fe K edge) and re-emission of fluorescence lines (such as Fe Kα). For low-ionization states of Fe we expect approximately one-third of photons absorbed in a K-edge photoionization to be re-emitted as Kα line photons. For highly-ionized material we expect $0.5 \lesssim \langle Y \rangle \lesssim 0.7$ (Krolik and Kallman 1987). Because the bound-free edge is observed in absorption along the line of sight, but the fluorescence photons are emitted isotropically, the equivalent width of the emission depends on the geometry of the absorber and in particular on the fraction of the source that is covered by the absorber. Only in the case of complete covering of the source by optically-thin gas do we expect to observe an equivalent width commensurate with the fluorescence yield.

For ionized material, the binding energies of the inner shells generally increase with ionization and so the energies of the K edges and emission and absorption lines usually increase with ionization (see Kallman et al. 2004). In neutral material the Fe Kα fluorescence line comprises a doublet at energies 6.404 and 6.391 keV, these being indistinguishable by current X-ray spectrometers. The Fe Kβ line at 7.06 keV is expected at about 13.5% of the flux of Kα (e.g. Leahy and Creighton 1993; Palmeri et al. 2003). In ionized gas the "Fe Kα line" becomes a complex of permitted, intercombination and forbidden transitions (depending on which ion is considered) with possible contributions also from satellite lines, that are largely unresolved with current instruments (see e.g. Bautista and Kallman 2000; Kallman et al. 2004; Bianchi et al. 2005), but which may be partly separable with future instruments (see Section 9). In photoionized gas in particular, Fe Kα fluorescence emission may be dominated by the intercombination and forbidden transitions (e.g. for Fe XXV, see Bautista and Kallman 2000; Bianchi et al. 2005 and references therein, see also Bautista and Kallman 2000; Porquet and Dubau 2000 for discussion of other He-like ions). The fluorescence yield is also a function of ionization state; the yield varies with ionization until the atom is down to H- and He-like states, where the Auger effect can no longer occur and the yield reaches a maximum (Krolik and Kallman 1987). Matt et al. (1997), Bianchi and Matt (2002) and Bianchi et al. (2005) give examples of the predicted line strengths and dependences on atomic number, column density, geometry, elemental abundance and ionization-state of the line-emission region.

Returning to consideration of resonance absorption lines, emission of Kα photons following a Kα absorption (the process of resonant scattering) can also occur, causing the absorption lines to be partially filled-in. Neglecting, for the moment, the destruction or absorption of line photons that can occur during successive resonant scatterings (see Section 2.3) and assuming the optically-thin limit, the strength F_{em} of resonance line emission accompanying the line absorption is expected in Li-like to F-like ions to be approximately $F_{em} \simeq F_{abs} Y' \Delta\Omega / 4\pi$, where F_{abs} is the absorbed flux, Y' is the fluorescence yield for the ionization state below that of the ion in question and $\Delta\Omega$ the solid angle subtended by the absorber at the illuminating source (Matt 1994). The fluorescence yield for the previous ionization state, Y', is close to, but not exactly the same as, the yield of Kα photons from the resonant transition. For H-like and He-like ions Y' should be replaced by a value of nearly unity, as Kα transitions in these ions are almost pure scattering events. The geometry of the gas is a crucial factor in determining the degree to which the absorption line is filled-in by re-emission and for a full sphere of highly-ionized optically-thin gas the emitted flux is typically about one-half the absorbed flux (but see below for further discussion of the effects of geometry on resonantly-scattered lines). Clearly the relative dominance of various emission and absorption features depends strongly on the gas geometry, and so conversely, the measured strengths of these could in principle be a powerful constraint on the gas distribution, if components can be adequately separated in observational data.

2.3 Resonant line scattering and the effects of geometry

In ionized material, for radiative transitions whose lower level is significantly populated, the photon mean free path may be much less than for continuum photons, and under these conditions line photons can resonantly scatter (e.g. the Fe Kα resonance line in the case where Fe is ionized at least to F-like states). Losses of line emission may occur for lines such as Fe Kα during resonant scattering. First, on each scattering there is some probability of photoelectric absorption, so on repeated resonant scattering events the line becomes increasingly attenuated. Second, for Li-like to F-like ions, at each resonant absorption there is a probability of auto-ionization rather than remission of a Kα photon - a process often referred to as "resonant Auger destruction". Detailed calculations of population levels are required to correctly assess the extent both of resonant scattering and of resonant Auger destruction (e.g. Liedahl 2005) but the effect can be significant for ionized absorbing zones. The extent of resonant scattering is also affected by the velocity structure in the gas: turbulent velocity structure lowers the optical depth in the line core but increases the range of photon energies over which resonant scattering can take place (Nicastro et al. 1999); macroscopic velocity structure can suppress resonant scattering, which ceases when line photons are Doppler-shifted away from the wings of the absorption profile.

The geometry of the absorbing material can play an even more important role for resonantly-scattered lines than it does for non-resonantly scattered lines. Not only is the covering fraction important but so also is the shape of the absorbing zone and orientation with respect to both illuminating source and observer. Consider radiation passing through an anisotropic absorber. When resonantly scattering, line photons random walk between successive absorption and emission events inside the absorber, and are last scattered from about an optical depth of unity inside its volume. If the absorber is oriented so that its surface is preferentially oriented away from the observer, there is a greater line intensity away from the observer than towards the observer. The effect has been simulated for resonant scattering in highly ionized gas by Matt et al. (1997). In addition, if the K-edge absorption optical depth is sufficiently high, most fluorescence photons are emitted from the surface nearest the illuminating source, again leading to anisotropy of the line emission, with the observed luminosity being significantly suppressed for lines-of-sight that pass through the absorber (Ferland et al. 1992).

Given that there is no spatial information available for the innermost X-ray-emitting regions, the geometry of the regions is unknown, making predictions of the observed strengths of resonantly-scattered lines such as ionized Fe Kα difficult and model-dependent.

2.4 X-ray reprocessing in the Compton-thick regime

In gas with a high column density, Compton scattering has a significant effect. For photons in the 2–10 keV band, where most X-ray data have been accumulated to date, $\mathrm{h}\nu << \mathrm{m_e c^2}$ and the Compton scattering cross-section for free electrons is approximately the energy-independent Thomson cross-section σ_{T}. For solar-abundance gas in which H and He are fully ionized, the dominant scattering is by free electrons and the continuum optical depth is $\tau \simeq \mathrm{N_e}\sigma_{\mathrm{T}}$, where $\mathrm{N_e}$ is the free electron column density (heavier ions also have significant energy-dependent individual scattering cross-sections but their net contribution is small). Thus the scattering optical depth has a value unity approximately at $\mathrm{N_H} \simeq 1/1.2\sigma_{\mathrm{T}} \simeq 1.25 \times 10^{24}\mathrm{cm^{-2}}$. For solar abundance material, the cross-sections for Compton scattering and photoelectric absorption, σ_{pe}, are comparable at 10 keV and this represents an energy that has been considered as the low threshold for studying the "Compton reflected" components of AGN. For column density up to about $10^{25}\mathrm{cm^{-2}}$, some transmitted radiation is still visible above 10 keV (Matt et al. 1999). Note that in this regime, computation of the expected transmitted spectrum should take account of Compton scattering, which is not included in one-dimensional radiative transfer codes such as XSTAR. For higher column densities still, the material allows essentially no direct transmission of photons through the structure. Compton scattering around the edges of absorbing zones may still allow some fraction of X-ray radiation to reach the observer (rather like the "silver-lining" effect around cloud edges).

Despite the presence of an intense field of radiation, relatively cold gas ($T \leq 10^6$K) can exist in the nuclear regions if the material is sufficiently dense (Guilbert and Rees 1988; Ferland and Rees 1988). It is thought that the inner radius of the accretion disk may extend very close to the black hole, and that this disk could provide a Compton-thick structure that plays an important role in reprocessing nuclear X-rays. Photons incident on the disk surface penetrate to a mean optical depth of unity into the disk. Continuum X-ray photons undergo either Compton scattering or photoelectric absorption in this surface layer. Compton scattering can redirect photons back out of the slab; in such an encounter, the typical Compton recoil energy loss ΔE by a photon of energy E is given by $\Delta E/E \simeq 2E/\mathrm{m_e c^2}$ which exceeds 10 percent at $E \gtrsim 30\,\mathrm{keV}$. Incident photons are downscattered in energy and a "hump" appears in the reflected spectrum through a combination of scattering and absorption effects. If we view the disk from the same side as the illumination there are not many scatterings per observed photon and for photon index $\Gamma = 2$ the hump is at most a factor two enhanced (Magdziarz and Zdziarski 1995) compared with a calculation in which Compton losses are neglected. Below 30 keV the photoelectric opacity of the material increases with decreasing energy, further enhancing the appearance of the reflection hump (Matt et al. 1991). A photoelectric absorption event results in either fluorescence line emission or ejection of an Auger electron. Thus the fate of incident photons is either to be destroyed by the Auger effect, scattered out of the slab or re-emitted from the slab as a fluorescence line (with some small contribution from two-photon emission). The net effect of these processes gives the so-called Compton reflection spectrum.

The shape of the reflection spectrum has been determined from theory (Guilbert and Rees 1988; Ferland and Rees 1988) and calculated in Monte Carlo simulations (George and Fabian 1991; Reynolds and Fabian 1997; Matt et al. 1991). The combination of absorption and scattering reduces the intensity of the reflected spectrum compared to that incident on the disk. To first order, valid for energies $\lesssim 10\,\mathrm{keV}$, the reflected spectrum is depressed by an energy-dependent factor about $\sigma_{\mathrm{T}}/(\sigma_{\mathrm{T}} + \sigma_{\mathrm{pe}})$ relative to the illuminating continuum and is a function of the ionization of the surface layers in the reflector. At energies $\gtrsim 10\,\mathrm{keV}$ the Compton "hump" discussed above enhances the reflected spectrum somewhat. The observed strength of the reflected spectrum relative to the illuminating continuum is a strong function of illuminating angle and viewing angle (Ghisellini et al. 1994; George and Fabian 1991; Matt et al. 1997), being highest for viewing normal to the surface, and, for an infinite disk illuminated by a point source, varying by a factor about 10 as viewing angle θ varies over the range $0.05 < \cos\theta < 0.95$ (Magdziarz and Zdziarski 1995: see also Nayakshin et al. 2000). In model fits to data the relative reflection strength at high energy (where the opacity is low) is often parameterized by a parameter R defined as the ratio of the reflected intensity relative to that expected from a uniform infinite disk with time-steady illumination from above and viewed normal to the surface: a surprising feature of some model fits to data is that they yield values $R \gtrsim 3$ (e.g. Miniutti et al. 2007), see Section 6.3.

X-ray missions to date have offered limited data above 10 keV, making it difficult to access this important part of the spectrum (without going to high redshift, where a dearth of photons limits progress). Fortunately however, there are other detectable signatures of reflection predicted below 10 keV. As noted above, some absorbed photons are re-emitted as fluorescence lines and the emission part of the spectrum is dominated by the Kα lines of the most abundant metals. Fe Kα is the strongest of these fluorescence lines and was predicted to have a detectable contribution from cold dense material close to the black hole whether in the form of clouds (Guilbert and Rees 1988;

Nandra and George 1994) or an accretion disk (Lightman and White 1988). At softer energies, emission is expected from other fluorescence lines, radiative recombination continuum and bremsstrahlung from the reflector surface layers leading to a rich spectrum that is highly dependent on the ionization parameter (Ross et al. 1999; Ross and Fabian 2005).

As noted above, the photons that escape from the disk are those that reprocess within an average of one optical depth of the surface, and thus it is the properties of the skin of the disk that determine the detailed shape of the reflected spectrum, i.e. the reflection spectrum can have the signature of ionized material without inferring any inconsistency with the conditions required for the disk to exist at that location. The strengths of the spectral features in the case of reflection also depend on the factors that are important for Compton-thin gas, i.e., elemental abundance, ionization-state, incident spectrum and geometry (in this case, the shape and orientation of the disk). Destruction of line photons during resonant scattering (Section 2.3) also occurs: for the Fe Kα emission this is important for the range $100\,\mathrm{erg\,cm\,s^{-1}} \lesssim \xi \lesssim 500\,\mathrm{erg\,cm\,s^{-1}}$, where Fe is dominated by ions in the range Fe XVII-XXIII (Kallman et al. 2004). As ξ increases above this level photoelectric absorption and the Auger destruction diminish, and although resonant scattering is still in effect, the line photons can eventually escape the disk and the observed line strength increases, up to a point where Fe is completely ionized and both line and edge disappear from the reflected spectrum (see Ross et al. 1999; Ross and Fabian 2005).

The X-ray spectra of AGN are likely complex, with contributions from a primary continuum that may have a high-energy cut-off (thought to be in the few hundred keV regime, Dadina 2008), absorption from several layers of gas with different ionization and likely differing covering fraction, and a contribution from reflection off Compton-thick gas. On this is superimposed the re-emission associated with each absorption and reflection process, and those components are subject to distortion by various kinematic and relativistic effects. We now consider the distortions important to the X-ray regime.

2.5 Thermal, kinematic and relativistic modifications of AGN spectra

The modification of the reprocessed spectrum by a variety of kinematic and relativistic effects complicates the effort to identify the physical state and geometry of reprocessing material. Consider first the effects that are expected for a cloud of gas experiencing no external effects. For the Fe Kα fluorescence line the natural line-width is about 3.5 eV, negligible given the spectral resolution available and given many other factors that broaden the line far more. Thermal broadening in gas of temperature T produces a Doppler spread in photon energy $\Delta E/E \sim \sqrt{2\mathrm{k}T/\mathrm{m_p c^2}}$. For $T \sim 10^6 - 10^7\,\mathrm{K}$, likely applicable to the X-ray gas, thermal widths are also negligible compared with instrumental resolution, although thermal broadening does affect the extent of resonant scattering of lines.

Compton scattering can also have a detectable effect on line profiles. At Fe Kα a single Compton scattering event can change the photon energy by an average of about 80 eV, comparable to the resolution of CCD detectors and resolvable by grating instruments, and leading to the possible development of a "Compton shoulder" to energies below the line core.

Other observational distortions depend on the gas geometry, radial location from the central black hole and our viewing line-of-sight. Spectral features imprinted from gas with some velocity are shifted in energy; in the non-relativistic regime this is a simple Doppler shift. The case of the symmetric sphere of outflowing gas is interesting and well studied within stellar astrophysics; the so-called P Cygni profile is produced in such a case, where the absorption component of a line is blue-shifted relative to the mean emission component, producing a characteristic spectral signature. In all cases except that of the symmetric sphere of gas, the observer's orientation to the material is clearly important as that determines the velocity component along the sight-line and hence the degree of Doppler shift experienced by each line component. For Compton-thin gas, absorption features can be seen from material in the line-of-sight to the continuum, and in this case broadening can occur where there is a velocity gradient along the line-of-sight. Line emission is similarly broadened both by bulk flow velocity gradients and by orbital motion. In some regimes of inclination angle and emitting radii, gas in a rotating annulus may produce emission lines with the classic "double-horned" profile, as the observer is viewing the sum of the approaching and receding sides of the disk.

As gas velocities reach the relativistic regime then spectral signatures suffer further distortion, as relativistic aberration boosts the blue peak of spectral lines and suppresses the red. For emitting material very close to the black hole, gravitational redshift of photons becomes significant, redistributing line photons to lower energies with a shift that depends on the radial location of the gas; in addition to gravitational redshift the Doppler effect from orbital motion provides an energy shift of comparable magnitude; and light bending around the black hole leads to potentially large distortions in the viewed emission region. In the case of emission from a disk, the latter effect is most significant for disks viewed at large inclination angles to the normal. Fabian et al. (1989), Laor (1991), Karas et al. (1995) and Reynolds and Nowak (2003), among others, plot the predicted spectra from an accretion disk, showing the expected line profile as a function of disk orbital parameters. As the radial location of the gas is a critical parameter for determining the degree of general relativistic effects, this, and other key parameters can, in principle, be derived from spectral line shapes. In the Schwarzschild metric, the general relativistic terms are factors $(1-2\mathrm{r_g}/r)^{-1/2}$ which become significant for radius coordinate $r \lesssim 20\,\mathrm{r_g}$. Thus general relativistic distortions are, in principle, measurable in current X-ray spectra for gas within such radii, although, as we discuss below, the ambiguity of spectral signatures limits progress in this regard.

3 Basic Models of AGN spectra

The above basic ingredients may be used to construct model spectra with a small number of parameters that may be used to fit to observations (see Sections 4 & 6). Fig. 2 illustrates the model components that are commonly used, all shown here for the same simple input continuum, a power-law with photon index $\Gamma = 2$. The first panel (a) shows the effect of a shell of absorbing gas in front of the primary source. In this case the gas is assumed to be neutral and hence has very high optical depth in the soft band. As discussed above, models to generate the effects of ionized absorption are also frequently used (e.g. XSTAR, Kallman and Bautista 2001; Kallman et al. 2004[3]). Curves show the transmitted spectrum for a full shell of gas of varying column density and the Fe Kα and Kβ line emission from the gas is also included based on the calculations of Leahy and Creighton (1993), assuming the Kβ line flux to be 13.5% of the Kα line.

---

[3] http://heasarc.nasa.gov/lheasoft/xstar/xstar.html

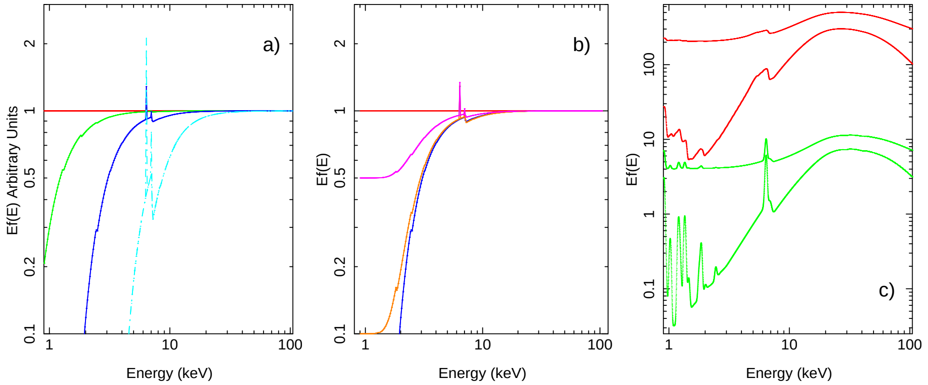

Fig. 2 Model lines for a) a simple power-law continuum with photon index $\Gamma = 2$, no high-energy cut-off and no absorption (red), modified by absorption by a full shell of neutral gas with column density $\mathrm{N_H} = 5 \times 10^{21}\mathrm{cm^{-2}}$ (green), $\mathrm{N_H} = 5 \times 10^{22}\mathrm{cm^{-2}}$ (dark blue), $\mathrm{N_H} = 5 \times 10^{23}\mathrm{cm^{-2}}$ (light blue dot-dash line); b) the same power law (red) absorbed by a full shell of gas with $\mathrm{N_H} = 5 \times 10^{23}\mathrm{cm^{-2}}$ (dark blue), 90% covered by the gas (orange) and 50% covered by the gas (magenta); c) the spectrum reflected by Compton-thick gas calculated from the REFLIONX model (Ross and Fabian 2005). We plot reflection alone (lower green line) and summed with the illuminating powerlaw (upper green line). The same reflection spectrum is shown blurred by the effect of orbiting of the material near the black hole (lower red line) and the sum of the blurred reflected spectrum and the powerlaw is also shown (upper red line). The two cases are each shown with an arbitrary normalization to allow clarity of display. See text for full details of the calculations.

The second panel (b) shows the effect of allowing only part of an extended source to be covered by the absorbing gas, showing covering fractions of 50, 90 and 100 percent. The dominant effect is to allow leakage of flux in the soft band, and to change the shape of the transmitted spectrum at intermediate energies. Emission lines are included as for (a). The third panel (c) shows the spectrum expected from reflection from optically-thick gas, here generated using the REFLIONX model (Ross and Fabian 2005) assuming $\xi = 10\,\mathrm{erg\,cm\,s^{-1}}$ and solar abundances. Also shown is the sum of the reflected spectrum and the illuminating powerlaw. For comparison, these are overlaid with the spectrum expected after general relativistic blurring appropriate to reflection within 3–20 $\mathrm{r_g}$ of the black hole, with a radial profile of reflected emissivity $I(r) \propto r^{-3}$ and assuming in the blurring calculation an inclination angle of 30°. This calculation was made using the KDBLUR convolving function, based on the model of Laor (1991), in the XSPEC package (Arnaud 1996).

These models are overly simplistic representations of the likely complex inner regions of AGN. Any absorbing material is unlikely to be in the form of a uniform shell and probably comprises multi-phase gas over a wide range of ionization, density and radii, and having spatial structure which, if comparable to the scale of the primary emission region, causes a mixture of spectral components to be received by the observer. Any absorbing gas of high optical depth also produces scattered components of radiation that should be taken into account. Similarly, although we expect there to be scattered/reflected radiation from optically-thick components in the inner regions, this is likely complex, again covering a wide range of radii, ionization states and spatial structures. Nayakshin et al. (2000) show how an accretion disk atmosphere in pressure equilibrium may produce substantially different reflection spectra from the constant-density calculation used for REFLIONX (Ross and Fabian 2005) for some range of disk states. Also, although the approach noted above to construct the reflection models is one that is commonly used, the one-dimensional calculation used for REFLIONX does not allow for the expected variation in line emissivity with both illumination incidence angle and viewing angle (e.g. Nayakshin et al. 2000) and thus the calculation for inclined disks is not self-consistent. For inclination angles $\lesssim 30^\circ$ the variation in emissivity is not thought to be large (Magdziarz and Zdziarski 1995) but would make a significant difference at inclinations $\gtrsim 60^\circ$. Near the black hole the combined effects of relativistic aberration of angles caused by the disk motion and the bending of light around the black hole may make such angle-dependent emissivity more important. Furthermore, although we adopted a reflected emissivity profile varying as r^{-3}, we do not in fact expect the reflection to vary with the same dependence as the black-body emissivity of the disk (Shakura and Syunyaev 1973), as the reflected emissivity depends on the radial dependence of the illuminating continuum, e.g. radiation from a corona, viewed at the disk's surface, as well as on the disk's structure and ionization. A large, extended corona would not be expected to result in such a steep reflection profile.

With the datasets currently available it is not possible to build models that can encapsulate such complexity in any unambiguous way, so the best that can be done for now is to try to model the generic features of the X-ray spectra to distinguish the most important spectral components. This has important consequences for the conclusions that may be drawn from model-fitting: if we wish to decide between two competing models of a spectrum, in reality either of the models being tested are likely gross simplifications of the true physical situation. A simple comparison of overall goodness-of-fit, e.g. using a standard χ^2 test, could be misleading. A better approach under these conditions is to attempt to identify key features, such as absorption lines or edges or emission lines, which might have the power of discriminating between models, and to test the data for the presence of those signatures. As the quality of data improves with each successive X-ray observatory, our ability to distinguish between such signatures increases. But even with current generations of instruments, CCD detectors with high effective area lack the energy resolution needed to clearly detect narrow absorption and emission features, whereas high resolution grating instruments lack sensitivity. This results in an ongoing ambiguity in the conclusions that may be drawn from modeling of X-ray spectra, but this ambiguity should be addressed in the next few years with a new generation of high-throughput, high-resolution and broad-band instruments (Section 9). In the following two sections we take a historical approach to describe how our knowledge of the inner regions of AGN has developed to date, and to summarize some of the current ambiguities in the interpretation of AGN X-ray spectra.

4 Early X-ray observations of AGN

In this section we summarize some of the strengths and notable properties of the X-ray missions that have had the most major impact on AGN research.

Observations using balloon and rocket-borne detectors flown during the 1960s detected X-rays from extra-galactic sources such as 3C 273 and Centaurus A (Bowyer et al. 1970). Following these successes, several dedicated X-ray astronomy satellites were approved that operated during the 1970s. One of these, the *Uhuru* satellite, confirmed the X-ray detection of several sources identified with AGN (Giacconi et al. 1974). *Ariel-V* data (e.g. Elvis et al. 1978) later showed that not only was X-ray emission a common property of AGN but that the X-ray flux varied by significant factors down to timescales shorter than one day in some sources (Marshall et al. 1981). Of the many instruments on *OSO-7* and *HEAO-1*, the proportional counters were the most useful for AGN studies. These, along with the *Ariel V* data, established that in the $2-20\,\mathrm{keV}$ regime AGN spectra could be parameterized by power-law continua with a mean photon index for the sample $\Gamma \sim 1.7$ (e.g. Tucker et al. 1973, Mushotzky 1976, Mushotzky 1984). Column densities were estimated assuming the absorbing gas to be a shell of neutral material covering the illuminating source. Compilations of spectral fits suggested column densities $\mathrm{N_H} \sim 10^{21}\,\mathrm{cm}^{-2}$ of gas existed around active nuclei, that this gas may be located in the BLR and that obscuration is more likely for low luminosity objects (e.g. Lawrence and Elvis 1982).

The second *HEAO* satellite, launched in 1978, was named the *Einstein* observatory. *Einstein* provided focusing X-ray optics and high sensitivity whose combined properties increased the number of X-ray detections of AGN by an order of magnitude. The focal plane detectors included proportional counters and a solid state spectrometer; observations using these instruments revealed soft-band (here used to mean 0.1–2 keV) complexity (e.g. Wilkes and Elvis 1987) that led to some suggestions that the gas covers only a fraction of the line-of-sight of AGN, comprising a so-called 'partial-covering absorber' (Reichert et al. 1985; Holt et al. 1980; see Section 3). *Einstein* observations of variations in absorption for the quasar MR 2251-178 led Halpern (1984) to the first suggested detection of a partially ionized absorber in AGN, dubbed the 'warm absorber', responding to variations in the continuum source.

The European X-ray Observing Satellite, *EXOSAT*, had a 3 year mission (1983-1986) and provided a variety of instruments of which the channel multiplier array (CMA) and the medium energy (ME) proportional counter were most useful for studies of AGN. The satellite had focusing optics in two Wolter type 1 Low Energy Telescopes each with a CMA in the focal plane that yielded data in the 0.05–2 keV band. As for previous proportional counters, the ME provided only modest spectral energy resolution ($\Delta E_{\mathrm{FWHM}}/E \simeq 0.21(E/6.0\mathrm{keV})^{-0.5}$ for the argon chambers) and useful data over 1–10 keV for weak sources such as AGN. *EXOSAT* also carried grating detectors (the Transmission Grating Spectrometers) but the sensitivity of the detector combination was not sufficiently high for any useful AGN observations to be carried out. Some notable contributions of *EXOSAT* to the study of AGN included detailed study of rapid variability in AGN (Green et al. 1993). Timing studies of AGN were aided by the eccentric orbit that allowed continuous observations for up to 76 hours of the 90 hour orbit. The broad bandpass of *EXOSAT* was also key to the detection of an excess of soft-band X-ray flux (the so-called 'soft excess') seen in about 50% of AGN compared to an extrapolation of model fits to data above a few keV (Turner and Pounds 1989). Some authors discussed how the reduced soft-band opacity of partially ionized C, N, O, Ne and other ions might explain the soft spectra and variability observed (e.g. Fiore et al. 1990; Warwick et al. 1988; Yaqoob et al. 1989; Pan et al. 1990) while others argued for an interpretation of the soft excess as emission closely related to the inner accretion disk (e.g. Arnaud et al. 1985; Kaastra and Barr 1989; Piro et al. 1988; Turner and Pounds 1988).

In addition to the soft-band spectral complexity, some detections of Fe emission had been made in the brightest and most heavily absorbed Seyfert galaxies from *OSO-8* data (Mushotzky et al. 1978), the Japanese *Tenma* satellite (Miyoshi et al. 1986) and some *EXOSAT* data (e.g. Ghosh et al. 1992; Leighly et al. 1989). Fe emission lines found in

Einstein spectra (Holt et al. 1980) were suggested to originate in the BLR, from the same gas observed to be providing partial-covering absorption of the X-ray source.

Ginga (launched by Japan in 1987) provided a large area proportional counter yielding good AGN spectra over the range $2-30$ keV, whose data established Fe Kα fluorescence emission to be a common property of local Seyfert galaxies (Pounds et al. 1989, 1990; Matsuoka et al. 1990; Nandra and Pounds 1994). Seyfert galaxies were detected at energies as high as 20 keV, and the detection of spectral hardening above 10 keV (Nandra et al. 1989; Piro et al. 1990; Matsuoka et al. 1990) and deep Fe K edge were consistent with an origin in neutral gas and supported the picture of a strong contribution from a reprocessed X-ray component. Various origins were discussed for the Fe Kα line, including the putative molecular torus, the BLR clouds and the accretion disk. In addition to the earlier suggestions of an origin in BLR clouds, a contribution was suggested from reflection off Compton-thick material out of the line-of-sight. The predicted Compton reflection component seemed consistent with some observed attributes of Seyfert galaxies (e.g. Guilbert and Rees 1988; Lightman and White 1988; George and Fabian 1991; Matt et al. 1991). Several physical origins of the Compton-thick material were suggested, including the accretion disk (Pounds et al. 1990) and the molecular torus (Krolik and Kallman 1987). However, the predicted spectra of AGN with partial-covering absorbers also provided a good explanation of the data (Matsuoka et al. 1990; Piro et al. 1990, 1992). Celotti et al. (1992) expanded on the Guilbert and Rees (1988) treatment of clouds by consideration of magnetic confinement, finding clouds in the density regime $10^{17} - 10^{19}\mathrm{cm}^{-3}$ could survive the intense irradiation likely to be experienced near the black hole. The hard-band properties of AGN were confirmed by missions such as the *Rossi X-ray Timing Explorer* (a proportional counter mission) and the Italian mission *BeppoSAX* (featuring proportional counters and a collimated Phoswich detector system giving a total overall bandpass 0.1–300 keV), although the ambiguity between Compton-thick reflection and complex absorption remained unresolved (e.g. Matsuoka et al. 1991). *Ginga* spectra also showed absorption edges from ionized species of Fe (XXIV-XXVI) in about 50% of Seyfert spectra (Nandra and Pounds 1994), indicating that a significant column density ($N_H \sim 10^{23}\,\mathrm{cm}^{-2}$) of very highly ionized material exists in these nuclei (a discovery that was to be confirmed by later grating observations).

The German-led *Roentgensatellit*, *ROSAT*, was launched in 1990, carrying a telescope of high spatial resolution with focal plane instruments covering the soft X-ray band. Individual absorption features were found in the Position-Sensitive Proportional Counter (PSPC) spectra covering the 0.1–2 keV regime, including detection of an absorption feature at 0.8 keV in MCG–6-30-15 (Nandra and Pounds 1992). Several other bright Seyfert I galaxies had sufficiently strong individual features that distinct zones of ionized gas could be isolated (e.g. Nandra et al. 1993; Turner et al. 1993a,b; Pounds et al. 1994; Ceballos and Barcons 1996). Most individual features detected using *ROSAT* were interpreted as a blend of O VII 739.3 eV and O VIII 871.4 eV bound-free edges. The soft absorption feature in MCG–6-30-15 was sufficiently well defined that it could be monitored and showed variations that indicated changes in absorbing gas opacity on timescales from about a day to weeks (Fabian 1994; Reynolds et al. 1995; Otani et al. 1996). As the mission progressed, further AGN observations confirmed the importance of ionized gas in Seyfert galaxies (e.g. Mihara et al. 1994; Ptak et al. 1994; Weaver et al. 1994; Yaqoob et al. 1994; Guainazzi et al. 1994). *ROSAT* observations of narrow-line Seyfert 1 galaxies showed some cases of extremely large amplitude variability, apparently exceeding what might be reasonably expected from variable continuum processes (Boller et al. 1997; Brandt et al. 1999) and arguably favoring X-ray absorption changes as the origin of the observed flux range. Motivated by such striking evidence for the importance of absorption variability in AGN, Abrassart and Czerny (2000) investigated how X-ray variability might be shaped by clouds partially covering the continuum, finding that random rearrangements of the cloud distribution could produce large amplitude variations on timescales of $10^2 - 10^6$s.

The launch of the Japanese *Advanced Satellite for Cosmology and Astrophysics*, *ASCA*, (Tanaka et al. 1994) in 1993 offered a significant improvement in spectral resolution with the first flight of CCDs on an X-ray observatory. The CCDs formed the Solid-State Imaging Spectrometers (SIS) (Burke et al. 1993) and offered the valuable combination of improved spectral resolution ($\Delta E/E \simeq 2\%$ at launch) and improved detector sensitivity with low detector background. While imaging optics had been in use for several years, *ASCA* was the first observatory allowing imaging in the hard X-ray regime. *ASCA* also carried a pair of gas imaging spectrometers (GIS) of lower spectral resolution. The SIS and GIS allowed determination of the X-ray background in an offset region of the detector (clear of target source photons), simultaneous to the accumulation of source counts. Prior to *ASCA*, hard-band detectors had relied on the use of non-simultaneous background determination, measurements made in a different detector part or the use of background models. The SIS CCDs allowed separation of some strong lines and edges that had previously been unresolved in proportional counter spectra, with the potential for constraining the shapes of very broad features. Of particular interest was the possibility of measuring strong distortions (blurring) of the Fe K emission line contributions produced within about 20 $\mathrm{r_g}$of the black hole, provided the line was strong and not confused with other spectral signatures. Indeed a strong spectral curvature around 6 keV was observed in many Seyfert galaxies and an interpretation made as an Fe K emission line, heavily broadened and redshifted by relativistic effects close to the event horizon (Tanaka et al. 1995; Nandra et al. 1997; Fabian et al. 2000). If one could be sure of the identification of this spectral component then a wealth of diagnostics could be obtained regarding the black hole and accretion disk (Fabian et al. 2000; Reynolds and Nowak 2003). The ambiguity of interpretation of X-ray spectra continued to be an issue however; blurred reflection, unblurred reflection and models of complex absorption all fit the mean spectra of AGN at a statistically similar level (e.g. Gondoin et al. 2001; Reeves et al. 2004; Turner et al. 2005).

ASCA performed some long observations that revealed spectral variability in both the overall observed shape and in individual features. For example, the absorbing gas in MCG–6-30-15 was confirmed to be variable by tracing changes in the O edges first observed using *ROSAT*. *ASCA* data showed the depth of the O VIII edge to be anti-correlated with continuum flux, while the O VII edge appeared unresponsive to variations in continuum flux. Otani et al. (1996) suggested that the absorber must be composed of at least two distinct gas zones, one of which has a significant recombination time (see also Orr et al. 1997). Towards the end of the 1990s a sufficient number of objects had been observed by *ASCA* and *BeppoSAX* that sample studies could start to address the overall absorption properties of AGN. George et al. (1998) and Reynolds (1997) agreed that about 60% of Seyfert I galaxies exhibited soft X-ray spectral features consistent with ionized gas having $\mathrm{N_H} \sim 10^{21} - 10^{23}\,\mathrm{cm^{-2}}$ and $\xi \sim 10 - 50\,\mathrm{erg\,cm\,s^{-1}}$. Nandra et al. (1997) discussed the hard X-ray properties of Seyfert 1 galaxies concentrating on the apparent profile of the Fe Kα line and discussing that in the context of blurred reflection models. Turner et al. (1997) discussed the X-ray parameters of Seyfert 2 galaxies, finding some surprising similarities between

Seyfert type 1 and 2 AGN with regard to hard X-ray variability and to the structure in the Fe K regime.

In light of the growing evidence for the importance of ionized gas in AGN systems, some authors revived the idea that partial-covering can explain observed spectral shapes and variability in AGN (Section 7.2). *ASCA* obtained data for key sources such as MCG–6-30-15, where Inoue and Matsumoto (2003) concluded that a significant part of the broad feature observed between 5–7 keV was the result of the superposition of ionized absorbers: this result was supported by analysis of the r.m.s. variability of the Fe line band compared with the rest of the spectrum (Matsumoto et al. 2003).

It is obvious that leaps in understanding have come from each new development in instrumentation. The early proportional counters provided low spectral resolution and often limited spatial resolution together with a need to take non-simultaneous background measurements. CCDs allowed some measure of the ratios and variability of broad and strong spectral features, although the detection of narrow features such as resonance lines was impossible. The next big steps came with the advent of grating spectrometers, as we discuss in the next section.

5 Current Observatories

In 1999 two new satellites were launched, the *Chandra* X-ray observatory and *XMM-Newton*, offering major steps forward in observational capabilities. With these missions the X-rays incident upon the grating instruments were dispersed on to sufficiently sensitive detectors that grating-resolution AGN spectra could be accumulated with useful signal, for the first time.

5.1 Chandra

The *Chandra* X-ray observatory carries high-resolution optics, providing $0.5''$ spatial resolution on-axis (an order of magnitude improvement over the best previous missions). *Chandra* provides the High Energy Transmission Grating (HETG) comprising two grating assemblies - the High Energy Grating (HEG) and the Medium Energy Grating (MEG), calibrated to an absolute wavelength accuracy about 100 km s^{-1}. HEG provides spectral resolution FWHM $\Delta\lambda = 0.012$ Å and calibration accurate to 0.006 Å across its effective energy range (0.8–8.5 keV/ 16–1.5 Å), approximately twice as good as that of the MEG which has FWHM $\Delta\lambda \simeq 0.023$ Å and calibration accurate to 0.011Å over 0.5–7 keV (25–2 Å). HEG has a higher effective area than the MEG above about 6 keV and is the only grating for which useful data can be accumulated in the Fe K region. Specifically, HEG provides energy resolution FWHM$\simeq$ 40 eV, equivalent to a velocity resolution about 1900 km s^{-1} at 6.4 keV, a factor of 4 improvement over the *ASCA* CCDs' best period of performance. The *Chandra* Low Energy Transmission Grating (LETG) is a single grating assembly that complements the HETG by providing grating data to very soft energies with $\Delta\lambda = 0.05$ Å covering the 0.07–6.0 keV/175-2 Å regime. Events dispersed by the gratings are collected by a focal plane detector and can be assigned an energy based on the position along the dispersion axis. The Advanced CCD Imaging Spectrometer (ACIS) comprises one focal plane instrument for *Chandra*. ACIS has two CCD configurations, ACIS-S and ACIS-I optimized for spectroscopy and imaging, respectively. A micro-channel High Resolution Counter

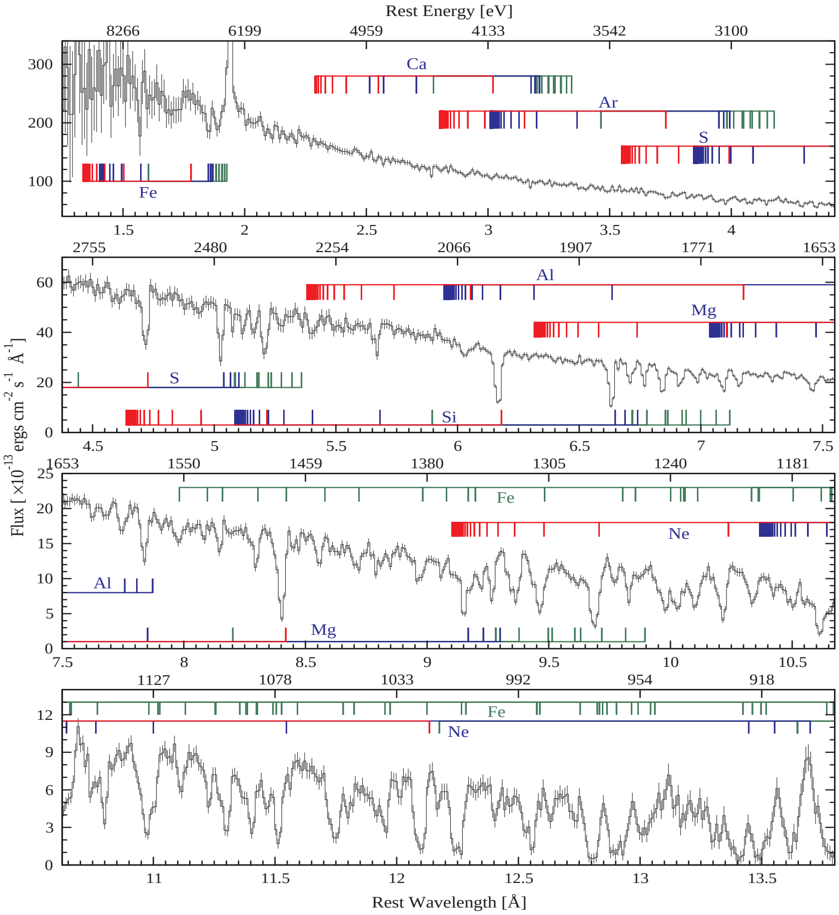

Fig. 3 NGC 3783, summed data from a 900 ks *Chandra* HETG observation. The combined MEG and HEG first-order spectrum has been binned to 0.01 Å. Each data point has an error bar representing its 1σ uncertainty. The H-like and He-like lines of the identified ions are marked in red and blue, respectively. Lines from other ions (lower ionization metals and Fe XVII, Fe XXIV) are marked in green. For each H-like or He-like ion the theoretically expected lines are plotted up to the ion's edge (not all lines are identified in the data). The ions' lines are marked at their expected wavelengths in the systemic rest frame of NGC 3783, and the blueshift of the absorption lines is noticeable. *From Kaspi et al. (2002): reproduced by permission of the AAS.*

(HRC) provides alternative focal plane instrumentation. While grating spectra can be dispersed onto either of the *Chandra* focal plane detectors, the usual configuration is to disperse HETG onto ACIS-S, whose CCDs are configured in a line suitable for the dispersed spectrum. Since the ACIS CCDs have intrinsic energy resolution, background events can be rejected with high efficiency, and different spectral orders can be discriminated easily, making ACIS-S a highly desirable focal plane detector choice for use in grating observations that do not require the very soft response of the LETG. The LETG grating data are dispersed onto the HRC or ACIS detector. The physical dimensions of the HRC can accommodate the large dispersion suffered by the softest photons (photons below 0.2 keV are dispersed off the edge of the ACIS-S array).

5.2 XMM-Newton

The *XMM-Newton* observatory has a pair of gratings that comprise the Reflection Grating Spectrometer (RGS) (den Herder et al. 2001), dispersing onto arrays of focal plane CCDs, providing a resolution FWHM $\simeq$ 2.9 eV at 1 keV, or $\Delta\lambda \simeq 0.07$ Å . The absolute wavelength calibration for the RGS is 0.008Å equivalent to $100\,\mathrm{km\,s^{-1}}$ at about 0.5 keV. *XMM-Newton* also carries both metal oxide semi-conductor (MOS) and pn-CCDs covering 0.5–10 keV with energy resolution FWHM $\simeq$ 130 eV at 6 keV, and FWHM $\simeq$ 55 eV at 1 keV, with throughput comparable to the previous CCD instruments on board *ASCA*. Useful RGS data can be accumulated over the range 0.4–2.0 keV/31–6 Å: data below 0.4 keV are not used because of a detector feature, and above 2.0 keV the effective area is very low. Although offering a lower spectral resolution than the *Chandra* gratings, RGS gratings offer greater effective area over this range then either HETG or LETG.

The choice of grating instrument for a given scientific observation is a complex function of anticipated source flux, spectrum and scientific objective. These grating detectors provide unprecedented resolution for many key diagnostic lines. Soft-band spectroscopy gained almost two orders of magnitude improvement in spectral resolution in the 0.5–1 keV regime, with He-like triplets of O and Ne becoming resolvable. Despite improvements in throughput, it is still the finite signal-to-noise that provides the limiting factor in error determination for many astrophysical features. The potential of existing gratings is arguably best illustrated by the 900 ks *HETG* exposure on NGC 3783, the deepest single AGN exposure to date with a grating detector (Figure 3); this dataset yielded more than 100 detections of absorption lines (Kaspi et al. 2002).

5.3 Suzaku

Complementing the grating facilities is the Japanese-led *Suzaku* mission launched in 2005. *Suzaku* (Mitsuda et al. 2007) carries four X-ray telescopes that each focus X-rays on to a CCD forming part of the X-ray Imaging Spectrometer array (XIS) (Koyama et al. 2007) . XIS CCDs 0, 2 and 3 are front-illuminated (FI) and cover about $0.6-10.0$ keV with energy resolution FWHM $\simeq 120-150$ eV at 6 keV. Use of XIS 2 was discontinued after 2006 November because of a charge leak that occurred. XIS 1 is a back-illuminated CCD with an enhanced soft-band response (down to 0.2 keV) compared to the FI units, but lower area at 6 keV than the FI CCDs as well as a larger background level at high energies. *Suzaku* also carries a non-imaging, collimator Hard X-ray Detector (HXD, Takahashi et al. 2007) made from silicon PIN diodes, providing useful AGN data typically over 15–70 keV, and a GSO well-type Phoswich counter, providing data over about 75–165 keV for the handful of AGN bright enough to be detected. The hard X-ray detector has a significantly lower background level than the previous *BeppoSAX* PDS instrument over most of its bandpass, and so the simultaneous XIS and PIN data obtained during a *Suzaku* observation have allowed some exciting new insight into AGN.

Suzaku also carries the now non-functioning X-ray calorimeter XRS-2, this was the first X-ray calorimeter to achieve orbit on a satellite. Calorimeters are highly desirable X-ray detectors because they can achieve excellent spectral resolution across a broad bandpass by converting the absorbed energy of incident X-ray photons into heat. The detectors are low heat-capacity absorbers, cooled to very low temperatures, about 0.1 K, and coupled to heat detectors (thermistors or Transition Edge Sensors). XRS-2 would have provided both high resolution and high throughput in a single instrument with resolution better than 6 eV across its bandpass. Unfortunately a problem with the instrument vent configuration rendered XRS-2 inoperable after a few days in orbit. This failure followed a previous loss of the XRS-1 calorimeter along with the entire *ASTRO-E* satellite, which failed to achieve orbit after a problem with the first stage rocket.

New results from *Chandra* and *XMM-Newton* and *Suzaku* have opened up our understanding of AGN and we now review some of the recent developments and their implications.

6 Recent Observational Results

6.1 Absorption in a new regime

At the turn of the millennium, ionized "warm absorbers" had been established as commonly occurring in AGN, with multiple zones detected across the source population, covering a range of ionization and showing variability on relatively short timescales (Section 4). AGN spectra were revealed to be complex when observed at grating resolution. As UV spectroscopy had already shown AGN to possess kinematically-complex absorption, the richness of the X-ray absorbers was no surprise. In the longest grating exposures several ionization zones of gas could be discerned in a single source (e.g. Kaspi et al. 2002; Steenbrugge et al. 2005). In one case, NGC 3783, Netzer et al. (2003) and Krongold et al. (2003) discussed the observed complexity in the context of several phases of absorbing gas having distinct temperatures and ionization states (see also Behar et al. 2003); this is the most common approach to modeling AGN spectra. In an alternative treatment, Gonçalves et al. (2006) modeled the data using a single medium in total pressure equilibrium; this showed a stratification of ionization structure yielding multiple temperature components within the cloud without a need to invoke separate absorber regions (although if zones are found to be kinematically distinct such a picture would need to be modified).

Grating spectra allowed separation of lines that had been unresolved using CCDs. Broader features such as radiative recombination continua could be measured (or fit) for the gas temperature; the components of some He-like triplets (O, Ne) could be separated and component ratios used as a temperature and density diagnostic. The gas temperatures indicated for the line-emitting gas were generally in the million-K regime based on soft-band absorption lines. An improved ability to identify individual lines also led to better estimates of gas kinematics, showing outflow velocities covering the range hundreds to thousands of $\mathrm{km\,s^{-1}}$ (Kaspi et al. 2002; Krongold et al. 2003; Blustin et al. 2005; McKernan et al. 2007; Blustin et al. 2007). The detection of some unresolved transition arrays (Sako et al. 2001; Krongold et al. 2005; Smith et al. 2007) and possible detection of dust absorption edges (Lee et al. 2001) also implied the iden-

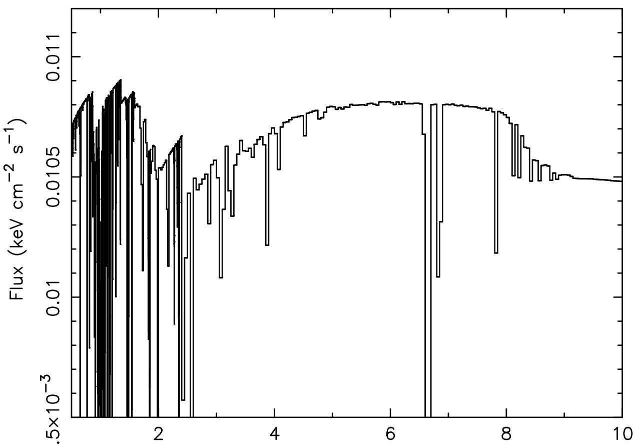

Fig. 4 Model of the high-ionization warm absorber fitted to the spectrum of NGC 3783 by Reeves et al. (2004). The model line shows the imprint of a column of gas having $\log \xi \sim 3$ and $N_H \sim 5 \times 10^{22}\,\mathrm{cm}^{-2}$ over a smooth $\Gamma = 2$ powerlaw continuum. The curvature is due to high ionization K-shell edges and lines from Mg, Si, S, as well as from the L-shell and K-shell of Fe. *Figure reproduced from Reeves et al. (2004) by permission of the AAS.*

tification of cool and dusty zones of the absorber complex, previously difficult to distinguish from absorption edges and broadened emission lines.

In addition to the detailed diagnostics of known gas layers, new observations by *Chandra* and *XMM-Newton* revealed that X-ray absorbers extend into a previously poorly-explored regime of high column density, high ionization gas. Deep K-shell absorption lines were found in grating and CCD spectra from very highly ionized species of Fe. The detection of a strong absorption line from highly ionized Fe in a long *XMM-Newton* observation of NGC 3783 (Reeves et al. 2004) confirmed the suggestion of Fe XXV absorption made in *Chandra* data (Kaspi et al. 2002). The absorption line showed variability in equivalent width over days, being strongest when the continuum level was highest. In the case of NGC 3783 the absorption line was found to be consistent with an origin in gas having $\log \xi \simeq 3$ and $N_H \simeq 5 \times 10^{22}\,\mathrm{cm}^{-2}$, likely existing about 0.1 pc from the nucleus. An interesting consequence of the high-ionization warm gas is that a large part of the curvature in the Fe K regime was accounted for by this zone, reducing the requirement for a relativistically blurred disk-line in the source (Figure 4).

Further examples of the presence of a highly-ionized X-ray absorber showed up in other long AGN exposures. Young et al. (2005) using *Chandra* HEG data, and Miniutti et al. (2007) in *Suzaku* data found lines at 6.7 and 6.9 keV in MCG–6-30-15 most likely identified with Fe XXV and Fe XXVI, with outflow velocity about 1800 km s^{-1}, supported by detection of Si XIV and S XVI (Young et al. 2005).

In analysis of *XMM-Newton* data from NGC 1365, Risaliti et al. (2005) described four absorption lines in the observed range 6.7–8.3 keV, identified as Fe XXV and Fe XXVI Kα and Kβ lines from gas outflowing at 1000–5000 km s^{-1}. This velocity range was interesting, being somewhat higher than that typical for the lower-ionization gas detected in the soft-band. Risaliti et al. (2005) found the absorption lines to have high equivalent widths (about 100 eV) and these, combined with the ratio of strengths of the

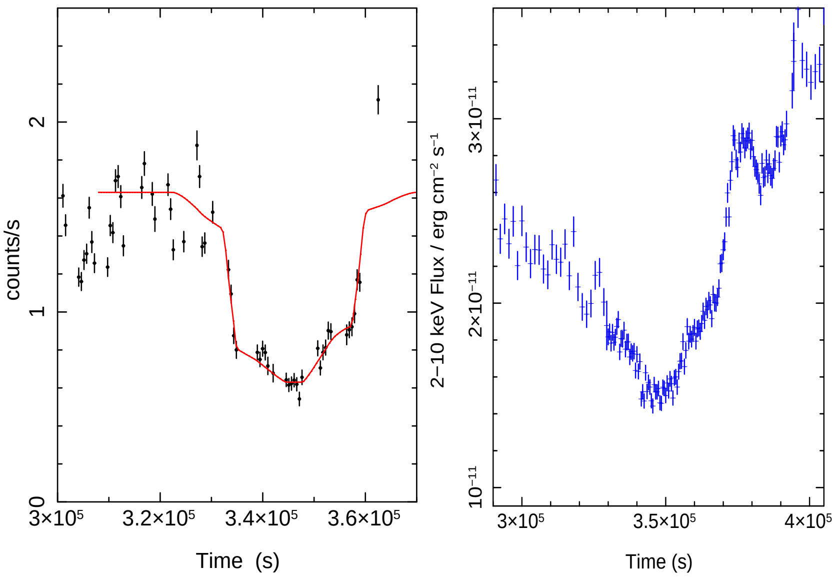

Fig. 5 A close-up view of the deep dip section of the light curve of: left) MCG–6-30-15 revealing the symmetric structure in the dip during an *ASCA* observation from 1994 July. SIS0 data are shown, binned at 512 s. The solid line is the predicted light curve based on a uniform cloud occulting a bright continuum point source situated within a ring of lower intensity extended emission. *Figure courtesy of Tahir Yaqoob, based on the analysis of McKernan and Yaqoob (1998)*; right) NGC 3516, showing the data discussed by Turner et al. (2008)

lines, implied the absorbing gas to have a column density about $5 \times 10^{23}\mathrm{cm}^{-2}$ and to reside about 50–100 $\mathrm{r_g}$ from the central source. In a follow-up campaign using *Chandra* the data showed variations consistent with an occultation by a Compton-thick cloud crossing the line-of-sight of the X-ray source. In the context of the occultation model the source was estimated to be less than 10^{14} cm in extent and residing within 10^{16} cm of the nucleus (Risaliti et al. 2007).

Mrk 766 also shows strong absorption features, observed at 6.9 and 7.2 keV: in this case an explanation as Fe Kα and Fe XXVI Lyα absorption is appealing, as a single outflow velocity of 13,000 $\mathrm{km\,s^{-1}}$ then fits both features (Miller et al. 2007). Similarly to the case of NGC 1365, a very high column density $\mathrm{N_H} > 10^{23}\mathrm{cm}^{-2}$ and high ionization, $\log\xi \gtrsim 2$, was found for the absorbing gas.

Analyzing NGC 3516, Turner et al. (2005) discovered a high-column absorber with $\mathrm{N_H} \sim 10^{23}\mathrm{cm}^{-2}$ and $\log\,\xi \sim 2$, covering about 50% of the continuum source. Data from a joint *XMM-Newton*/*Chandra* campaign during 2006 showed that changes in covering fraction of the high-column absorber could explain the spectral variability observed in this source (Turner et al. 2008). Intriguingly, a deep dip in flux showed a complex but well-defined and symmetric flux profile that was similar to that observed in *ASCA* data from MCG–6-30-15 (McKernan and Yaqoob 1998, Figure 5). The dip profiles could be explained as an eclipse of the continuum by a cloud moving across the sight-line (McKernan and Yaqoob 1998; Turner et al. 2008). If an occultation origin for such deep dips could be proved then the potential would be enormous: the angular size of black hole event horizons is $\sim 10^{-6}$ arcsec for the nearest AGN, so imaging of these systems is not possible in the foreseeable future, however, using the occultation event in MCG–6-30-15, McKernan and Yaqoob (1998) effectively mapped the nuclear regions on a size scale of $\sim 10^{-7}$ arcsec. Such angular scales may otherwise only be probed by analysis of micro-lensing events (Chartas et al. 2004, 2008). For NGC 3516, the *XMM-Newton* data showed that an additional gas zone was evident at a similar column density to that responsible for the spectral variability, but with higher ionization, log $\xi \sim 4$, producing deep absorption lines from the K shell of Fe XXV and Fe XXVI ions (Turner et al. 2008).

As existing AGN observations cover a wide range of signal-to-noise ratio it is too early to make a definitive assessment of the occurrence rate of these high column X-ray absorbers with $N_H \sim 10^{23} - 10^{24}\mathrm{cm}^{-2}$ and having Fe XXV and Fe XXVI as the dominant ions. However, as these lines have shown up in a number of well-exposed AGN observations, the gas, with typical outflow velocities of a few to many thousand $\mathrm{km\,s}^{-1}$, appears common in local AGN.

In addition to the strong observational effects attributed to changes in gas covering and/or opacity, any circumnuclear gas must respond to changes in its local ionizing continuum. Whether ionization changes can be observed depends on not only the signal-to-noise of the data but also whether the gas lies in a regime where changes in the illuminating continuum produce an observable change in the gas state. Some results have been published in this regard, with Kraemer et al. (2005) finding changes in the X-ray absorbers of NGC 4151 consistent with a response of the gas to changes in the ionizing continuum. Also, Netzer et al. (2002) found evidence for a response of the absorbing gas to continuum variations in NGC 3516 (see also Netzer et al. 2003).

Some sources show evidence for extremely high velocities in the outflowing gas. Outflows seem often to be associated with the more luminous AGN, and typically have velocities in the range 0.1–0.2 c (Reeves et al. 2008). *RXTE* data for PDS 456 first showed a very deep Fe K edge revealing the existence of a column of gas with $N_H \sim 5 \times 10^{23}\mathrm{cm}^{-2}$ and $\log \xi \sim 2.5$ in the source. A later *XMM-Newton* observation allowed a determination of an outflow velocity of 50,000 $\mathrm{km\,s}^{-1}$ (Reeves et al. 2003). Most recently, a long *Suzaku* observation has resolved the deep absorption feature into absorption lines from Fe XXV and XXVI yielding a revised estimate for the flow velocity of 0.25–0.3 c. Other early reports of such features included APM 08279+5255 (Chartas et al. 2002), PG 1115+80 (Chartas et al. 2003), PG 1211+143 (Pounds et al. 2003), IRAS 13197–1627 (Dadina and Cappi 2004), Mrk 509 (Dadina et al. 2005), IC 4329A (Markowitz et al. 2006) and MCG–5-23-16 (Braito et al. 2007). Further to these outflows, high-velocity inflows have been suggested to explain apparent redshifted resonance absorption lines detected in some sources (e.g. Mrk 335, Longinotti et al. 2007; Mrk 509, Dadina et al. 2005; E1821+643, Yaqoob and Serlemitsos 2005) with velocities in the range 0.1–0.4 c (see Reeves et al. 2008, and references within).

Not just restricted to the X-ray data, high velocity outflows are a well-known general phenomenon in AGN, being observed unambiguously in optical and ultraviolet spectra, especially in broad absorption line quasars (e.g. Weymann et al. 1991). The general existence of significant outflows is also implied by the existence of jets in AGN (e.g. Axon et al. 1989), although we likely need to make a distinction between the highly collimated jet outflows and possible wind-type outflows with wide opening angles (e.g. Pounds and Reeves 2008). However, the X-ray results remain contentious, with some authors claiming a possible correlation between the cosmological recession velocity of the AGN and the absorption outflow velocity for a number of

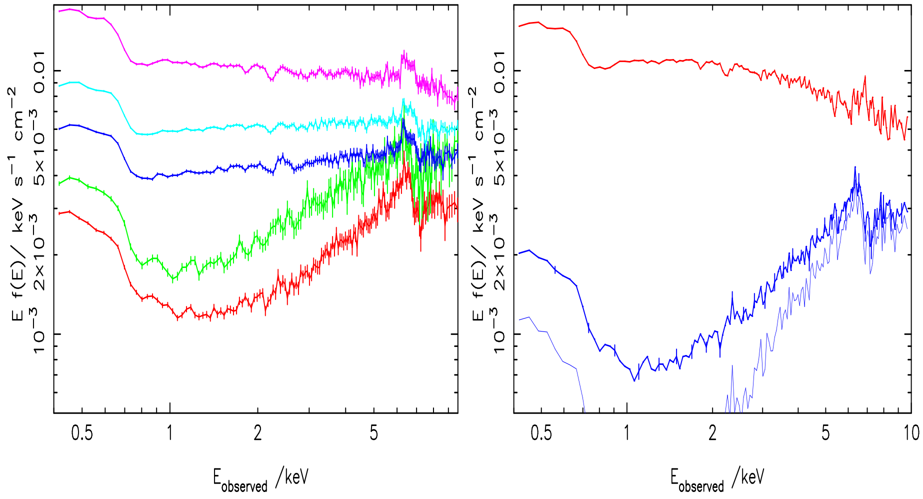

Fig. 6 Left: Data used for the principal components analysis of Mrk 766, from *XMM-Newton*, averaged into five logarithmically spaced flux states based upon the 1–2 keV flux, and ratio-ed to a power-law of photon index $\Gamma = 2$ with unit normalization, illustrating how the source hardens to low fluxes, behavior typical of Seyfert galaxies. Based upon data and analysis presented by Miller et al. (2007). Right: Principal component spectra of Mrk 766, 0.4–10 keV. The first, varying, principal component is the upper line (red), the possible range of an unvarying zero-point spectrum is shown by the lower set of spectra (blue). For clarity, error bars are only plotted on every fifth spectral point on both panels.

sources (McKernan et al. 2005), suggesting the absorbers have an origin in local gas, particularly since some of the sources in question lie behind the local hot bubble of gas known as the Northern Polar Spur. Countering these arguments, Reeves et al. (2008) calculate that the variability observed in PG1211+143 over 4 years shows the absorber to be too compact, and the surface brightness of the gas too high, for the observed absorption signature to arise in local gas; furthermore, Reeves et al. (2008) contend that the velocity coincidence observed in PG 1211+143 does not extend to other AGN. Finally, claims have been made that some of the detections of narrow absorption (and emission) lines are not statistically significant and we return to that issue in Section 6.5.

6.2 Broad-band spectral variability

While the existence of spectral curvature in the $2-8$ keV regime, dubbed the “red wing”, was confirmed by *XMM-Newton*, *Suzaku* and *Chandra* data (Wilms et al. 2001, Vaughan and Fabian 2004, Miniutti et al. 2007, Nandra et al. 2007), it has continued to prove difficult to make a convincing distinction between models dominated by either complex absorption or blurred reflection to explain how that curvature arises (c.f. Miniutti et al. 2007, Miller et al. 2008).

The most progress has come from consideration of the spectral changes that occur in these sources over timescales as short as tens of ks (e.g. Miller et al. 2007, Figure 6). Local AGN commonly show a systematic hardening as a source dims to a low flux level (e.g. Papadakis et al. 2002; Pounds et al. 2004a,b; Vaughan and Fabian 2004; Miller et al. 2007, 2008; Turner et al. 2008). As significant spectral variability occurs on much shorter timescales than a typical observation duration, the commonly-fitted mean spectrum is actually a superposition of source spectra from differing states. Fitting to mean spectra alone misses key information. Worse, if source variations are non-additive, such as in the case of variations caused by varying opacity, then fitting to the mean spectrum is unlikely to give a good representation of the physical construction of these systems.

A simple method to address the problem is to take time- or intensity-selected spectra to try to isolate the physical origin of the spectral variations. When sufficient photons have been accumulated, one can examine the flux correlations at different energies and look for the spectral forms of the smallest number of spectral components that can be used to describe the data.

More versatile than time-resolved spectroscopy, a powerful mathematical tool used to analyze systematic variations is principal components analysis (PCA). Its use in analysis of AGN X-ray spectra, albeit with low energy resolution, was first demonstrated by Vaughan and Fabian (2004), who showed that MCG–6-30-15 could be described by a constant hard component and a variable softer one. The steady spectral component carries the so-called red wing, showing that component to be surprisingly constant in amplitude while the observed continuum flux varies, contrary to the line/continuum correlation that would be expected if the line is produced very close to the continuum source. This behavior has been addressed with models that invoke variable light-bending effects driven by variations in the height of the continuum source above the disk (Fabian and Vaughan 2003; Miniutti et al. 2003; Miniutti and Fabian 2004). In the light-bending model, as the continuum source moves closer to the disk and black hole, general relativistic effects become more pronounced and some of the photons that were previously able to reach the observer instead arrive at either the disk surface or the black hole. For appropriate choices of height and range in height of the source, the fractional change in the primary source intensity viewed by the observer can be significant with the fractional change in the disk reflection intensity remaining relatively small (Miniutti et al. 2003). In this model, the continuum variations seen by the observer are thus primarily due to the effect of the moving source of X-ray continuum. For the effect to be isotropic, a ring-like structure for the illuminating source could be envisaged (Miniutti et al. 2003). The model has been applied to explain the variable spectra of a number of sources, including MCG–6-30-15 (Miniutti et al. 2003, 2007). The interpretation of the observed hard spectral component as blurred reflection requires significant contributions from within $6\,\mathrm{r_g}$ in order to obtain a component that extends to low enough energies to fit the data, a result that has been used to infer that the black hole in MCG–6-30-15 is spinning (e.g. Brenneman and Reynolds 2006).

Miller et al. (2007) address the problem in standard PCA applied to X-ray spectra where the number of data slices (often limited by the requirement of having adequate signal-to-noise in each data slice) is less than the number of energy intervals (determined by instrument energy resolution) and consequently the covariance matrix is singular and the eigenvectors are not uniquely defined. In this case the leading eigenvectors may be extracted using Singular Value Decomposition (SVD) (Press et al. 1992) and employment of this technique led to extraction of the leading eigenvectors at the full instrument resolution. Application of PCA with SVD was performed on Mrk 766 (Miller et al. 2007) yielding a spectral decomposition into a variable amplitude power-law of slope $\Gamma \simeq 2.4$ with a modestly broadened ionized component of Fe K emission superposed on this (Figure 6). The data showed a correlation of the flux in the continuum and Fe line with no detectable lag (Miller et al. 2006). This result was supported by apparent variations in the peak energy of the ionized line component. The energy variations, lack of lag and the width of the ionized emission line are all consistent with the line being produced at around $100\,\mathrm{r_g}$. Another line response to continuum was seen as a one-time event in MCG–6-30-15 where Ponti et al. (2004) found evidence for a Fe Kα component that appeared 3000 s after one strong continuum flare, suggesting some contributions to the observed emission line may come from regions located close to the continuum source ($< 240\,\mathrm{r_g}$) but outside the regime where light-bending effects are significant. In the analysis of Mrk 766, Miller et al. (2007) found in addition a hard-spectrum, less time-variable component that could be fit either as a blurred reflector, unblurred reflection from an ionized wind or absorption from a disk wind whose variable covering of the power-law explained the spectral variability observed. While the decomposition of X-ray data had isolated the variable spectral component, the interpretation of this ‘steady’ component was still unclear.

Turning to analysis of the well-studied source MCG–6-30-15, Miller et al. (2008) compiled all the best long-exposure, high-quality data, obtained from 522 ks with *Chandra* HETG, 282 ks with *XMM-Newton* EPIC-pn/RGS and 253 ks with *Suzaku* XIS/PIN and decomposed the spectral variations using the SVD-PCA. The Miller et al. approach was to make the spectral decomposition and then fit the variable and steady components as for Mrk 766. The model for the variable component was found to be a simple power-law $\Gamma \simeq 2.3$ covered by the complex warm absorber. The warm absorber in MCG–6-30-15 has long been known to consist of at least three zones of ionized gas whose signatures are seen in grating observations (Lee et al. 2001; Turner et al. 2003, 2004a). In modeling the hard component it was found that a variable partial-covering zone of absorption plus absorbed low-ionization reflection (distant from the source) resulted in a full model that fits all flux states of the data over its entire observed energy range. The construction of this model was different to that of Young et al. (2005) in allowing some of the ionized absorption to have a covering fraction < 1: the spectral shape is then reproduced by gas of intermediate ionization, $\log\xi \lesssim 2$, and consequently the absorption model of Miller et al. does not predict the resonance Fe Kα absorption lines at 6.5 keV that Young et al. had previously suggested would be expected if absorption does cause the red wing. In the Miller et al. model, the relative lack of variation of the red wing is an artifact of variation in the partial covering fraction of the absorber.

Seyfert behavior is sometimes complicated by the observation of spectral changes *within* the lowest flux states. Reynolds et al. (2004) interpreted spectral variations during the low state for MCG–6-30-15 as correlated changes between the line and continuum and explained the lack of correlated behavior at higher fluxes as due to a saturation of line production beyond a critical continuum level. It has been suggested that such complex low-state behavior could be expected either from patchy ionization of the disk surface (Reynolds and Wilms 2000) or in light-bending models if the continuum source is located close to the axis of spin for the black hole (Miniutti and Fabian 2004). In the alternative absorption models, behavior within the low-states may be explained either as opacity or ionization changes in the absorbers or as systematic evolution in the relative sizes of the source and the absorbing structure (Miller et al. 2008).

Interestingly, fluxes observed above 10 keV often exceed those expected from reflection from the surface of a disk subtending 2π steradians to a continuum source. Relative reflection strengths in the range $2 \lesssim R \lesssim 4.8$ are inferred in MCG–6-30-15, (e.g. Ballantyne et al. 2003; Miniutti et al. 2007). Ballantyne et al. (2003) proposed a model of double reflection to explain both the spectrum around the Fe Kα line and the high R value. The light-bending model, by design, enhances the reflected component over that expected in the absence of relativistic aberration and thus is constructed to produce enhanced R values. Other explanations for the relative lack of variability of the "red wing" (e.g. Merloni et al. 2006, Nayakshin and Kazanas 2002, Życki 2004) do not naturally explain the high R values, although it is possible that deeply-embedded emission hotspots in an inhomogeneous disk might be able to produce such an effect.

For NGC 4051, reflection models yielded $R \sim 7$ (Terashima et al. 2008). Light-bending models appear not to work for this source as they cannot simultaneously account for the high R value and the weak Fe Kα emission, leading Terashima et al. to conclude that partial-covering absorption is required. Attempts to model the spectrum of Mrk 335 also required $R \sim 2.8$ (Larsson et al. 2008).

An observed feature of the hard-band flux is that it appears less variable than the 2–10 keV flux (Miniutti et al. 2007), consistent with having a joint origin with the steady red wing. In the blurred reflection explanation this is consistent with the light-bending model. In absorption-dominated models the inference would be that much of the 2–10 keV band variability is caused by variations in absorption, with the steady continuum source being relatively unaffected by absorption above 10 keV.

A *Suzaku* observation of 1H 0419–577 appears to provide a rare case of a distinction between models. A marked 'hard excess' of counts was detected in the PIN data relative to the predicted flux based on model fits below 10 keV. The *Suzaku* data can be fit using an absorption-dominated model but not with any reasonable blurred reflection model. The detailed fits show that Compton-thick partial-covering gas must exist in 1H 0419–577 (Turner et al. 2009, ApJ in press). This result supports the earlier contention that partial-covering shapes the observed spectrum and much of the flux variability in 1H 0419–577 (Page et al. 2002; Pounds et al. 2004a,b). Considering the broad-band properties of 1H 0419–577, the source is consistent with spectral modification by a clumpy disk wind that provides the X-ray absorption from gas residing at radii inside or comparable to the radius of the optical/UV BLR. Importantly, the observed Fe Kα line luminosity is consistent with an origin in an equatorial disk wind in that case (Turner et al. 2009).

The luminous AGN PDS 456 also exhibits a hard excess (at the 3σ level) that similarly can be explained only by partial-covering models (Reeves et al. 2009, submitted). These two sources provide the first strong evidence for Compton-thick partial-covering gas in type 1 AGN and show that the intrinsic luminosity of such sources is underestimated significantly when based on data below 10 keV. The *Swift* BAT survey has discovered many new AGN based on their flux above 10 keV, suggesting that there may be a much higher fraction of heavily absorbed sources in the AGN population than previously known (Tueller et al. 2008). Further study of these absorbed AGN should give us a much better understanding of the properties of the absorbing gas in accreting systems.

6.4 Origin of the soft excess

The soft X-ray spectra of AGN often show a marked rise in flux below about 1 keV, the so-called 'soft excess', relative to the downwards extrapolation of the higher energy spectrum (Arnaud et al. 1985; Turner and Pounds 1989). Such excesses are particularly prevalent in narrow-line Seyfert 1 galaxies (Boller et al. 1996). While AGN have a soft-band contribution from extended emission (binaries, hot gas and in Seyfert type 2 a few percent of scattered nuclear radiation), this is observed at a low flux level and typically comprises only a few percent of the soft-band flux: the soft excess discussed here is not dominated by those extended components.

Historically, the soft excess has often been fit using a black body model, yielding best-fit temperatures in the range 0.1–0.2 keV (Walter and Fink 1993; Czerny et al. 2003). Although the temperature of the soft excess is too high to be direct emission from the inner disk (unless photon trapping is invoked, see Abramowicz et al. 1988; Mineshige et al. 2000), it could represent Compton-scattered disk photons (e.g. Czerny and Elvis 1987). However, Gierliński and Done (2004) fit models representing a Compton-scattered disk component to a sample of AGN, finding a surprisingly narrow range of temperatures for sources covering such a large range ($10^6 - 10^8 \mathrm{M}_\odot$) in mass.

Grating data have clearly shown strong emission and absorption features in the soft X-ray spectra of most AGN, these arise in the warm absorber and other circumnuclear reprocessors in and out of the line-of-sight. As discussed by Gierliński and Done (2004), the imprint of strong spectral features such as O VII, VIII and the Fe M-shell unresolved transition array (UTA) in the 0.7 keV regime could affect the perceived shape of the soft excess. The problem with assigning an 'atomic interpretation' to explain the similarities of soft excesses across the Seyfert population is that some sections of the soft excess often appear smooth and certain predicted features are not evident. This led Gierliński and Done (2004) to consider the possibility of relativistic blurring of absorption features arising in a relativistic outflow, whose reduced opacity in the soft X-ray regime (owing to the high ionization of the gas) would then explain the spectral soft excesses. In the context of such a picture, Schurch and Done (2007, 2008) computed the X-ray spectra of columns of outflowing gas as functions of density and velocity, demonstrating that very high outflow velocities would be required if absorption in outflows are solely to explain soft excesses observed in AGN spectra. The high velocities at about 0.9 c exceed even the relativistic wind components detected through energy-shifted absorption lines, and Schurch et al. (2008) have found that models of line-driven accretion-disk winds do not attain sufficiently high velocities. Schurch and Done (2008) note that magnetic driving is likely the only acceleration mechanism that could achieve the high velocities required in this case, and that the wind itself would have to be clumpy, only partially covering the source.

Chevallier et al. (2006) assert that a blurred absorber would have to be in pressure equilibrium, otherwise the predicted spectral variability exhibited by a source and across a sample would be much larger than that observed. Done and Nayakshin (2007), however, have disagreed with this conclusion. A relativistically blurred absorber would have associated relativistically-blurred line emission, that might dominate in sources viewed from certain angles. Models composed of blurred emission lines from an ionized reflector have been invoked to explain some RGS spectra (Branduardi-Raymont et al. 2001), although that result was challenged by Lee et al. (2001) and Turner et al. (2003, 2004a) who find that the soft X-ray spectrum of MCG–6-30-15 may, instead, be influenced by the presence of a dusty warm absorber.

Interestingly, detailed analysis of Mrk 766 and MCG–6-30-15 found the soft excess in those cases to be satisfactorily accounted for by the combined opacity profile of several layers of unblurred absorption (Turner et al. 2007; Miller et al. 2008). It may be that a complex of ionized absorption may yet turn out to be the dominant cause of apparent 'soft excesses and that extreme velocities and other effects are not required to explain these sources (Nicastro et al. 1999), with only the extreme soft-excess AGN such as RE J1034+396 requiring an accretion disk contribution (e.g. Pounds et al. 1995).

Other attempts (Crummy et al. 2006) to explain the soft excess of AGN include modeling the broad X-ray spectra using blurred, ionized reflection models. As discussed by Sobolewska and Done (2007), a reflection origin strongly constrains the strength of the soft excess relative to the incident continuum and the observation of several extremely strong soft excesses would require anisotropy of the continuum or light-bending, such that the disk *consistently* sees more of the continuum radiation than the observer in those sources. In contrast, the absorption-based models fit the data without recourse to any radiation anisotropy. Taking an overview of models, Middleton et al. (2007) find that absorption-based models for the soft excess provide a clearer correspondence with black holes in the stellar mass class, compared to reflection models. Aside from the compelling nature of such an extrapolation, how might the issue be resolved? If the general lack of variability of the Fe-line 'red wing' is caused by light bending, one should expect a blurred reflection component of the soft excess to show similar non-variable behavior. More complete studies of the variability of the soft excess would then provide this critical test of the reflection hypothesis.

6.5 Variable narrow emission lines

While the evidence for a relativistically-broadened line is contentious, the existence of a narrow 'core' component of Fe emission is common among observed local AGN. The energy of this core component is generally consistent with 6.4 keV (Yaqoob and Padmanabhan 2004) implying an origin in low-ionization material. Line equivalent widths lie in the range a few tens of eV up to about 200 eV (e.g. Nandra et al. 1997; Sulentic et al. 1998; Reeves et al. 2002), allowing some constraints to be placed on the covering fraction of the emitting cloud (which must be high) and the optical depth of the emitting gas (Leahy and Creighton 1993). The observed widths of the narrow line 'core' components are typically a few thousand $\mathrm{km\,s^{-1}}$, consistent with previous suggestions of an origin in the BLR (Yaqoob et al. 2001; Kaspi et al. 2001; Yaqoob and Padmanabhan 2004; Bianchi et al. 2008) although some contribution from the material at large distances is likely (e.g. Reeves et al. 2007). A study by Nandra (2006) showed there to be no correlation between the width of the narrow Fe Kα emission component and either Hβ width or black hole mass; that result suggested significant contributions to the narrow line may arise from regions other than the optical BLR, including the outer parts of the accretion disk. A disk contribution to the narrow component had also been suggested from study of MCG–6-30-15 *Chandra* data (Lee et al. 2002).

Additional evidence for narrow lines originating in the accretion disk came from the observation of variations in the narrow Fe Kα line in Mrk 841 (Petrucci et al. 2002) and the discovery of narrow and rapidly (tens of ks) variable lines in NGC 3516 (Turner et al. 2002). In the case of NGC 3516 the lines appeared at energies redward of the neutral Fe Kα line and were fully separated in the data from the narrow line core at 6.4 keV; considerations of those line energies and strengths led to a conclusion that they were likely Doppler-shifted Fe lines, originating in the accretion disk or in an outflow, such as a disk wind (Turner et al. 2002, 2004b). Further examples of the phenomenon, dubbed 'transient Fe lines' soon came from observations of other AGN (e.g. Yaqoob et al. 2003; Guainazzi 2003; Longinotti et al. 2004).

The periodic pattern of line-energy/profile changes expected from a hotspot orbiting a black hole are very distinctive, so long as the emitting gas is not viewed too close to the polar axis (i.e. so long as there is a significant velocity component along the line-of-sight). The line evolution with azimuthal angle (around the disk) is particularly distinctive for lines originating within $20\,\mathrm{r_g}$ where general relativistic effects are measurable (Dovčiak et al. 2004; Czerny et al. 2004; Goosmann et al. 2007; Dovčiak et al. 2008). Lines originating in a wind would also suffer relativistic and Doppler effects related to motion along the sight-line, but these are different to the periodic energy shifts due to disk rotation. Both possibilities are interesting: confirmation of a disk origin would allow derivation of parameters such as the radius of emission and inclination of the system, confirmation of a wind origin might allow us to trace the velocity distribution of emitting knots to help determine launch radius, acceleration/deceleration mechanisms and mass loss rate. In principle, one could confirm a line origin using time-resolved spectroscopy with available instrumentation; in practice, sufficient signal has to be accumulated in distinct azimuthally selected slices to see the line energy evolution, without integrating so long that the azimuthal variations are averaged out. Few observations to date have had the combination of sufficient source brightness, hotspot radial location and observation duration to track line evolution in any useful way and so the origin of these features has been poorly tested. Iwasawa et al. (2004b) claim tentative evidence for periodic flux variability for a line in NGC 3516, although only viewing 3 cycles of repetition. Perhaps the most positive development in this area was the previously noted discovery of a line/continuum flux correlation in Mrk 766 (Miller et al. 2006) with associated changes in line energy (Turner et al. 2006). This flux correlation and peak-energy variability was discovered in data from a 500 ks *XMM-Newton* observation and would not have been significantly detected in a shorter observation.

Given the large number of claims of energy-shifted absorption and emission features now in the literature, Vaughan and Uttley (2008) have questioned the significance of the mass of results reported. Reviewing 38 published detections of features having energy shifts $v \geq 0.05$c, Vaughan and Uttley find a tight linear relationship between the estimated feature strength and its uncertainty, demonstrating that more accurate data tend to show weaker lines, whereas if these are true features then the stronger lines should show up in a well-defined way with improved signal-to-noise. The inference is that many of the reported detections are merely statistical fluctuations. However, a number of these features have been detected on multiple occasions in the same source, e.g. features in NGC 3516 show up repeatedly in the 5–6 keV band (Turner et al. 2002; Bianchi et al. 2004; Dovčiak et al. 2004; Iwasawa et al. 2004b) and others have been assessed using Monte Carlo simulations (e.g. Yaqoob and Serlemitsos 2005). Further long observations of AGN detecting characteristic changes in line energy or flux with time, coupled with a rigorous statistical analysis, are required to settle the issue.

7 Summary of status and a review of model-space

That the X-ray spectra of AGN show marked curvature in the 2–8 keV regime is now well-established and in itself, no longer controversial (e.g. Nandra et al. 2007), although the interpretation of this curvature is still not agreed upon. Taking the ensemble of results both from sample studies and across the literature, summarized above, it appears that models dominated either by blurred reflection or by complex absorption provide statistically-comparable fits to the *mean* X-ray spectra of most AGN. We now summarize the points for and against the hypotheses that one or other process dominates, before discussing more general models, arguably more realistic, in section 8.

In the following section we concentrate on "reprocessing" origins for spectral signatures. It should be born in mind however that we still have no established model for the continuum production, and that process itself may imprint spectral signatures and spectral variability on the observed spectra. In particular the corona-plus-disk emission models of Haardt and Maraschi (1991, 1993) suppose a coupling between photons from the accretion disk and the hot Comptonizing corona, acting as the primary cooling source, and between the Comptonized photons and the accretion disk, acting as a heating source. In this picture, the illuminating spectrum should not be considered as being a component independent of the reflection or absorption arising from cooler material in the accretion disk.

7.1 Blurred reflection

The approach of many teams to modeling the curvature observed over the 2–8 keV band is to use blurred reflection models obtained by convolving reflection spectra from Ross and Fabian (2005) with the effects of emission from a rotating disk deep in a black hole's potential well (c.f. Laor 1991). First, any obvious absorbing gas is isolated by measurement of narrow features in grating data (e.g. Wilms et al. 2001). The absorbing gas is thus parameterized and model components or tables included in the fit to allow for that; it is common to then assume a power-law continuum and blurred reflector to model the rest of the spectrum. We assess the motivation for and implications of modeling using this approach.

7.1.1 Motivation

One of the compelling aspects of blurred reflection models is that the signatures from material within a few tens of gravitational radii might reasonably be expected to be produced in AGN at a level that could be measured with existing instrumentation. If the X-ray continuum is produced on size-scales of a few $\mathrm{r_g}$ then for certain disk geometries one would expect to see significant reflection component contributions from within $20\,\mathrm{r_g}$ and these should show measurable general relativistic effects. However, the integrated spectrum from disk reflection depends on the illumination pattern across the accretion disk and thus depends on the size, geometry and location of the continuum source and the structure and ionization of the accretion disk.

7.1.2 Continuum size

Production of the X-ray continuum over an extended corona would not result in disk reflection that was strongly weighted towards small radii and consequently one would not expect to observe significant blurring in the integrated disk reflection spectrum. The size of the X-ray continuum source is therefore a key issue in predicting the integrated reflection spectrum and assessing the consistency of the data with that prediction. One intriguing and potentially strong constraint is the result of observations of X-ray variability in gravitationally lensed images of quasar RXJ 1131-1231, which, if interpreted as due to micro-lensing variations suggests the continuum region to have half-light radius $\lesssim 6\mathrm{r_g}$ (Chartas et al. 2008).

The case has long been made that the rapid variability observed in X-ray light curves of AGN demonstrates, from arguments based upon light-crossing timescales, that the X-ray emitter must be very compact (Rees 1977): variations observed with current missions would suggest the size to be on the order of a thousand light seconds across. It is now unclear however, whether such rapid variability should be interpreted in terms of absorption variations. For example, constraints on the continuum source size have estimated the region to be a few $\mathrm{r_g}$ in extent based on what appear to be (de-)occultation events in AGN (e.g. NGC 1365 Risaliti et al. 2007). Whichever way one views the data, there are reasons to think the illumination of the disk might indeed be centrally concentrated and thus that there could be significant reflection within $20\,\mathrm{r_g}$ if the accretion disk also extends that close to the black hole.

7.1.3 Disk parameters

The most recent systematic study of local AGN was that of Nandra et al. (2007) based on available *XMM-Newton* data. It was concluded that a large fraction of local AGN show emission that appeared best-fitted with a blurred reflection model, but with a large dispersion in the characteristic radius of emission. However, the study did not allow the X-ray absorbers to have covering fractions less than unity when absorption models were tested, nor was it able to test models against the spectral variability of AGN. Once covering fraction is allowed as a free parameter then absorption-based models are also acceptable fits to the time-averaged X-ray spectra of AGN (e.g. Mrk 766, c.f. Nandra et al. 2007, Miller et al. 2007; Turner et al. 2007).

7.1.4 Variability

Perhaps the biggest problem for the blurred-reflection-dominated picture is the lack of any simple correlation observed between continuum and reflection. Light bending models rely on the continuum flux being intrinsically steady and then explain the observed phenomena by invoking changes in the height of the continuum source above the disk, opponents of this picture argue that such variation in continuum placement is *ad hoc* and might require fine-tuning if it is observed that there is universally no line-continuum correlation in samples of AGN. Some other models seek to explain the observed constancy of the red wing (e.g. Merloni et al. 2006; Nayakshin and Kazanas 2002; Życki 2004) but these may have difficulty reproducing the high apparent R values observed above 10 keV.

7.1.5 Strength of the reflection component

Analysis of AGN over the broad bandpass afforded by *Suzaku* has shown that some individual sources have very hard spectra indicating nominal solid angles much greater than 2π for blurred reflection (Section 6.3). High geometrical factors may be feasible if the disk has a deep funnel or other favorable inner geometry, but as always, the strength of the reflected spectrum depends critically on the surface illumination pattern, illumination angle and viewing angle. Another possibility for producing a high observed R value is that the illuminating continuum is partly hidden from direct view and so what we see is only the Thomson-scattered radiation (i.e. the reflector sees some continuum that is hidden from the observer, such that the observed ratio of continuum to reflection is not directly interpretable). Some hard excesses are sufficiently extreme that model fitting disfavors reflection with all reasonable modifications (1H 0419–577, Turner et al. 2009; PDS 456, Reeves et al 2009, submitted).

7.1.6 The question of spin

In principle, if one has a clean view of the reflection spectrum then the extent of the 'red wing' could constrain the inner radius of the emission and thus the black hole spin: if it is found that emission from radii $r < 6\,\mathrm{r_g}$ is required in the reflection model then one may interpret the data as favoring an innermost stable circular orbit $r_{\mathrm{ISCO}} < 6\,\mathrm{r_g}$ and thus indicative of a Kerr metric. Claims for detection of black hole spin have been made in MCG–6-30-15 and IRAS 18325–5926 (Iwasawa et al. 2004a) where curvature is evident down to $\sim 2\,\mathrm{keV}$. With the uncertainty and debate on the physical processes that dominate the X-ray spectrum in this energy range (e.g. Miller et al. 2008), in the view of these authors it is not currently possible to constrain the black hole spin in a model-independent way.

7.2 Absorption

An alternative view is that spectral signatures from complex absorption dominate the X-ray spectra and may explain the spectral variability of AGN.

7.2.1 Motivation

High-resolution UV spectroscopy shows that multi-layered, complex absorbers are common in AGN comprising low-column, low-ionization systems, often showing several kinematic components (Crenshaw et al. 2003). The highest ionization UV emission lines in high accretion-rate objects show systematic asymmetry (e.g. Gaskell 1982; Richards et al. 2002) supporting a disk wind origin for the UV absorbers (Murray and Chiang 1998) and by extension, possibly supporting a wind origin for the X-ray gas. Theoretically, we should not be surprised to find winds being driven off accretion disks (King and Pounds 2003) and as it appears likely such winds would extend to relatively close to the black hole (e.g. Proga et al. 2000), this motivates a consideration of X-ray spectra in terms of absorption-dominated models. Indeed, X-ray spectroscopy directly detects absorption signatures indicative of an origin in a disk wind, as we now discuss.

7.2.2 Parameter space for the X-ray absorbers

X-ray observations show that absorbing gas exists over higher column densities, and ionization-states than are measured in the UV band. Most local type 1 AGN show numerous narrow absorption lines in the soft X-ray regime where the effective area and spectral resolution of various X-ray grating instruments are relatively high, and detected zones cover the full range of ionization state to which observations are sensitive (Blustin et al. 2005; McKernan et al. 2007; Blustin et al. 2007, and references therein).

Details of the zones of absorbing gas, especially for $N_H \lesssim 10^{23} cm^{-2}$ are confirmed from grating observations of absorption lines. At the low-ionization end, outflow velocities are typically in the range 100–2000 $km\,s^{-1}$ (these are usually consistent with having turbulent velocities of a similar order) and zones with $\log \xi < 0$ are commonly found (e.g. Kaastra et al. 2000; Kaspi et al. 2002; Netzer et al. 2003; Crenshaw et al. 2003). Spectral modeling to date has assumed the gas zones to be discrete, but a more realistic picture may be that there is a wide range of ionization across a large-scale outflow, with possibly multi-phase components present. Some of the higher columns to date have been inferred from broad-band fits, as the opacity tends to be too high to be able to detect discrete lines in soft-band grating observations. An exception is the highest ionization zones that have $\log \xi \gtrsim 3$, evident only from their telltale absorption lines from Fe XXV and Fe XXVI; these lines have equivalent widths of many tens of eV and those observed to date likely arise from gas in the range $10^{23} - 5 \times 10^{24}\,cm^{-2}$ (e.g Turner et al. 2007, 2008) with outflow velocities ranging from several thousands of km s^{-1} up to relativistic flows. In many cases leakage of flux towards low energies is a strong indication that at least some absorbing zones only partially cover the source, with covering fractions suggested to be anything from a few tens of percent to a full shell of gas. An unambiguous signature of partial covering absorption would be the detection of saturated line profiles that have non-zero flux in the line core, as in UV spectroscopy of AGN: unfortunately, as many of the X-ray absorption lines are not resolved even in grating data, line profiles cannot yet be used in this way.

Spectral variability in type 1 AGN is consistent with variations in covering fraction of the gas. Detections of sources partially covered by gas at the high end of this column density range may prove key to settling the absorption/reflection debate (e.g. as in 1H 0419–577, Turner et al. 2009). Of course, absorbers that are Compton-thick lead to an expectation of some accompanying reflection from the same gas. As previously discussed, the level of accompanying reflection or re-emission from the gas depends critically on ionization-state and gas geometry.

7.2.3 Reasonableness of partial covering as a concept

In absorption models the covering fractions found for key gas zones often come out $\lesssim 1$ and variations of tens of percent (with mean values often about 50%) may be used to explain observed spectral variability (e.g. Reeves et al. 2002, 2003; Miller et al. 2007; Turner et al. 2007).

The most common argument against partial-covering models is one based upon probability. The key point is that for an absorber to have some (possibly varying) covering fraction $\lesssim 1$ it should contain structure on the same scale as the source it is obscuring. If that structure arises because the absorber is composed of discrete clouds of some size, then we should expect that size to be comparable to the source size. Then, if the absorbing clouds are distant from the source, there is some implied coincidence between the source and absorber sizes, and furthermore to have a reasonable chance of seeing a partial-covering absorption event there must be many such clouds distributed across the region. Alternatively, the clouds might exist at radii comparable to that of the source.

A more likely scenario, however, is that the X-ray absorber exists as part of a clumpy disk wind or as part of the broad-line region. In this case we would expect it to comprise a wide range of scale sizes, perhaps with some power-spectrum of fluctuations as expected for turbulent fluids, rather than being in the form of discrete clouds of some fixed size. Such distributions of clumpy absorbers are apparent in disk wind models (e.g. Proga et al. 2008). If the X-ray absorption is in the form of a wind then the argument about probability is not so relevant, an equatorial disk wind has a preferred plane and the incidence of observation of rapidly varying partial-covering absorption depends on viewing angle to the accretion disk.

A test of the reasonableness of absorption models may be possible by comparing emission-line strengths with those expected from the absorbing gas (Section 2.3). For non-resonantly-scattered lines this may lead to an estimate of the fraction of the sky subtended by the wind as seen from the source: if that fraction turns out to be extremely small that might argue against the absorption model, or if it turns out to be some intermediate value that may instead allow some estimate of wind geometry to be made. If the ionization of the absorbing gas is sufficiently high that the emission-line in question would be resonantly scattered, the problem becomes much more difficult (Section 2.3). We emphasize that the *absorber* model parameters should be used to determine whether the material is sufficiently ionized that a line could be resonantly scattered. A line observed in emission from apparently low ionization material may simply originate in a different location.

In model fits, partial-covering models are indistinguishable from ‘Thomson scattering’ models: i.e. a source that appears to be partially covered cannot be distinguished from one where we are viewing a fully covered, absorbed continuum source plus some fraction of continuum that has been scattered energy-independently, and this may provide an alternative explanation for the spectra of some sources.

7.2.4 Variability

If absorption changes do produce the observed spectral variability they must also produce variability in the observed broad-band X-ray flux. The profiles of flux changes during AGN deep dips (Section 6.1) may support this possibility. In this case, even if the continuum source is constant, we would expect to observe large amplitude and rapid X-ray variability in type 1 AGN and this must be accounted for when interpreting the detailed characteristics of X-ray variations. It is not yet clear whether **all** of the observed fluctuations are an artifact of such absorber variations.

A corollary of the above is that if the variations in spectral shape are explained as arising from partial-covering changes, then the observation of systematic spectral flattening as a source dims implies that the observed flux variations in such AGN are dominated by the variable absorption and not by intrinsic continuum variations, as these would not result in a correlation between brightness and spectral shape.

7.2.5 Location and geometry of the gas

The distance of the absorbers from the ionizing source may be estimated from the value of ionization parameter ξ obtained from model fits to spectra. Since $\xi = L/r^2 n$ (section 2.2), then provided we can obtain estimates for the other quantities we may make an estimate of the location of the absorber, r. For an absorber of any substantial opacity, ξ varies through the material and it is usual to assume that the absorber has a discrete inner face, and to define r as being the distance of the inner face from the ionizing source and ξ the value of ionization parameter at that face. The ionizing luminosity is usually fairly well constrained by the knowledge of X-ray flux, power-law photon index Γ and source cosmological redshift, although assumptions have to be made both about the form of the continuum (e.g. power-law) and its extrapolation outside the observed energy range. The largest uncertainty arises from lack of information about the gas density n, so estimates of distance based on this method should always be parameterized in terms of the unknown density (e.g. Turner et al. 2008). A plausibility argument can be used to choose a range for the most likely value of density and distance: for example the constraint $\Delta r \simeq \mathrm{N_H}/n \lesssim r$ might be applied in the case where the depth through the absorber is thought to be smaller than the distance of the absorber from the central source and this would then yield an approximate lower bound on n and a corresponding approximate upper bound on $r \lesssim L/\xi \mathrm{N_H}$.

Analysts should also be aware of the degeneracies in model fits between column density $\mathrm{N_H}$, ξ and n. For example, for a given column density, an absorber with low n must be proportionally larger along the line-of-sight than one with high n. In that case there may be substantial inverse-square-law dilution of the radiation field through the gas, if the required source depth is comparable to the distance from the source, so that at the outer face ξ may be much lower than in a higher-density, smaller-depth, model. This condition arises for $\mathrm{N_H}/n \gtrsim \sqrt{L/n\xi}$ or $n \lesssim {\mathrm{N_H}}^2 \xi/L$. In this case the mean ξ though the material would be lower than in a high-density model, and a given dataset thus tends to be best-fit by a degenerate family of models in which ξ is anti-correlated with n. Appropriate choices of ionizing luminosity and density need to be made when calculating the expected opacity with code such as XSTAR. Even then, such code assumes the absorber to have invariant density, whereas this is unlikely to be true in practice: for example, in a steady wind, density may fall off inversely as distance-squared, canceling out in the value of ξ the inverse-square-law fall-off in the illuminating radiation. These considerations should always be born in mind when assessing model choice.

Based on such estimates, some Compton-thick partial-covering absorbers appear to lie within the BLR (e.g. Turner et al 2009) while lower column gas generally appears to exist outside the BLR (Blustin et al. 2005), possibly associated with the dusty torus. Other estimates of the location of the gas come from observation of column variations that imply origins typically on the inner edge of the BLR (e.g. Puccetti et al. 2004). However, taking an overview of the recent observational findings for this class of source it appears that the inferred absorption arguably should be considered in the context of outflow models rather than orbiting clouds and therefore we do not review discussions in the literature based upon the latter.

Mass flow rates can be estimated from an assumed volume filling factor, measured velocity and the fitted gas parameters. In a review of soft-band absorbers, Blustin et al. (2005) found that for a sample of local AGN the median mass outflow rate was about $0.3\,\mathrm{M_\odot\,yr^{-1}}$ compared to a median mass accretion rate approximately an order of magnitude lower at about $0.04\,\mathrm{M}_{\odot}\,\mathrm{yr}^{-1}$: other studies suggest the outflow and accretion rates may be comparable (Chelouche and Netzer 2005; McKernan et al. 2007). The kinetic luminosity in those flows was unimportant compared to the bolometric luminosity. As yet there are too few tightly constrained results from the high-velocity gas zones to draw many global conclusions. However, a recent analysis of PG 1211+143 (Pounds and Reeves 2008) found a P Cygni signature of high-velocity gas that implied an outflow with solid angle around π steradians. The constraint on global covering allowed Pounds and Reeves (2008) to estimate the outflow energetics and to conclude that this zone of gas makes an energetically significant contribution to feedback to the host galaxy.

8 Towards a complete picture of AGN X-ray emission

Whatever the origin of spectral curvature around 6 keV, AGN carry unambiguous evidence, from grating data, for absorption covering a wide range of column, ionization-state and radial locations. When absorption models are considered to explain the observed systematic spectral and flux variability then the parameters implied for the gas suggest the material includes clumps of high column density with low covering fraction, that indicate that it would be a misleading oversimplification to continue to think in terms of individual single clouds. The most natural gas geometry is likely an equatorial disk wind.

Physically, we should expect that a black hole accreting at close to the Eddington limit should generate significant outflows, and it seems likely that such an accretion disk would have an atmosphere and that the atmosphere would be outflowing. The column densities required to significantly affect the observed X-ray spectra are not extreme compared with theoretical expectation: estimates by King and Pounds (2003) indicate that sources with a high Eddington ratio would be expected to have Compton-thick winds outflowing at high velocity. Early wind models for supercritical AGN had also suggested the winds would be optically thick in the central regions and that the continuum source would be hidden from direct observation (Camenzind and Courvoisier 1983). In many ways then, it is more incumbent upon modelers to justify why absorption can be ignored in model fits rather than to justify why absorption should be included.

Whether variable absorption can explain the full range of X-ray spectral variability is more contentious, although SWIFT observations of the brightest nearby AGN show that the X-ray emission from AGN is more variable in those that are more absorbed (Beckmann et al. 2007), implying that opacity variations play a significant role in source variability. It has been found that a model of variable partial covering for the variable X-ray spectrum of MCG–6-30-15 can explain the spectral shape, including red wing and hard X-ray excess without requiring any inner disk reflection (Miller et al. 2008). The model seems to require an anti-correlation between illuminating luminosity and covering fraction, although the model fits are not unique and other possible solutions exist. If a systematic dependence between covering fraction and luminosity is confirmed, this may point to a picture in which the continuum source changes in size systematically with luminosity, appearing and disappearing behind an absorption structure such as a clumpy disk wind or atmosphere. Changes in source size have previously been discussed in the context of models of coronal plus disk emission (e.g. Haardt et al. 1997).

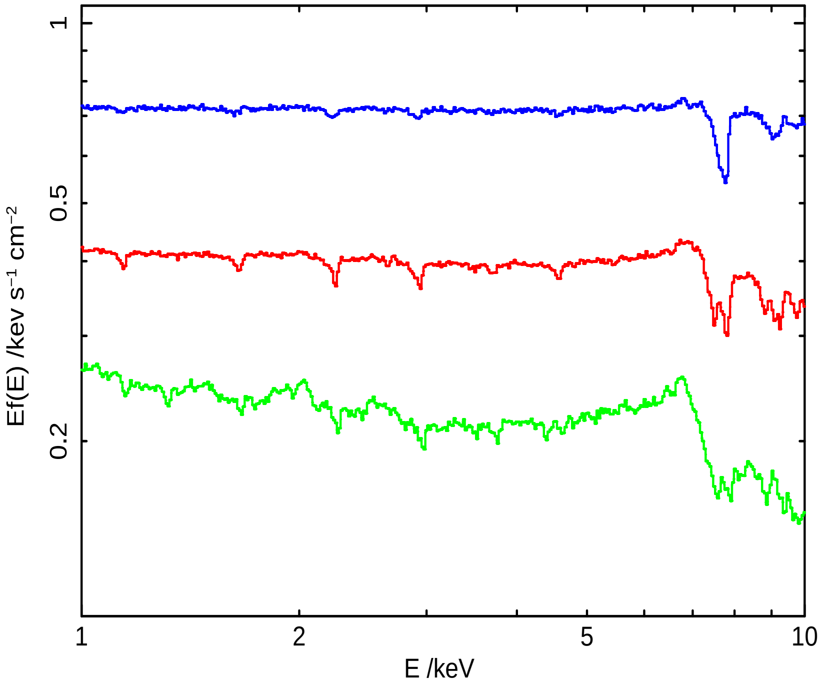

Fig. 7 Sample spectra computed for a viewing angle 60° from the polar axis for the equatorial smooth wind models of Sim et al. (2008). System parameters are chosen to be appropriate for the case of Mrk 766 with a wind originating at radius $100\,\mathrm{r_g}$ (see Sim et al. 2008). The wind opening half angle in this case is 45°. From top to bottom are shown mass flow rates of 0.1, 0.3 and $1.0\,\mathrm{M_{\odot} yr^{-1}}$. The plotted spectra are all normalized to the input primary power-law spectrum with photon index $\mathit{\Gamma} = 2$.

In spectral fitting and in the above discussion, attempts to describe complex AGN X-ray spectra, beyond simple power-law models, have tended to be classed as either "absorption-dominated", in which case a radiative transfer code such as XSTAR (Kallman and Bautista 2001; Kallman et al. 2004) is used to model a foreground absorber, or else as "reflection-dominated", where the dominant spectral signatures are assumed to arise from a slab-like reflecting surface modeled by e.g. REFLION (Ross and Fabian 2005). In practice it is likely that *both* absorption and reflection occur naturally, and in fact that both processes may arise simultaneously in a clumpy wind from an accretion disk. Such an environment is much more difficult to model because the distribution of absorbing/reflecting gas is completely unknown, but recent modelers have attempted to predict the X-ray spectra of these more complex scenarios in order to make a comparison with observation. Schurch and Done (2007) and Schurch et al. (2008) have modeled the absorption component expected from a disk wind by taking shells of XSTAR-modeled absorbing zones (noting that XSTAR is strictly a 1D radial calculation of absorption in an assumed spherically symmetric absorber and that it neglects scattering). Schurch et al. (2008) have shown how even this simple approach, when applied to the disk wind simulations of Proga and Kallman (2004), can yield complex spectra that carry many features that are observed in actual AGN. Sim et al. (2008) have used a

Monte Carlo method to calculate disk wind spectra, so far for simple wind geometries, but making a more complete treatment of the radiative transfer that includes the effects of scattering/reflection as well as absorption. Their initial treatment was limited to highly ionized material and to consideration of K shell ions, but further work is extending the models to lower charge states and to more complex wind geometries. The wind spectra produced by Schurch et al. (2008) and Sim et al. (2008) naturally explain the energy-shifted absorption lines observed in recent X-ray spectra, and Sim et al. (2008) also show that electron scattering, line scattering and recombination contribute to a significant emission of Fe Kα with a pronounced red wing, which may provide another possible explanation of the common observational signatures in AGN spectra. Earlier work on outflows by Titarchuk et al. (2003) had also shown that significant line broadening would occur from Thomson scattering in outflows around black hole systems and that this scattering can produce broad features that match the observed data around 6 keV. Such scattering effects are difficult to separate from strong relativistic effects in current data.

9 Future prospects

In the crucial energy range covering the Fe K-shell spectral features, current X-ray data offer either high throughput with modest spectral resolution, e.g. the CCDs of *XMM-Newton* and *Suzaku* with energy resolution FWHM $\simeq$ 130 eV at 6 keV, or improved spectral resolution with low effective area, e.g. *Chandra* HEG having energy resolution FWHM $\simeq$ 40 eV at 6 keV. These data limitations have made it difficult to distinguish between absorption and reflection models for the curvature around 6 keV. Successful flight of an X-ray calorimeter should resolve the issue. The calorimeter design is currently being improved compared to that used for the previous attempts with the *ASTRO-E* XRS-1 and *Suzaku* XRS-2 calorimeters. The spectral resolution now achievable with calorimeters is FWHM $\simeq$ 7 eV, but resolution FWHM $\simeq$ 4 eV is projected for the calorimeters that should fly aboard *ASTRO-H* and FWHM $\simeq$ 2.5 eV for those on the *International X-ray Observatory* (*IXO*).

ASTRO-H is planned for a launch around 2013 and, in addition to the calorimeter, it will carry the first imaging hard-X-ray detector contributing to a total bandpass covering 0.3–600 keV. Closely following *ASTRO-H* will be the *Simbol-X* mission, jointly supported by the French (CNES) and Italian (ASI) space agencies and having a target launch date of 2014. *Simbol-X* will provide X-ray imaging up to 80 keV with approximately two orders of magnitude improvement in sensitivity compared to the non-focusing instruments that have operated above 10 keV so far. *ASTRO-H* and *Simbol-X* will yield a wealth of valuable new information on Compton-thick absorbed systems in AGN. *IXO* will be a collaborative mission involving ESA, JAXA and NASA, and is planned to be launched sometime beyond 2018. In addition to the calorimeter, *IXO* will carry a wide field imager and a X-ray grating spectrometer dispersed onto CCDs. Possible additional instruments for *IXO* include an X-ray polarimeter, a hard-band instrument or a high-resolution timing instrument. The effective area of *IXO* is currently planned to be 10,000 cm^2 at 6 keV and thus *IXO* is poised to offer a factor of 20 improvement over the best effective area offered by current CCD instruments, and the same factor improvement over the best resolution available (at 6 keV). The scientific return however should be even greater than these numbers indicate because the high throughput and resolution will be available together. With the likely combination

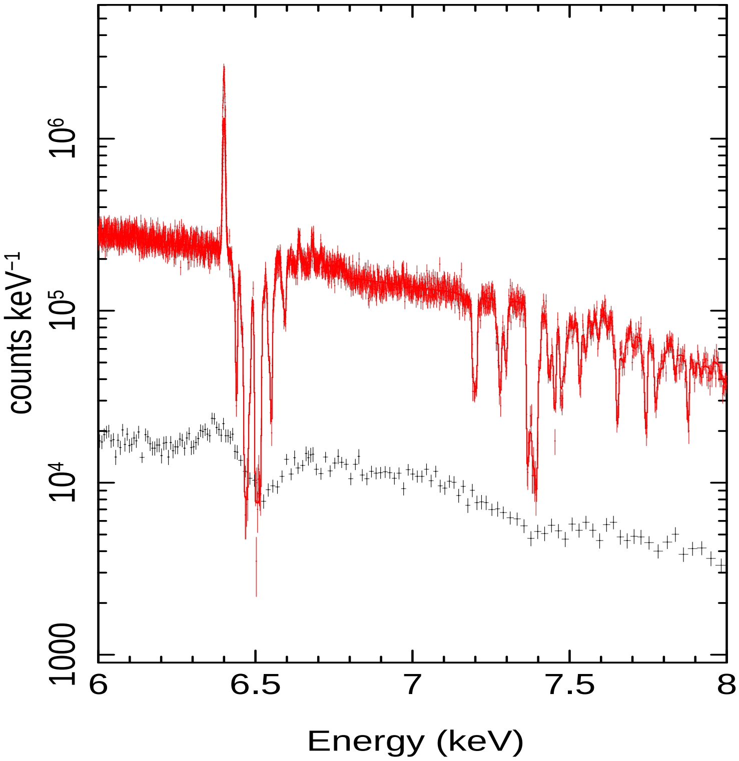

Fig. 8 A comparison of a model AGN spectrum as would be viewed by IXO (red) and *Suzaku* XIS0 plus XIS3 CCDs (black). Both spectra represent a 100 ks exposure on a source of flux $F_{2-10\mathrm{keV}} = 2.5 \times 10^{-11}\mathrm{erg\,cm^{-2}\,s^{-1}}$ having a power-law with photon index $\Gamma = 2$ viewed through an absorbing column with $\mathrm{N_H} = 5 \times 10^{23}\mathrm{cm^{-2}}$ and $\log \xi = 2.75$. The line emission is shown from the absorbing gas plus an additional Fe Kα emission line from neutral material with equivalent width 100 eV and line width $\sigma = 3$ eV. The simulation includes no velocity shift for either emitter or absorber.

of calorimeter and high throughput, *IXO* observation exposures of 10 ks would be sufficient to detect key diagnostic features such as the Fe Kβ UTA in bright Seyfert galaxies; this complex is predicted based on some absorption models for particular AGN but is not detectable with current instruments (e.g. Miller et al. 2008). Thus calorimeter observations with reasonable exposure times would offer the possibility of resolving the origin of the curvature around 6 keV by isolating weak absorption features so that we can build up a clearer picture of the nuclear regions. Figure 8 shows an example of how clearly spectral structure would be measured by a future calorimeter compared to data obtained for the same intrinsic spectrum and exposure time with *Suzaku* CCDs.

Another area of current interest are the rapidly variable narrow lines: the rapid variability in energy observed for these energy-shifted features means that one cannot simply make a long integration and obtain a stronger detection. Tracking the line changes for a sufficiently long time however, would allow the pattern of changes in these weak lines to be compared with predictions from hotspot and wind models and compared to random noise fluctuations. Changes in the flux and spectrum above 10 keV,

Table 1 Flux (2–10 keV) and orbital timescale at 10 r_g for the Tartarus database sample of bright AGN.

Target	2-10 keV flux $/10^{-11}$ erg s^{-1} cm^{-2}	T_{orb} /ks
IC 4329A[a]	7.0	1.0
MCG-6-30-15[b]	4.0	2.0
NGC 4051 [a]	2.0	2.0
NGC 5506[c]	7.0	2.0
Mrk 766[d]	2.0	4.0
Mrk 335[e]	1.0	5.1
NGC 7314[f]	4.0	5.1
NGC 7469[e]	3.2	7.1
NGC 4593[e]	4.5	8.1
NGC 4151[a]	10.0	13.2
MCG+8-11-11[g]	2.3	15.2
NGC 3516[e]	5.0	23.3
NGC 3783[a]	7.0	29.3
NGC 3227[e]	2.8	44.5
NGC 2992[e]	0.4	52.6
MCG–5-23-16[g]	9.0	70.8
Mrk 509[e]	6.6	72.9
Fairall 9[e]	2.5	82.0
MR 2251-178[h]	5.0	99.2
NGC 7213[e]	3.0	99.2
Mrk 841[e]	1.0	101.2
NGC 5548[e]	5.0	111.3
Arp 102B[i]	1.1	141.7
NGC 2110[e]	3.5	202.4
MCG–2-58-22[g]	3.3	354.2

[a] Peterson et al. (2004)
[b] Wang et al. (2004)
[c] Bianchi et al. (2003)
[d] Wandel (2002)
[e] Woo and Urry (2002)
[f] Padovani and Rafanelli (1988)
[g] Bian and Zhao (2003)
[h] Morales and Fabian (2002)
[i] Wu and Liu (2004)

where the reflection continuum excess peaks, are expected to be associated with line signatures having a disk hotspot origin. Clearly, a hard-band detector would be invaluable for use in conjunction with a calorimeter. We should be able to confirm the line origin using time-resolved spectroscopy with *IXO*, because we could accumulate sufficient photons in azimuthal samples round the disk orbit to see what patterns emerge; we are currently limited to integrating much longer than the likely timescales of interest to obtain sufficient photons for spectral analysis.

Considering the case where lines are observed from hotspots orbiting the black hole, the Keplerian orbital time varies with the mass of the central black hole as $t_{orb} \simeq (r/9\mathrm{r_g})^{3/2}\,\mathrm{M_8}$ days, where $\mathrm{M_8}$ is the central mass in units $10^8\,\mathrm{M_\odot}$. At $r = 10\,\mathrm{r_g}$ the orbital timescale is just 1000 s for an AGN with a non-rotating (Schwarzschild metric) $10^6\,\mathrm{M_\odot}$ black hole, rising to 100 ks for a source with a $10^8\,\mathrm{M_\odot}$ black hole; even for the latter case the timescale is approximately equal to the integration time required to detect the weak features of interest in an AGN spectrum. While there have been indications of line profile evolution matching that expected from an orbiting hotspot in a few tantalizing cases (Longinotti et al. 2004; Turner et al. 2006) observational progress has been very limited. The detect-ability of hotspot lines is a function of both the orbital timescale (and therefore black hole mass) and the source flux, as both quantities determine the accumulated photons in time-selected spectral bins that would reveal detectable profile evolution.

To track the evolution in line profile at $10\mathrm{r_g}$ one might wish to take a minimum of four spectral samples around the disk orbit. Figure 9 shows the signal-to-noise that would be obtained in an IXO exposure corresponding to one quarter of a disk orbit, as a function of black hole mass. For the simulation, a simple line was used to represent a sample of the profile falling on the red side of the rest energy, with the integration azimuthal section giving a line energy of 5.5 keV. The line was conservatively taken to have an equivalent width of 30 eV, and a width $\sigma = 30\,\mathrm{eV}$. The simulation assumed an effective area of $9000\,\mathrm{cm}^2$ at 5.5 keV for IXO. Points on the figure represent the same line seen at $10\mathrm{r_g}$ in different sources comprising a sample of bright AGN (Table 1), those with flux in the 2–10 keV band greater than $5 \times 10^{-11}\,\mathrm{erg\,s^{-1}\,cm^{-2}}$ in the Tartarus[4] compilation of AGN (having systematically reduced and fit *ASCA* spectral results). It can be seen that many sources have timescales at $10\,\mathrm{r_g}$ in the range of a few tens of ks, ideal for study with *IXO*. The plot can be used to assess potential observations using *ASTRO-H* if the values are scaled appropriately using the ratio of the effective areas. As noted previously, details of the line variability should yield key system parameters such as emitting radius and system inclination in the case of a hotspot origin; launch radius, acceleration/deceleration mechanism and mass loss rate if a wind origin were confirmed.

10 Conclusions

Almost a decade of grating data from *Chandra* and *XMM-Newton* has helped shape our understanding of the circumnuclear environments in AGN. The warm absorber generally appears as a multi-layered gas complex spanning a range of ionization parameter. It is likely that this absorption is largely responsible for the soft excesses seen in many AGN X-ray spectra and must be taken into account when fitting models to spectra. Higher columns of gas are also detected: data from *XMM-Newton* CCDs, the *Chandra* HEG and the *Suzaku* XIS have recently revealed K-shell absorption lines from Fe XXV and Fe XXVI ions in a number of AGN, tracing near Compton-thick gas. In a number of AGN, such gas appears outflowing with velocities from hundreds of $\mathrm{km\,s^{-1}}$ to $\sim 0.3\,\mathrm{c}$. It is expected that disk winds develop in high Eddington-ratio AGN, and such a phenomenon would be consistent with the asymmetric UV emission lines seen in AGN. The most recent observations at energies above 10 keV also indicate the presence of high column densities of gas that partially cover the source and provide a natural explanation for the hard-band excesses that are often observed. Partial-covering by additional gas lying within the known range of column and ionization can explain observed X-ray spectral curvature and variability at lower energies, 2–8 keV. The key layers associated with such partial-covering solutions have not yet been unambiguously identified via narrow spectral features . However, occultation and de-occultation events also indicate the importance of dynamically variable absorbers. It now seems highly

---

[4] http://tartarus.gsfc.nasa.gov/

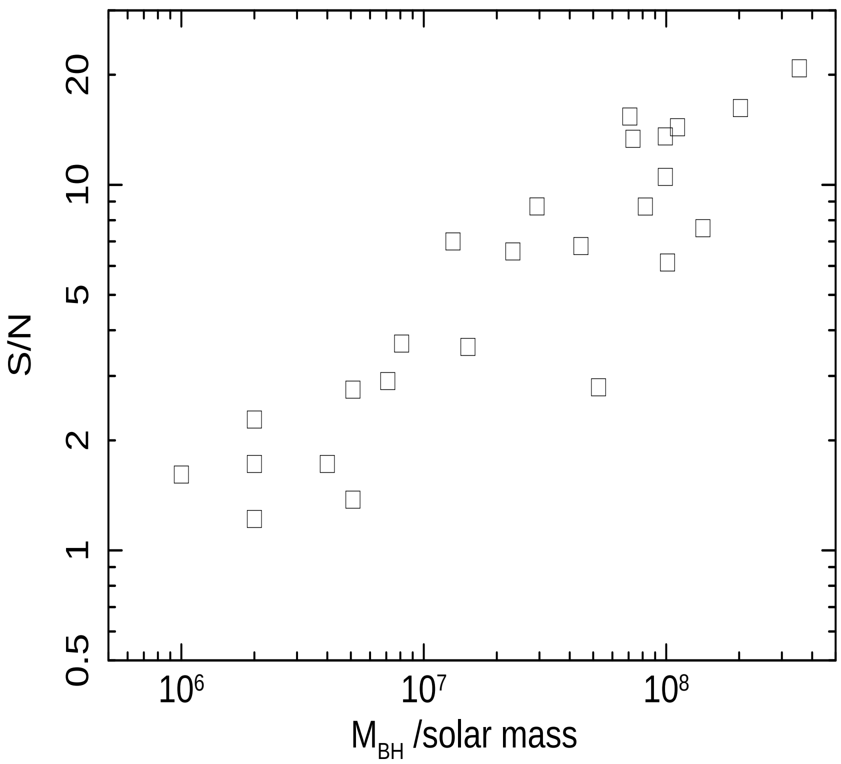

Fig. 9 The signal-to-noise that would be obtained for a line detection in one azimuthal portion, covering a 90 degree section of an orbit, at emitting radius $10\,r_g$ plotted against the black hole mass for a number of bright AGN. Each plotted point represents a source listed in Table 1.

likely that, rather than having a direct view of a "naked" accretion disk dominated by a power-law continuum plus disk reflected emission, the view to the central regions is in fact complex, with absorption covering a wide range of densities, ionization and dynamics, likely coupled with reflection from material over a wide range of radii. With the recognition of the greater complexity of AGN X-ray spectra, the inference of black hole spin from model fits is seen to be difficult with the current generation of data. However, there is much to learn about the accretion process from studying the complex inner regions at radii $\lesssim 100\,r_g$. New models are currently being developed to study the radiative transfer through disk winds and new high resolution data, and imaging data in the hard X-ray band, should provide crucial new insights in the coming decade.

Acknowledgements The authors thank Stuart Sim, Ian George, Tahir Yaqoob and James Reeves for comments that significantly improved this manuscript. TJT acknowledges NASA grant NNX08AJ41G. LM acknowledges STFC grant number PP/E001114/1.

References

1. Abramowicz MA, Czerny B, Lasota JP, Szuszkiewicz E (1988) Slim accretion disks.

ApJ332:646–658, DOI 10.1086/166683

2. Abramowicz MA, Chen X, Kato S, Lasota JP, Regev O (1995) Thermal equilibria of accretion disks. ApJ438:L37–L39, DOI 10.1086/187709, `arXiv:astro-ph/9409018`
3. Abrassart A, Czerny B (2000) Toy model of obscurational variability in active galactic nuclei. A&A356:475–489, `arXiv:astro-ph/0001515`
4. Antonucci R (1993) Unified models for active galactic nuclei and quasars. ARA&A31:473–521, DOI 10.1146/annurev.aa.31.090193.002353
5. Arnaud KA (1996) XSPEC: The First Ten Years. In: Jacoby GH, Barnes J (eds) Astronomical Data Analysis Software and Systems V, Astronomical Society of the Pacific Conference Series, vol 101, pp 17–+
6. Arnaud KA, Branduardi-Raymont G, Culhane JL, Fabian AC, Hazard C, McGlynn TA, Shafer RA, Tennant AF, Ward MJ (1985) EXOSAT observations of a strong soft X-ray excess in MKN 841. MNRAS217:105–113
7. Axon DJ, Pedlar A, Unger SW, Meurs EJA, Whittle DM (1989) The jets of 3C120. Nature341:631–633, DOI 10.1038/341631a0
8. Ballantyne DR, Vaughan S, Fabian AC (2003) A two-component ionized reflection model of MCG-6-30-15. MNRAS342:239–248, DOI 10.1046/j.1365-8711.2003.06533.x, `arXiv:astro-ph/0302288`
9. Bassani L, Dadina M, Maiolino R, Salvati M, Risaliti G, della Ceca R, Matt G, Zamorani G (1999) A Three-dimensional Diagnostic Diagram for Seyfert 2 Galaxies: Probing X-Ray Absorption and Compton Thickness. ApJS121:473–482, DOI 10.1086/313202, `arXiv:astro-ph/9811074`
10. Bautista MA, Kallman TR (2000) Recombination Spectra of Helium-like Ions. ApJ544:581–591, DOI 10.1086/317206, `arXiv:astro-ph/0006371`
11. Beckmann V, Barthelmy SD, Courvoisier TJL, Gehrels N, Soldi S, Tueller J, Wendt G (2007) Hard X-ray variability of active galactic nuclei. A&A475:827–835, DOI 10.1051/0004-6361:20078355
12. Behar E, Rasmussen AP, Blustin AJ, Sako M, Kahn SM, Kaastra JS, Branduardi-Raymont G, Steenbrugge KC (2003) A Long Look at NGC 3783 with the XMM-Newton Reflection Grating Spectrometer. ApJ598:232–241, DOI 10.1086/378853, `arXiv:astro-ph/0307467`
13. Bian W, Zhao Y (2003) On X-ray variability in narrow-line and broad-line active galactic nuclei. MNRAS343:164–168, DOI 10.1046/j.1365-8711.2003.06650.x, `arXiv:astro-ph/0303546`
14. Bianchi S, Matt G (2002) Ionized iron Kalpha lines in AGN X-ray spectra. A&A387:76–81, DOI 10.1051/0004-6361:20020372, `arXiv:astro-ph/0203178`
15. Bianchi S, Matt G, Balestra I, Perola GC (2003) The origin of the iron lines in NGC 7213. A&A407:L21–L24, DOI 10.1051/0004-6361:20031054, `arXiv:astro-ph/0307143`
16. Bianchi S, Matt G, Balestra I, Guainazzi M, Perola GC (2004) X-ray reprocessing in Seyfert galaxies: Simultaneous XMM-Newton/BeppoSAX observations. A&A422:65–76, DOI 10.1051/0004-6361:20047128, `arXiv:astro-ph/0404308`
17. Bianchi S, Matt G, Nicastro F, Porquet D, Dubau J (2005) FeXXV and FeXXVI lines from low-velocity, photoionized gas in the X-ray spectra of active galactic nuclei. MNRAS357:599–607, DOI 10.1111/j.1365-2966.2005.08661.x, `arXiv:astro-ph/0411603`
18. Bianchi S, La Franca F, Matt G, Guainazzi M, Jimenez Bailón E, Longinotti AL, Nicastro F, Pentericci L (2008) A broad-line region origin for the iron Kα line in NGC 7213. MNRAS389:L52–L56, DOI 10.1111/j.1745-3933.2008.00521.x, `0806.3876`
19. Blustin AJ, Page MJ, Fuerst SV, Branduardi-Raymont G, Ashton CE (2005) The nature and origin of Seyfert warm absorbers. A&A431:111–125, DOI 10.1051/0004-6361:20041775, `arXiv:astro-ph/0411297`
20. Blustin AJ, Kriss GA, Holczer T, Behar E, Kaastra JS, Page MJ, Kaspi S, Branduardi-Raymont G, Steenbrugge KC (2007) The mass-energy budget of the ionised outflow in NGC 7469. A&A466:107–118, DOI 10.1051/0004-6361:20066883, `arXiv:astro-ph/0702311`
21. Boller T, Brandt WN, Fink H (1996) Soft X-ray properties of narrow-line Seyfert 1 galaxies. A&A305:53–+, `arXiv:astro-ph/9504093`
22. Boller T, Brandt WN, Fabian AC, Fink HH (1997) ROSAT monitoring of persistent giant and rapid variability in the narrow-line Seyfert 1 galaxy IRAS 13224-3809. MNRAS289:393–405, `arXiv:astro-ph/9703114`
23. Bowyer CS, Lampton M, Mack J, de Mendonca F (1970) Detection of X-Ray Emission from 3c 273 and NGC 5128. ApJ161:L1+
24. Boyle BJ, Shanks T, Croom SM, Smith RJ, Miller L, Loaring N, Heymans C (2000) The

2dF QSO Redshift Survey - I. The optical luminosity function of quasi-stellar objects. MNRAS317:1014–1022, `arXiv:astro-ph/0005368`

25. Braito V, Reeves JN, Dewangan GC, George I, Griffiths RE, Markowitz A, Nandra K, Porquet D, Ptak A, Turner TJ, Yaqoob T, Weaver K (2007) Relativistic Iron K Emission and Absorption in the Seyfert 1.9 Galaxy MCG -5-23-16. ApJ670:978–991, DOI 10.1086/521916, `0707.2950`
26. Brandt WN, Boller T, Fabian AC, Ruszkowski M (1999) ROSAT High-Resolution Imager monitoring of extreme X-ray variability in the narrow-line quasar PHL 1092. MNRAS303:L53–L57, DOI 10.1046/j.1365-8711.1999.02411.x, `arXiv:astro-ph/9901353`
27. Branduardi-Raymont G, Sako M, Kahn SM, Brinkman AC, Kaastra JS, Page MJ (2001) Soft X-ray emission lines from a relativistic accretion disk in ¡ASTROBJ¿MCG -6-30-15¡/ASTROBJ¿ and ¡ASTROBJ¿Mrk 766¡/ASTROBJ¿. A&A365:L140–L145, DOI 10.1051/0004-6361:20000209, `arXiv:astro-ph/0011167`
28. Brenneman LW, Reynolds CS (2006) Constraining Black Hole Spin via X-Ray Spectroscopy. ApJ652:1028–1043, DOI 10.1086/508146, `arXiv:astro-ph/0608502`
29. Burke BE, Mountain RW, Daniels PJ, Cooper MJ, Dolat VS (1993) CCD soft x-ray imagers for ASCA and AXAF. In: Siegmund OH (ed) Society of Photo-Optical Instrumentation Engineers (SPIE) Conference Series, Society of Photo-Optical Instrumentation Engineers (SPIE) Conference Series, vol 2006, pp 272–285
30. Camenzind M, Courvoisier TJL (1983) A wind and shock model for active galactic nuclei. ApJ266:L83–L87, DOI 10.1086/183983
31. Ceballos MT, Barcons X (1996) Soft versus hard X-ray emission in active galactic nuclei: partial-covering and warm-plus-cold absorber models. MNRAS282:493–500, `arXiv:astro-ph/9604097`
32. Celotti A, Fabian AC, Rees MJ (1992) Dense thin clouds in the central regions of active galactic nuclei. MNRAS255:419–422
33. Chartas G, Brandt WN, Gallagher SC, Garmire GP (2002) CHANDRA Detects Relativistic Broad Absorption Lines from APM 08279+5255. ApJ579:169–175, DOI 10.1086/342744, `arXiv:astro-ph/0207196`
34. Chartas G, Brandt WN, Gallagher SC (2003) XMM-Newton Reveals the Quasar Outflow in PG 1115+080. ApJ595:85–93, DOI 10.1086/377299, `arXiv:astro-ph/0306125`
35. Chartas G, Eracleous M, Agol E, Gallagher SC (2004) Chandra Observations of the Cloverleaf Quasar H1413+117: A Unique Laboratory for Microlensing Studies of a LoBAL Quasar. ApJ606:78–84, DOI 10.1086/382743, `arXiv:astro-ph/0401240`
36. Chartas G, Kochanek CS, Dai X, Poindexter S, Garmire G (2008) X-ray Microlensing in RXJ1131-1231 and HE1104-1805. ArXiv e-prints `0805.4492`
37. Chelouche D, Netzer H (2005) Dynamical and Spectral Modeling of the Ionized Gas and Nuclear Environment in NGC 3783. ApJ625:95–107, DOI 10.1086/429580, `arXiv:astro-ph/0502272`
38. Chevallier L, Collin S, Dumont AM, Czerny B, Mouchet M, Gonçalves AC, Goosmann R (2006) The role of absorption and reflection in the soft X-ray excess of Active Galactic Nuclei. I. Preliminary results. A&A449:493–508, DOI 10.1051/0004-6361:20053730, `arXiv:astro-ph/0510700`
39. Collin S, Dumont AM, Godet O (2004) A new type of photoionized code required for the new era of X-ray spectroscopy. A&A419:877–886, DOI 10.1051/0004-6361:20041019, `arXiv:astro-ph/0403009`
40. Crenshaw DM, Kraemer SB, George IM (2003) Mass Loss from the Nuclei of Active Galaxies. ARA&A41:117–167, DOI 10.1146/annurev.astro.41.082801.100328
41. Crummy J, Fabian AC, Gallo L, Ross RR (2006) An explanation for the soft X-ray excess in active galactic nuclei. MNRAS365:1067–1081, DOI 10.1111/j.1365-2966.2005.09844.x, `arXiv:astro-ph/0511457`
42. Czerny B, Elvis M (1987) Constraints on quasar accretion disks from the optical/ultraviolet/soft X-ray big bump. ApJ321:305–320, DOI 10.1086/165630
43. Czerny B, Nikołajuk M, Różańska A, Dumont AM, Loska Z, Zycki PT (2003) Universal spectral shape of high accretion rate AGN. A&A412:317–329, DOI 10.1051/0004-6361:20031441, `arXiv:astro-ph/0309242`
44. Czerny B, Różańska A, Dovčiak M, Karas V, Dumont AM (2004) The structure and radiation spectra of illuminated accretion disks in AGN. II. Flare/spot model of X-ray variability. A&A420:1–16, DOI 10.1051/0004-6361:20035741, `arXiv:astro-ph/0402394`
45. Dadina M (2008) Seyfert galaxies in the local Universe z< 1: the average X-ray spectrum as

seen by BeppoSAX. A&A485:417–424, DOI 10.1051/0004-6361:20077569, `0801.4338`

46. Dadina M, Cappi M (2004) Complex absorption hides a Type II QSO in IRAS 13197-1627. A&A413:921–927, DOI 10.1051/0004-6361:20031561, `arXiv:astro-ph/0310272`
47. Dadina M, Cappi M, Malaguti G, Ponti G, de Rosa A (2005) X-ray absorption lines suggest matter infalling onto the central black-hole of Mrk 509. A&A442:461–468, DOI 10.1051/0004-6361:20042487, `arXiv:astro-ph/0506697`
48. den Herder JW, Brinkman AC, Kahn SM, Branduardi-Raymont G, Thomsen K, Aarts H, Audard M, Bixler JV, den Boggende AJ, Cottam J, Decker T, Dubbeldam L, Erd C, Goulooze H, Güdel M, Guttridge P, Hailey CJ, Janabi KA, Kaastra JS, de Korte PAJ, van Leeuwen BJ, Mauche C, McCalden AJ, Mewe R, Naber A, Paerels FB, Peterson JR, Rasmussen AP, Rees K, Sakelliou I, Sako M, Spodek J, Stern M, Tamura T, Tandy J, de Vries CP, Welch S, Zehnder A (2001) The Reflection Grating Spectrometer on board XMM-Newton. A&A365:L7–L17, DOI 10.1051/0004-6361:20000058
49. Done C, Nayakshin S (2007) Can the soft excess in AGN originate from disc reflection? MNRAS377:L59–L63, DOI 10.1111/j.1745-3933.2007.00303.x, `arXiv:astro-ph/0701410`
50. Dovčiak M, Bianchi S, Guainazzi M, Karas V, Matt G (2004) Relativistic spectral features from X-ray-illuminated spots and the measure of the black hole mass in active galactic nuclei. MNRAS350:745–755, DOI 10.1111/j.1365-2966.2004.07683.x, `arXiv:astro-ph/0401607`
51. Dovčiak M, Karas V, Matt G, Goosmann RW (2008) Variation in the primary and reprocessed radiation from an orbiting spot around a black hole. MNRAS384:361–369, DOI 10.1111/j.1365-2966.2007.12713.x, `0712.1122`
52. Elvis M, Maccacaro T, Wilson AS, Ward MJ, Penston MV, Fosbury RAE, Perola GC (1978) Seyfert galaxies as X-ray sources. MNRAS183:129–157
53. Ercolano B, Young PR, Drake JJ, Raymond JC (2008) X-Ray Enabled MOCASSIN: A Three-dimensional Code for Photoionized Media. ApJS175:534–542, DOI 10.1086/524378, `0710.2103`
54. Fabian AC (1994) Hot plasmas and the generation of gamma rays. ApJS92:555–558, DOI 10.1086/192015
55. Fabian AC (2008) XMM-Newton and broad iron lines. Astronomische Nachrichten 329:155–+, DOI 10.1002/asna.200710902, `arXiv:0711.2976`
56. Fabian AC, Vaughan S (2003) The iron line in MCG-6-30-15 from XMM-Newton: evidence for gravitational light bending? MNRAS340:L28–L32, DOI 10.1046/j.1365-8711.2003.06465.x, `arXiv:astro-ph/0301588`
57. Fabian AC, Rees MJ, Stella L, White NE (1989) X-ray fluorescence from the inner disc in Cygnus X-1. MNRAS238:729–736
58. Fabian AC, Iwasawa K, Reynolds CS, Young AJ (2000) Broad Iron Lines in Active Galactic Nuclei. PASP112:1145–1161, `arXiv:astro-ph/0004366`
59. Ferland GJ, Rees MJ (1988) Radiative equilibrium of high-density clouds with application to active galactic nucleus continua. ApJ332:141–156, DOI 10.1086/166639
60. Ferland GJ, Peterson BM, Horne K, Welsh WF, Nahar SN (1992) Anisotropic line emission and the geometry of the broad-line region in active galactic nuclei. ApJ387:95–108, DOI 10.1086/171063
61. Ferland GJ, Korista KT, Verner DA, Ferguson JW, Kingdon JB, Verner EM (1998) CLOUDY 90: Numerical Simulation of Plasmas and Their Spectra. PASP110:761–778
62. Ferrarese L, Merritt D (2000) A Fundamental Relation between Supermassive Black Holes and Their Host Galaxies. ApJ539:L9–L12, DOI 10.1086/312838, `arXiv:astro-ph/0006053`
63. Fiore F, Perola GC, Romano M (1990) X-ray spectral variations in NGC 4151. MNRAS243:522–528
64. Gaskell CM (1982) A redshift difference between high and low ionization emission-line regions in QSOs - Evidence for radial motions. ApJ263:79–86, DOI 10.1086/160481
65. Gebhardt K, Bender R, Bower G, Dressler A, Faber SM, Filippenko AV, Green R, Grillmair C, Ho LC, Kormendy J, Lauer TR, Magorrian J, Pinkney J, Richstone D, Tremaine S (2000) A Relationship between Nuclear Black Hole Mass and Galaxy Velocity Dispersion. ApJ539:L13–L16, DOI 10.1086/312840, `arXiv:astro-ph/0006289`
66. George IM, Fabian AC (1991) X-ray reflection from cold matter in active galactic nuclei and X-ray binaries. MNRAS249:352–367
67. George IM, Turner TJ, Netzer H, Nandra K, Mushotzky RF, Yaqoob T (1998) ASCA Observations of Seyfert 1 Galaxies. III. The Evidence for Absorption and Emission Due to Photoionized Gas. ApJS114:73–+, DOI 10.1086/313067, `arXiv:astro-ph/9708046`
68. Ghisellini G, Haardt F, Matt G (1994) The Contribution of the Obscuring Torus to the X-

Ray Spectrum of Seyfert Galaxies - a Test for the Unification Model. MNRAS267:743–+, `arXiv:astro-ph/9401044`

69. Ghosh KK, Soundararajaperumal S, Kalai Selvi M, Sivarani T (1992) X-ray spectrum of NGC 3783 - Detection of soft excess and an emission line. A&A255:119–123
70. Giacconi R, Murray S, Gursky H, Kellogg E, Schreier E, Matilsky T, Koch D, Tananbaum H (1974) The Third UHURU Catalog of X-Ray Sources. ApJS27:37–+
71. Gierliński M, Done C (2004) Is the soft excess in active galactic nuclei real? MNRAS349:L7–L11, DOI 10.1111/j.1365-2966.2004.07687.x, `arXiv:astro-ph/0312271`
72. Gonçalves AC, Collin S, Dumont AM, Mouchet M, Różańska A, Chevallier L, Goosmann RW (2006) A new model for the Warm Absorber in NGC 3783: a single medium in total pressure equilibrium. A&A451:L23–L26, DOI 10.1051/0004-6361:20064849, `arXiv:astro-ph/0603641`
73. Gondoin P, Barr P, Lumb D, Oosterbroek T, Orr A, Parmar AN (2001) Simultaneous XMM-Newton and BeppoSAX observation of the Seyfert I galaxy IC 4329A. A&A378:806–816, DOI 10.1051/0004-6361:20011258
74. Goosmann RW, Mouchet M, Czerny B, Dovčiak M, Karas V, Różańska A, Dumont AM (2007) Iron lines from transient and persisting hot spots on AGN accretion disks. A&A475:155–168, DOI 10.1051/0004-6361:20078273, `0709.1356`
75. Graham AW, Erwin P, Caon N, Trujillo I (2001) A Correlation between Galaxy Light Concentration and Supermassive Black Hole Mass. ApJ563:L11–L14, DOI 10.1086/338500, `arXiv:astro-ph/0111152`
76. Green AR, McHardy IM, Lehto HJ (1993) On the nature of rapid X-ray variability in active galactic nuclei. MNRAS265:664–+
77. Guainazzi M (2003) The history of the iron K_α line profile in the Piccinotti AGN ESO 198-G24. A&A401:903–910, DOI 10.1051/0004-6361:20030160, `arXiv:astro-ph/0302117`
78. Guainazzi M, Matsuoka M, Piro L, Mihara T, Yamauchi M (1994) Iron line emission and two-component spectral behavior in the ASCA observation of the Seyfert 1 galaxy NGC 7469. ApJ436:L35–L39, DOI 10.1086/187627
79. Guilbert PW, Rees MJ (1988) 'Cold' material in non-thermal sources. MNRAS233:475–484
80. Haardt F, Maraschi L (1991) A two-phase model for the X-ray emission from Seyfert galaxies. ApJ380:L51–L54, DOI 10.1086/186171
81. Haardt F, Maraschi L (1993) X-ray spectra from two-phase accretion disks. ApJ413:507–517, DOI 10.1086/173020
82. Haardt F, Maraschi L, Ghisellini G (1997) X-Ray Variability and Correlations in the Two-Phase Disk-Corona Model for Seyfert Galaxies. ApJ476:620–+, DOI 10.1086/303656, `arXiv:astro-ph/9609050`
83. Halpern JP (1984) Variable X-ray absorption in the QSO MR 2251 - 178. ApJ281:90–94, DOI 10.1086/162077
84. Heckman TM (1980) An optical and radio survey of the nuclei of bright galaxies - Activity in normal galactic nuclei. A&A87:152–164
85. Heckman TM, Kauffmann G, Brinchmann J, Charlot S, Tremonti C, White SDM (2004) Present-Day Growth of Black Holes and Bulges: The Sloan Digital Sky Survey Perspective. ApJ613:109–118, DOI 10.1086/422872, `arXiv:astro-ph/0406218`
86. Ho LC (1999) The Spectral Energy Distributions of Low-Luminosity Active Galactic Nuclei. ApJ516:672–682, DOI 10.1086/307137, `arXiv:astro-ph/9905012`
87. Ho LC (2008) Nuclear Activity in Nearby Galaxies. ArXiv e-prints 803, `0803.2268`
88. Holt SS, Mushotzky RF, Boldt EA, Serlemitsos PJ, Becker RH, Szymkowiak AE, White NE (1980) X-ray spectral constraints on the broad-line cloud geometry of NGC 4151. ApJ241:L13–L17, DOI 10.1086/183350
89. Inoue H, Matsumoto C (2003) Another Interpretation of the Disk-Line Profile for the Seyfert 1 Galaxy MCG-6-30-15. PASJ55:625–629
90. Iwasawa K, Lee JC, Young AJ, Reynolds CS, Fabian AC (2004a) The hard X-ray spectrum of the Seyfert galaxy IRAS 18325-5926: reflection from an ionized disc and variable iron K emission. MNRAS347:411–420, DOI 10.1111/j.1365-2966.2004.07206.x, `arXiv:astro-ph/0309432`
91. Iwasawa K, Miniutti G, Fabian AC (2004b) Flux and energy modulation of redshifted iron emission in NGC 3516: implications for the black hole mass. MNRAS355:1073–1079, DOI 10.1111/j.1365-2966.2004.08392.x, `arXiv:astro-ph/0409293`
92. Kaastra JS, Barr P (1989) Soft and hard X-ray variability from the accretion disk of NGC 5548. A&A226:59–68

93. Kaastra JS, Mewe R, Liedahl DA, Komossa S, Brinkman AC (2000) X-ray absorption lines in the Seyfert 1 galaxy NGC 5548 discovered with Chandra-LETGS. A&A354:L83–L86, `arXiv:astro-ph/0002345`
94. Kaastra JS, Mewe R, Raassen T (2003) New Results on X-Ray Models and Atomic Data. Atomic Data for X-Ray Astronomy, 25th meeting of the IAU, Joint Discussion 17, 22 July 2003, Sydney, Australia 17
95. Kallman T, Bautista M (2001) Photoionization and High-Density Gas. ApJS133:221–253, DOI 10.1086/319184
96. Kallman TR, Palmeri P, Bautista MA, Mendoza C, Krolik JH (2004) Photoionization Modeling and the K Lines of Iron. ApJS155:675–701, DOI 10.1086/424039, `arXiv:astro-ph/0405210`
97. Karas V, Lanza A, Vokrouhlicky D (1995) Emission-line profiles from self-gravitating thin disks. ApJ440:108–115, DOI 10.1086/175252, `arXiv:astro-ph/9409035`
98. Kaspi S, Smith PS, Netzer H, Maoz D, Jannuzi BT, Giveon U (2000) Reverberation Measurements for 17 Quasars and the Size-Mass-Luminosity Relations in Active Galactic Nuclei. ApJ533:631–649, DOI 10.1086/308704, `arXiv:astro-ph/9911476`
99. Kaspi S, Brandt WN, Netzer H, George IM, Chartas G, Behar E, Sambruna RM, Garmire GP, Nousek JA (2001) High-Resolution X-Ray Spectroscopy and Modeling of the Absorbing and Emitting Outflow in NGC 3783. ApJ554:216–232, DOI 10.1086/321333, `arXiv:astro-ph/0101540`
100. Kaspi S, Brandt WN, George IM, Netzer H, Crenshaw DM, Gabel JR, Hamann FW, Kaiser ME, Koratkar A, Kraemer SB, Kriss GA, Mathur S, Mushotzky RF, Nandra K, Peterson BM, Shields JC, Turner TJ, Zheng W (2002) The Ionized Gas and Nuclear Environment in NGC 3783. I. Time-averaged 900 Kilosecond Chandra Grating Spectroscopy. ApJ574:643–662, DOI 10.1086/341113, `arXiv:astro-ph/0203263`
101. King AR, Pounds KA (2003) Black hole winds. MNRAS345:657–659, DOI 10.1046/j.1365-8711.2003.06980.x, `arXiv:astro-ph/0305541`
102. Kormendy J, Richstone D (1995) Inward Bound—The Search For Supermassive Black Holes In Galactic Nuclei. ARA&A33:581–+, DOI 10.1146/annurev.aa.33.090195.003053
103. Koyama K, Tsunemi H, Dotani T, Bautz MW, Hayashida K, Tsuru TG, Matsumoto H, Ogawara Y, Ricker GR, Doty J, Kissel SE, Foster R, Nakajima H, Yamaguchi H, Mori H, Sakano M, Hamaguchi K, Nishiuchi M, Miyata E, Torii K, Namiki M, Katsuda S, Matsuura D, Miyauchi T, Anabuki N, Tawa N, Ozaki M, Murakami H, Maeda Y, Ichikawa Y, Prigozhin GY, Boughan EA, Lamarr B, Miller ED, Burke BE, Gregory JA, Pillsbury A, Bamba A, Hiraga JS, Senda A, Katayama H, Kitamoto S, Tsujimoto M, Kohmura T, Tsuboi Y, Awaki H (2007) X-Ray Imaging Spectrometer (XIS) on Board Suzaku. PASJ59:23–33
104. Kraemer SB, George IM, Crenshaw DM, Gabel JR, Turner TJ, Gull TR, Hutchings JB, Kriss GA, Mushotzky RF, Netzer H, Peterson BM, Behar E (2005) Simultaneous Ultraviolet and X-Ray Observations of Seyfert Galaxy NGC 4151. I. Physical Conditions in the X-Ray Absorbers. ApJ633:693–705, DOI 10.1086/466522, `arXiv:astro-ph/0507354`
105. Krolik JH, Kallman TR (1987) Fe K features as probes of the nuclear reflection region in Seyfert galaxies. ApJ320:L5–L8, DOI 10.1086/184966
106. Krolik JH, Kriss GA (1995) Observable Properties of X-Ray–heated Winds in Active Galactic Nuclei: Warm Reflectors and Warm Absorbers. ApJ447:512–+, DOI 10.1086/175896, `arXiv:astro-ph/9501089`
107. Krolik JH, McKee CF, Tarter CB (1981) Two-phase models of quasar emission line regions. ApJ249:422–442, DOI 10.1086/159303
108. Krongold Y, Nicastro F, Brickhouse NS, Elvis M, Liedahl DA, Mathur S (2003) Toward a Self-Consistent Model of the Ionized Absorber in NGC 3783. ApJ597:832–850, DOI 10.1086/378639, `arXiv:astro-ph/0306460`
109. Krongold Y, Nicastro F, Brickhouse NS, Elvis M, Mathur S (2005) Opacity Variations in the Ionized Absorption in NGC 3783: A Compact Absorber. ApJ622:842–846, DOI 10.1086/427621, `arXiv:astro-ph/0411554`
110. Laor A (1991) Line profiles from a disk around a rotating black hole. ApJ376:90–94, DOI 10.1086/170257
111. Larsson J, Miniutti G, Fabian AC, Miller JM, Reynolds CS, Ponti G (2008) Suzaku observations of Markarian 335: evidence for a distributed reflector. MNRAS384:1316–1326, DOI 10.1111/j.1365-2966.2008.12844.x, `0712.1906`
112. Lawrence A, Elvis M (1982) Obscuration and the various kinds of Seyfert galaxies. ApJ256:410–426, DOI 10.1086/159918

113. Lawrence A, Watson MG, Pounds KA, Elvis M (1985) Continuous rapid X-ray variability and spectral changes in NGC 4051. MNRAS217:685–699
114. Leahy DA, Creighton J (1993) Montecarlo Simulations of X-Ray Spectra for Internally Illuminated Spherical Matter Distributions. MNRAS263:314–+
115. Lee JC, Ogle PM, Canizares CR, Marshall HL, Schulz NS, Morales R, Fabian AC, Iwasawa K (2001) Revealing the Dusty Warm Absorber in MCG -6-30-15 with the Chandra High-Energy Transmission Grating. ApJ554:L13–L17, DOI 10.1086/320912, `arXiv:astro-ph/0101065`
116. Lee JC, Iwasawa K, Houck JC, Fabian AC, Marshall HL, Canizares CR (2002) The Shape of the Relativistic Iron Kα Line from MCG -6-30-15 Measured with the Chandra High Energy Transmission Grating Spectrometer and the Rossi X-Ray Timing Explorer. ApJ570:L47–L50, DOI 10.1086/340992
117. Leighly KM (1999) A Comprehensive Spectral and Variability Study of Narrow-Line Seyfert 1 Galaxies Observed by ASCA. I. Observations and Time Series Analysis. ApJS125:297–316, DOI 10.1086/313277, `arXiv:astro-ph/9907294`
118. Leighly KM, Pounds KA, Turner TJ (1989) A search for iron features in the EXOSAT spectral survey sources. In: Hunt J, Battrick B (eds) Two Topics in X-Ray Astronomy, Volume 1: X Ray Binaries. Volume 2: AGN and the X Ray Background, ESA Special Publication, vol 296, pp 961–967
119. Liedahl DA (2005) Resonant Auger Destruction and Iron Kα Spectra in Compact X-ray Sources. In: Smith R (ed) X-ray Diagnostics of Astrophysical Plasmas: Theory, Experiment, and Observation, American Institute of Physics Conference Series, vol 774, pp 99–108, DOI 10.1063/1.1960918
120. Lightman AP, White TR (1988) Effects of cold matter in active galactic nuclei - A broad hump in the X-ray spectra. ApJ335:57–66, DOI 10.1086/166905
121. Longinotti AL, Nandra K, Petrucci PO, O'Neill PM (2004) On the variability of the iron Kα line in Mrk 841. MNRAS355:929–934, DOI 10.1111/j.1365-2966.2004.08369.x, `arXiv:astro-ph/0409459`
122. Longinotti AL, Sim SA, Nandra K, Cappi M (2007) Evidence for relativistic features in the X-ray spectrum of Mrk 335. MNRAS374:237–247, DOI 10.1111/j.1365-2966.2006.11138.x, `arXiv:astro-ph/0609414`
123. Magdziarz P, Zdziarski AA (1995) Angle-dependent Compton reflection of X-rays and gamma-rays. MNRAS273:837–848
124. Magorrian J, Tremaine S, Richstone D, Bender R, Bower G, Dressler A, Faber SM, Gebhardt K, Green R, Grillmair C, Kormendy J, Lauer T (1998) The Demography of Massive Dark Objects in Galaxy Centers. AJ115:2285–2305, DOI 10.1086/300353, `arXiv:astro-ph/9708072`
125. Marconi A, Hunt LK (2003) The Relation between Black Hole Mass, Bulge Mass, and Near-Infrared Luminosity. ApJ589:L21–L24, DOI 10.1086/375804, `arXiv:astro-ph/0304274`
126. Marconi A, Risaliti G, Gilli R, Hunt LK, Maiolino R, Salvati M (2004) Local supermassive black holes, relics of active galactic nuclei and the X-ray background. MNRAS351:169–185, DOI 10.1111/j.1365-2966.2004.07765.x, `arXiv:astro-ph/0311619`
127. Markowitz A, Reeves JN, Braito V (2006) Fe K Emission and Absorption in the XMM-EPIC Spectrum of the Seyfert Galaxy IC 4329a. ApJ646:783–800, DOI 10.1086/505107, `arXiv:astro-ph/0604353`
128. Marshall N, Warwick RS, Pounds KA (1981) The variability of X-ray emission from active galaxies. MNRAS194:987–1002
129. Matsumoto C, Inoue H, Fabian AC, Iwasawa K (2003) Iron Line Properties of the Seyfert 1 Galaxy MCG-6-30-15 Observed with ASCA. PASJ55:615–623
130. Matsuoka M, Piro L, Yamauchi M, Murakami T (1990) X-ray spectral variability and complex absorption in the Seyfert 1 galaxies NGC 4051 and MCG -6-30-15. ApJ361:440–458, DOI 10.1086/169209
131. Matsuoka M, Yamauchi M, Piro L (1991) A spectral signature of thick matter in the X-ray spectrum from the Seyfert 1 galaxy, IC4329A. Advances in Space Research 11:41–43, DOI 10.1016/0273-1177(91)90147-C
132. Matt G (1994) Iron K-alpha resonant absorption in warm absorbers around active galactic nuclei. MNRAS267:L17–L20
133. Matt G, Perola GC, Piro L (1991) The iron line and high energy bump as X-ray signatures of cold matter in Seyfert 1 galaxies. A&A247:25–34
134. Matt G, Fabian AC, Reynolds CS (1997) Geometrical and chemical dependence of K-shell

X-ray features. MNRAS289:175–184

135. Matt G, Pompilio F, La Franca F (1999) X-ray spectra transmitted through Compton-thick absorbers. New Astronomy 4:191–195, DOI 10.1016/S1384-1076(99)00021-4, `arXiv:astro-ph/9904341`
136. McKernan B, Yaqoob T (1998) Occultation Mapping of the Central Engine in the Active Galaxy MCG -6-30-15. ApJ501:L29+, DOI 10.1086/311457, `arXiv:astro-ph/9804265`
137. McKernan B, Yaqoob T, Reynolds CS (2005) Constraints on hot metals in the vicinity of the Galaxy. MNRAS361:1337–1344, DOI 10.1111/j.1365-2966.2005.09291.x, `arXiv:astro-ph/0506346`
138. McKernan B, Yaqoob T, Reynolds CS (2007) A soft X-ray study of type I active galactic nuclei observed with Chandra high-energy transmission grating spectrometer. MNRAS379:1359–1372, DOI 10.1111/j.1365-2966.2007.11993.x
139. Merloni A, Malzac J, Fabian AC, Ross RR (2006) On the X-ray spectra of luminous, inhomogeneous accretion flows. MNRAS370:1699–1712, DOI 10.1111/j.1365-2966.2006.10676.x, `arXiv:astro-ph/0606262`
140. Middleton M, Done C, Gierliński M (2007) An absorption origin for the soft excess in Seyfert 1 active galactic nuclei. MNRAS381:1426–1436, DOI 10.1111/j.1365-2966.2007.12341.x, `0704.2970`
141. Mihara T, Matsuoka M, Mushotzky RF, Kunieda H, Otani C, Miyamoto S, Yamauchi M (1994) Soft X-ray spectral features in the Seyfert 1 Galaxy NGC4051. PASJ46:L137–L140
142. Miller L, Turner TJ, Reeves JN, George IM, Porquet D, Nandra K, Dovciak M (2006) Variable iron-line emission near the black hole of Markarian 766. A&A453:L13–L16, DOI 10.1051/0004-6361:20065276, `arXiv:astro-ph/0605130`
143. Miller L, Turner TJ, Reeves JN, George IM, Kraemer SB, Wingert B (2007) The variable X-ray spectrum of Markarian 766. I. Principal components analysis. A&A463:131–143, DOI 10.1051/0004-6361:20066548, `arXiv:astro-ph/0611673`
144. Miller L, Turner TJ, Reeves JN (2008) An absorption origin for the X-ray spectral variability of MCG-6-30-15. A&A483:437–452, DOI 10.1051/0004-6361:200809590, `0803.2680`
145. Mineshige S, Kawaguchi T, Takeuchi M, Hayashida K (2000) Slim-Disk Model for Soft X-Ray Excess and Variability of Narrow-Line Seyfert 1 Galaxies. PASJ52:499–508, `arXiv:astro-ph/0003017`
146. Miniutti G, Fabian AC (2004) A light bending model for the X-ray temporal and spectral properties of accreting black holes. MNRAS349:1435–1448, DOI 10.1111/j.1365-2966.2004.07611.x, `arXiv:astro-ph/0309064`
147. Miniutti G, Fabian AC, Goyder R, Lasenby AN (2003) The lack of variability of the iron line in MCG-6-30-15: general relativistic effects. MNRAS344:L22–L26, DOI 10.1046/j.1365-8711.2003.06988.x, `arXiv:astro-ph/0307163`
148. Miniutti G, Fabian AC, Anabuki N, Crummy J, Fukazawa Y, Gallo L, Haba Y, Hayashida K, Holt S, Kunieda H, Larsson J, Markowitz A, Matsumoto C, Ohno M, Reeves JN, Takahashi T, Tanaka Y, Terashima Y, Torii K, Ueda Y, Ushio M, Watanabe S, Yamauchi M, Yaqoob T (2007) Suzaku Observations of the Hard X-Ray Variability of MCG -6-30-15: the Effects of Strong Gravity around a Kerr Black Hole. PASJ59:315–325, `arXiv:astro-ph/0609521`
149. Mitsuda K, Bautz M, Inoue H, Kelley RL, Koyama K, Kunieda H, Makishima K, Ogawara Y, Petre R, Takahashi T, Tsunemi H, White NE, Anabuki N, Angelini L, Arnaud K, Awaki H, Bamba A, Boyce K, Brown GV, Chan KW, Cottam J, Dotani T, Doty J, Ebisawa K, Ezoe Y, Fabian AC, Figueroa E, Fujimoto R, Fukazawa Y, Furusho T, Furuzawa A, Gendreau K, Griffiths RE, Haba Y, Hamaguchi K, Harrus I, Hasinger G, Hatsukade I, Hayashida K, Henry PJ, Hiraga JS, Holt SS, Hornschemeier A, Hughes JP, Hwang U, Ishida M, Ishisaki Y, Isobe N, Itoh M, Iyomoto N, Kahn SM, Kamae T, Katagiri H, Kataoka J, Katayama H, Kawai N, Kilbourne C, Kinugasa K, Kissel S, Kitamoto S, Kohama M, Kohmura T, Kokubun M, Kotani T, Kotoku J, Kubota A, Madejski GM, Maeda Y, Makino F, Markowitz A, Matsumoto C, Matsumoto H, Matsuoka M, Matsushita K, McCammon D, Mihara T, Misaki K, Miyata E, Mizuno T, Mori K, Mori H, Morii M, Moseley H, Mukai K, Murakami H, Murakami T, Mushotzky R, Nagase F, Namiki M, Negoro H, Nakazawa K, Nousek JA, Okajima T, Ogasaka Y, Ohashi T, Oshima T, Ota N, Ozaki M, Ozawa H, Parmar AN, Pence WD, Porter FS, Reeves JN, Ricker GR, Sakurai I, Sanders WT, Senda A, Serlemitsos P, Shibata R, Soong Y, Smith R, Suzuki M, Szymkowiak AE, Takahashi H, Tamagawa T, Tamura K, Tamura T, Tanaka Y, Tashiro M, Tawara Y, Terada Y, Terashima Y, Tomida H, Torii K, Tsuboi Y, Tsujimoto M, Tsuru TG, Turner MJL, Ueda Y, Ueno S, Ueno M, Uno S, Urata Y, Watanabe S, Yamamoto N, Yamaoka K, Yamasaki

NY, Yamashita K, Yamauchi M, Yamauchi S, Yaqoob T, Yonetoku D, Yoshida A (2007) The X-Ray Observatory Suzaku. PASJ59:1–7

150. Miyoshi S, Hayakawa S, Kunieda H, Nagase F, Tawara Y (1986) X-ray observation of AGN's from TENMA. Ap&SS119:185–190
151. Morales R, Fabian AC (2002) Weighing black holes with warm absorbers. MNRAS329:209–220, DOI 10.1046/j.1365-8711.2002.04951.x, `arXiv:astro-ph/0109050`
152. Murray N, Chiang J (1998) Photoionization of Disk Winds. ApJ494:125–+, DOI 10.1086/305183
153. Mushotzky RF (1976) Observations of hard X-rays from extra-galactic objects. PhD thesis, AA(California Univ., San Diego.)
154. Mushotzky RF (1984) X-ray spectra and time variability of active galactic nuclei. Advances in Space Research 3:157–165, DOI 10.1016/0273-1177(84)90081-4
155. Mushotzky RF, Holt SS, Serlemitsos PJ (1978) X-ray observations of a flare in NGC 4151 from OSO 8. ApJ225:L115–L118, DOI 10.1086/182806
156. Nandra K (2006) On the origin of the iron Kα line cores in active galactic nuclei. MNRAS368:L62–L66, DOI 10.1111/j.1745-3933.2006.00158.x, `arXiv:astro-ph/0602081`
157. Nandra K, George IM (1994) X-Ray Reprocessing by Cold Clouds in Active Galactic Nuclei. MNRAS267:974–+
158. Nandra K, Pounds KA (1992) Highly ionized gas in the nucleus of the active galaxy MCG-6-30-15. Nature359:215–+, DOI 10.1038/359215a0
159. Nandra K, Pounds KA (1994) GINGA Observations of the X-Ray Spectra of Seyfert Galaxies. MNRAS268:405–+
160. Nandra K, Pounds KA, Stewart GC, Fabian AC, Rees MJ (1989) Detection of iron features in the X-ray spectrum of the Seyfert I galaxy MCG-6-30-15. MNRAS236:39P–46P
161. Nandra K, Fabian AC, George IM, Branduardi-Raymont G, Lawrence A, Mason KO, McHardy IM, Pounds KA, Stewart GC, Ward MJ, Warwick RS (1993) A ROSAT observation of NGC 5548. MNRAS260:504–512
162. Nandra K, George IM, Mushotzky RF, Turner TJ, Yaqoob T (1997) ASCA Observations of Seyfert 1 Galaxies. II. Relativistic Iron K alpha Emission. ApJ477:602–+, DOI 10.1086/303721, `arXiv:astro-ph/9606169`
163. Nandra K, O'Neill PM, George IM, Reeves JN (2007) An XMM-Newton survey of broad iron lines in Seyfert galaxies. MNRAS382:194–228, DOI 10.1111/j.1365-2966.2007.12331.x, `0708.1305`
164. Narayan R, Yi I (1994) Advection-dominated accretion: A self-similar solution. ApJ428:L13–L16, DOI 10.1086/187381, `arXiv:astro-ph/9403052`
165. Nayakshin S, Kazanas D (2002) On Time-dependent X-Ray Reflection by Photoionized Accretion Disks: Implications for Fe Kα Line Reverberation Studies of Active Galactic Nuclei. ApJ567:85–96, DOI 10.1086/338333, `arXiv:astro-ph/0106450`
166. Nayakshin S, Kazanas D, Kallman TR (2000) Thermal Instability and Photoionized X-Ray Reflection in Accretion Disks. ApJ537:833–852, DOI 10.1086/309054, `arXiv:astro-ph/9909359`
167. Netzer H (1993) Ionized absorbers, ionized emitters, and the X-ray spectrum of active galactic nuclei. ApJ411:594–601, DOI 10.1086/172861
168. Netzer H (1996) X-Ray Lines in Active Galactic Nuclei and Photoionized Gases. ApJ473:781–+, DOI 10.1086/178190
169. Netzer H, Chelouche D, George IM, Turner TJ, Crenshaw DM, Kraemer SB, Nandra K (2002) The Density and Location of the X-Ray-absorbing Gas in NGC 3516. ApJ571:256–264, DOI 10.1086/338967, `arXiv:astro-ph/0112027`
170. Netzer H, Kaspi S, Behar E, Brandt WN, Chelouche D, George IM, Crenshaw DM, Gabel JR, Hamann FW, Kraemer SB, Kriss GA, Nandra K, Peterson BM, Shields JC, Turner TJ (2003) The Ionized Gas and Nuclear Environment in NGC 3783. IV. Variability and Modeling of the 900 Kilosecond Chandra Spectrum. ApJ599:933–948, DOI 10.1086/379508, `arXiv:astro-ph/0309096`
171. Nicastro F, Fiore F, Matt G (1999) Resonant Absorption in the Active Galactic Nucleus Spectra Emerging from Photoionized Gas: Differences between Steep and Flat Ionizing Continua. ApJ517:108–122, DOI 10.1086/307187, `arXiv:astro-ph/9812392`
172. Onken CA, Ferrarese L, Merritt D, Peterson BM, Pogge RW, Vestergaard M, Wandel A (2004) Supermassive Black Holes in Active Galactic Nuclei. II. Calibration of the Black Hole Mass-Velocity Dispersion Relationship for Active Galactic Nuclei. ApJ615:645–651, DOI 10.1086/424655, `arXiv:astro-ph/0407297`

173. Orr A, Molendi S, Fiore F, Grandi P, Parmar AN, Owens A (1997) Soft X-ray observations of the complex warm absorber in MCG-6-30-15 with BeppoSAX. A&A324:L77–L80, `arXiv:astro-ph/9706133`
174. Osterbrock DE, Ferland GJ (2006) Astrophysics of gaseous nebulae and active galactic nuclei. Astrophysics of gaseous nebulae and active galactic nuclei, 2nd. ed. by D.E. Osterbrock and G.J. Ferland. Sausalito, CA: University Science Books, 2006
175. Osterbrock DE, Pogge RW (1985) The spectra of narrow-line Seyfert 1 galaxies. ApJ297:166–176, DOI 10.1086/163513
176. Otani C, Kii T, Reynolds CS, Fabian AC, Iwasawa K, Hayashida K, Inoue H, Kunieda H, Makino F, Matsuoka M, Tanaka Y (1996) The Variable O,VIII Warm Absorber in MCG-6-30-15. PASJ48:211–218, `arXiv:astro-ph/9511063`
177. Padovani P, Rafanelli P (1988) Mass-luminosity relationships and accretion rates for Seyfert 1 galaxies and quasars. A&A205:53–70
178. Page KL, Pounds KA, Reeves JN, O'Brien PT (2002) The highly variable X-ray spectrum of the luminous Seyfert 1 galaxy 1H 0419-577. MNRAS330:L1–L5, DOI 10.1046/j.1365-8711.2002.05184.x, `arXiv:astro-ph/0112215`
179. Palmeri P, Mendoza C, Kallman TR, Bautista MA, Meléndez M (2003) Modeling of iron K lines: Radiative and Auger decay data for Fe II-Fe IX. A&A410:359–364, DOI 10.1051/0004-6361:20031262, `arXiv:astro-ph/0306321`
180. Pan HC, Stewart GC, Pounds KA (1990) The variable X-ray absorption and soft X-ray excess of the QSO MR2251 - 178. MNRAS242:177–187
181. Panessa F, Bassani L (2002) Unabsorbed Seyfert 2 galaxies. A&A394:435–442, DOI 10.1051/0004-6361:20021161, `arXiv:astro-ph/0208496`
182. Papadakis IE, Petrucci PO, Maraschi L, McHardy IM, Uttley P, Haardt F (2002) Long-Term Spectral Variability of Seyfert Galaxies from Rossi X-Ray Timing Explorer Color-Flux Diagrams. ApJ573:92–104, DOI 10.1086/340497, `arXiv:astro-ph/0202498`
183. Peterson BM (1993) Reverberation mapping of active galactic nuclei. PASP105:247–268
184. Peterson BM, Wandel A (2000) Evidence for Supermassive Black Holes in Active Galactic Nuclei from Emission-Line Reverberation. ApJ540:L13–L16, DOI 10.1086/312862, `arXiv:astro-ph/0007147`
185. Peterson BM, Ferrarese L, Gilbert KM, Kaspi S, Malkan MA, Maoz D, Merritt D, Netzer H, Onken CA, Pogge RW, Vestergaard M, Wandel A (2004) Central Masses and Broad-Line Region Sizes of Active Galactic Nuclei. II. A Homogeneous Analysis of a Large Reverberation-Mapping Database. ApJ613:682–699, DOI 10.1086/423269, `arXiv:astro-ph/0407299`
186. Petrucci PO, Henri G, Maraschi L, Ferrando P, Matt G, Mouchet M, Perola C, Collin S, Dumont AM, Haardt F, Koch-Miramond L (2002) A rapidly variable narrow X-ray iron line in Mkn 841. A&A388:L5–L8, DOI 10.1051/0004-6361:20020534, `arXiv:astro-ph/0204095`
187. Piro L, Massaro E, Perola GC, Molteni D (1988) An exceptional change in the X-ray flux and spectrum of the Seyfert 1 galaxy E1615 + 061. ApJ325:L25–L28, DOI 10.1086/185102
188. Piro L, Yamauchi M, Matsuoka M (1990) X-ray spectral signatures of very thick cold matter in the spectra of the Seyfert 1 galaxies NGC 7469 and IC 4329A. ApJ360:L35–L38, DOI 10.1086/185806
189. Piro L, Yamauchi M, Matsuoka M (1992) X-ray spectral signatures of very thick cold matter in the spectra of Seyfert galaxies. Nuovo Cimento C Geophysics Space Physics C 15:811–818
190. Ponti G, Cappi M, Dadina M, Malaguti G (2004) Mapping the inner regions of MCG-6-30-15 with XMM-Newton. A&A417:451–459, DOI 10.1051/0004-6361:20031758, `arXiv:astro-ph/0312250`
191. Porquet D, Dubau J (2000) X-ray photoionized plasma diagnostics with helium-like ions. Application to warm absorber-emitter in active galactic nuclei. A&AS143:495–514, DOI 10.1051/aas:2000192, `arXiv:astro-ph/0002319`
192. Pounds KA, Reeves JN (2008) Resolving a broad PCygni line profile to quantify the fast outflow in the luminous Seyfert galaxy PG1211+143. ArXiv e-prints `0811.3108`
193. Pounds KA, Turner TJ, Warwick RS (1986) Rapid X-ray variability of the Seyfert galaxy MCG-6-30-15. MNRAS221:7P–12P
194. Pounds KA, Nandra K, Stewart GC, Leighly K (1989) Iron features in the X-ray spectra of three Seyfert galaxies. MNRAS240:769–783
195. Pounds KA, Nandra K, Stewart GC, George IM, Fabian AC (1990) X-ray reflection from cold matter in the nuclei of active galaxies. Nature344:132–+, DOI 10.1038/344132a0

196. Pounds KA, Nandra K, Fink HH, Makino F (1994) Constraining the complexities in Seyfert X-ray spectra - an analysis of simultaneous observations with GINGA and ROSAT. MNRAS267:193–+
197. Pounds KA, Done C, Osborne JP (1995) RE 1034+39: a high-state Seyfert galaxy? MNRAS277:L5–L10
198. Pounds KA, Reeves JN, King AR, Page KL, O'Brien PT, Turner MJL (2003) A high-velocity ionized outflow and XUV photosphere in the narrow emission line quasar PG1211+143. MNRAS345:705–713, DOI 10.1046/j.1365-8711.2003.07006.x, `arXiv:astro-ph/0303603`
199. Pounds KA, Reeves JN, Page KL, O'Brien PT (2004a) An XMM-Newton Observation of the Seyfert 1 Galaxy 1H 0419-577 in an Extreme Low State. ApJ605:670–676, DOI 10.1086/382678, `arXiv:astro-ph/0401026`
200. Pounds KA, Reeves JN, Page KL, O'Brien PT (2004b) Resolving the Large-Scale Spectral Variability of the Luminous Seyfert 1 Galaxy 1H 0419-577: Evidence for a New Emission Component and Absorption by Cold Dense Matter. ApJ616:696–706, DOI 10.1086/424992, `arXiv:astro-ph/0407045`
201. Press WH, Teukolsky SA, Vetterling WT, Flannery BP (1992) Numerical recipes in FORTRAN. The art of scientific computing. Cambridge: University Press, —c1992, 2nd ed.
202. Proga D, Kallman TR (2004) Dynamics of Line-driven Disk Winds in Active Galactic Nuclei. II. Effects of Disk Radiation. ApJ616:688–695, DOI 10.1086/425117, `arXiv:astro-ph/0408293`
203. Proga D, Stone JM, Kallman TR (2000) Dynamics of Line-driven Disk Winds in Active Galactic Nuclei. ApJ543:686–696, DOI 10.1086/317154, `arXiv:astro-ph/0005315`
204. Proga D, Ostriker JP, Kurosawa R (2008) Dynamics of Rotating Accretion Flows Irradiated by a Quasar. ApJ676:101–112, DOI 10.1086/527535, `0708.4037`
205. Ptak A, Yaqoob T, Serlemitsos PJ, Mushotzky R, Otani C (1994) Rapid X-ray spectral variability in NGC 3227. ApJ436:L31–L34, DOI 10.1086/187626
206. Puccetti S, Risaliti G, Fiore F, Elvis M, Nicastro F, Perola GC, Capalbi M (2004) Rapid N_H changes in NGC 4151. Nuclear Physics B Proceedings Supplements 132:225–228, DOI 10.1016/j.nuclphysbps.2004.04.039, `arXiv:astro-ph/0311446`
207. Rees MJ (1977) George DARWIN Lecture 1976 - Quasars and young galaxies. QJRAS18:429–442
208. Reeves J, Done C, Pounds K, Terashima Y, Hayashida K, Anabuki N, Uchino M, Turner M (2008) On why the iron K-shell absorption in AGN is not a signature of the local warm/hot intergalactic medium. MNRAS385:L108–L112, DOI 10.1111/j.1745-3933.2008.00443.x, `0801.1587`
209. Reeves JN, Wynn G, O'Brien PT, Pounds KA (2002) Extreme X-ray variability in the luminous quasar PDS 456. MNRAS336:L56–L60, DOI 10.1046/j.1365-8711.2002.06038.x, `arXiv:astro-ph/0209120`
210. Reeves JN, O'Brien PT, Ward MJ (2003) A Massive X-Ray Outflow from the Quasar PDS 456. ApJ593:L65–L68, DOI 10.1086/378218, `arXiv:astro-ph/0307127`
211. Reeves JN, Nandra K, George IM, Pounds KA, Turner TJ, Yaqoob T (2004) The XMM-Newton Iron Line Profile of NGC 3783. ApJ602:648–658, DOI 10.1086/381091, `arXiv:astro-ph/0310820`
212. Reeves JN, Awaki H, Dewangan GC, Fabian AC, Fukazawa Y, Gallo L, Griffiths R, Inoue H, Kunieda H, Markowitz A, Miniutti G, Mizuno T, Mushotzky R, Okajima T, Ptak A, Takahashi T, Terashima Y, Ushio M, Watanabe S, Yamasaki T, Yamauchi M, Yaqoob T (2007) Revealing the High Energy Emission from the Obscured Seyfert Galaxy MCG-5-23-16 with Suzaku. PASJ59:301–314, `arXiv:astro-ph/0610434`
213. Reichert GA, Mushotzky RF, Holt SS, Petre R (1985) Soft X-ray spectral observations of low-luminosity active galaxies. ApJ296:69–89, DOI 10.1086/163421
214. Reynolds CS (1997) An X-ray spectral study of 24 type 1 active galactic nuclei. MNRAS286:513–537, `arXiv:astro-ph/9610127`
215. Reynolds CS, Fabian AC (1997) Special relativistic effects on the strength of the fluorescent Kalpha iron line from black hole accretion discs. MNRAS290:L1–L5, `arXiv:astro-ph/9707082`
216. Reynolds CS, Nowak MA (2003) Fluorescent iron lines as a probe of astrophysical black hole systems. Phys. Rep.377:389–466, `arXiv:astro-ph/0212065`
217. Reynolds CS, Wilms J (2000) On the Inability of Comptonization to Produce the Broad X-Ray Iron Lines Observed in Seyfert Nuclei. ApJ533:821–825, DOI 10.1086/308712, `arXiv:astro-ph/9912120`

218. Reynolds CS, Fabian AC, Inoue H (1995) ASCA observations of the Seyfert 1 galaxies MRK 1040 and MS 0225.5+3121. MNRAS276:1311–1319, `arXiv:astro-ph/9504095`
219. Reynolds CS, Wilms J, Begelman MC, Staubert R, Kendziorra E (2004) On the deep minimum state in the Seyfert galaxy MCG-6-30-15. MNRAS349:1153–1166, DOI 10.1111/j.1365-2966.2004.07596.x, `arXiv:astro-ph/0401305`
220. Richards GT, Vanden Berk DE, Reichard TA, Hall PB, Schneider DP, SubbaRao M, Thakar AR, York DG (2002) Broad Emission-Line Shifts in Quasars: An Orientation Measure for Radio-Quiet Quasars? AJ124:1–17, DOI 10.1086/341167, `arXiv:astro-ph/0204162`
221. Risaliti G, Bianchi S, Matt G, Baldi A, Elvis M, Fabbiano G, Zezas A (2005) Highly Ionized Iron Absorption Lines from Outflowing Gas in the X-Ray Spectrum of NGC 1365. ApJ630:L129–L132, DOI 10.1086/491646, `arXiv:astro-ph/0508608`
222. Risaliti G, Elvis M, Fabbiano G, Baldi A, Zezas A, Salvati M (2007) Occultation Measurement of the Size of the X-Ray-emitting Region in the Active Galactic Nucleus of NGC 1365. ApJ659:L111–L114, DOI 10.1086/517884, `arXiv:astro-ph/0703173`
223. Ross RR, Fabian AC (2005) A comprehensive range of X-ray ionized-reflection models. MNRAS358:211–216, DOI 10.1111/j.1365-2966.2005.08797.x, `arXiv:astro-ph/0501116`
224. Ross RR, Fabian AC, Young AJ (1999) X-ray reflection spectra from ionized slabs. MNRAS306:461–466, `arXiv:astro-ph/9902325`
225. Sako M, Kahn SM, Behar E, Kaastra JS, Brinkman AC, Boller T, Puchnarewicz EM, Starling R, Liedahl DA, Clavel J, Santos-Lleo M (2001) Complex resonance absorption structure in the X-ray spectrum of ¡ASTROBJ¿IRAS 13349+2438¡/ASTROBJ¿. A&A365:L168–L173, DOI 10.1051/0004-6361:20000081, `arXiv:astro-ph/0010660`
226. Schurch NJ, Done C (2007) The impact of accretion disc winds on the X-ray spectrum of AGN - I. XSCORT. MNRAS381:1413–1425, DOI 10.1111/j.1365-2966.2007.12336.x, `0706.1885`
227. Schurch NJ, Done C (2008) Funnel wall jets and the nature of the soft X-ray excess. MNRAS386:L1–L4, DOI 10.1111/j.1745-3933.2007.00395.x, `0709.2650`
228. Schurch NJ, Done C, Proga D (2008) The impact of accretion disk winds on the X-ray spectrum of AGN: Part 2 - XSCORT + Hydrodynamic Simulations. ArXiv e-prints `0810.0884`
229. Shakura NI, Syunyaev RA (1973) Black holes in binary systems. Observational appearance. A&A24:337–355
230. Sim SA, Long KS, Miller L, Turner TJ (2008) Multidimensional modelling of X-ray spectra for AGN accretion disc outflows. MNRAS388:611–624, DOI 10.1111/j.1365-2966.2008.13466.x, `0805.2251`
231. Smith RAN, Page MJ, Branduardi-Raymont G (2007) The XMM-Newton RGS spectrum of the high luminosity Seyfert 1 galaxy Markarian 509. A&A461:135–142, DOI 10.1051/0004-6361:20065348, `arXiv:astro-ph/0609746`
232. Sobolewska MA, Done C (2007) What is the origin of the soft excess in active galactic nuclei? MNRAS374:150–158, DOI 10.1111/j.1365-2966.2006.11117.x, `arXiv:astro-ph/0609223`
233. Soltan A (1982) Masses of quasars. MNRAS200:115–122
234. Steenbrugge KC, Kaastra JS, Crenshaw DM, Kraemer SB, Arav N, George IM, Liedahl DA, van der Meer RLJ, Paerels FBS, Turner TJ, Yaqoob T (2005) Simultaneous X-ray and UV spectroscopy of the Seyfert galaxy NGC 5548. II. Physical conditions in the X-ray absorber. A&A434:569–584, DOI 10.1051/0004-6361:20047138, `arXiv:astro-ph/0501122`
235. Sulentic JW, Marziani P, Zwitter T, Calvani M, Dultzin-Hacyan D (1998) On the Origin of Broad Fe K alpha and H i H alpha Lines in Active Galactic Nuclei. ApJ501:54–+, DOI 10.1086/305795, `arXiv:astro-ph/9712336`
236. Takahashi T, Abe K, Endo M, Endo Y, Ezoe Y, Fukazawa Y, Hamaya M, Hirakuri S, Hong S, Horii M, Inoue H, Isobe N, Itoh T, Iyomoto N, Kamae T, Kasama D, Kataoka J, Kato H, Kawaharada M, Kawano N, Kawashima K, Kawasoe S, Kishishita T, Kitaguchi T, Kobayashi Y, Kokubun M, Kotoku J, Kouda M, Kubota A, Kuroda Y, Madejski G, Makishima K, Masukawa K, Matsumoto Y, Mitani T, Miyawaki R, Mizuno T, Mori K, Mori M, Murashima M, Murakami T, Nakazawa K, Niko H, Nomachi M, Okada Y, Ohno M, Oonuki K, Ota N, Ozawa H, Sato G, Shinoda S, Sugiho M, Suzuki M, Taguchi K, Takahashi H, Takahashi I, Takeda S, Tamura KI, Tamura T, Tanaka T, Tanihata C, Tashiro M, Terada Y, Tominaga S, Uchiyama Y, Watanabe S, Yamaoka K, Yanagida T, Yonetoku D (2007) Hard X-Ray Detector (HXD) on Board Suzaku. PASJ59:35–51, `arXiv:astro-ph/0611232`
237. Tanaka Y, Inoue H, Holt SS (1994) The X-ray astronomy satellite ASCA. PASJ46:L37–L41
238. Tanaka Y, Nandra K, Fabian AC, Inoue H, Otani C, Dotani T, Hayashida K, Iwasawa K, Kii T, Kunieda H, Makino F, Matsuoka M (1995) Gravitationally Redshifted Emission

Implying an Accretion Disk and Massive Black-Hole in the Active Galaxy MCG:-6-30-15. Nature375:659–+, DOI 10.1038/375659a0

239. Tarter CB, Tucker WH, Salpeter EE (1969) The Interaction of X-Ray Sources with Optically Thin Environments. ApJ156:943–+
240. Terashima Y, Gallo LC, Inoue H, Markowitz AG, Reeves JN, Anabuki N, Fabian AC, Griffiths RE, Hayashida K, Itoh T, Kokubun N, Kubota A, Miniutti G, Takahashi T, Yamauchi M, Yonetoku D (2008) X-Ray Spectral Variability of the Seyfert Galaxy NGC 4051 Observed with Suzaku. ArXiv e-prints `0811.0692`
241. Titarchuk L, Kazanas D, Becker PA (2003) Broad Redshifted Line as a Signature of Outflow. ApJ598:411–418, DOI 10.1086/378701, `arXiv:astro-ph/0307486`
242. Titarchuk LG, Hua XM (1997) Comptonization models and spectroscopy of X-ray and gamma-ray sources. Advances in Space Research 19:99–108, DOI 10.1016/S0273-1177(97)00043-4
243. Tremaine S, Gebhardt K, Bender R, Bower G, Dressler A, Faber SM, Filippenko AV, Green R, Grillmair C, Ho LC, Kormendy J, Lauer TR, Magorrian J, Pinkney J, Richstone D (2002) The Slope of the Black Hole Mass versus Velocity Dispersion Correlation. ApJ574:740–753, DOI 10.1086/341002, `arXiv:astro-ph/0203468`
244. Tucker W, Kellogg E, Gursky H, Giacconi R, Tananbaun H (1973) X-Ray Observations of NGC 5128 (centaurus a) from UHURU. ApJ180:715–724
245. Tueller J, Mushotzky RF, Barthelmy S, Cannizzo JK, Gehrels N, Markwardt CB, Skinner GK, Winter LM (2008) Swift BAT Survey of AGNs. ApJ681:113–127, DOI 10.1086/588458, `0711.4130`
246. Turner AK, Fabian AC, Vaughan S, Lee JC (2003) A softer look at MCG-6-30-15 with XMM-Newton. MNRAS346:833–840, DOI 10.1111/j.1365-2966.2003.07127.x, `arXiv:astro-ph/0303418`
247. Turner AK, Fabian AC, Lee JC, Vaughan S (2004a) The soft X-ray absorption lines of the Seyfert 1 galaxy MCG-6-30-15. MNRAS353:319–328, DOI 10.1111/j.1365-2966.2004.08075.x, `arXiv:astro-ph/0405570`
248. Turner TJ, Pounds KA (1988) Variability of the soft excess in the Seyfert I galaxy MKN 335. MNRAS232:463–471
249. Turner TJ, Pounds KA (1989) The EXOSAT spectral survey of AGN. MNRAS240:833–880
250. Turner TJ, George IM, Mushotzky RF (1993a) ROSAT Position Sensitive Proportional Counter spectra of six Seyfert 1 galaxies. ApJ412:72–81, DOI 10.1086/172901
251. Turner TJ, Nandra K, George IM, Fabian AC, Pounds KA (1993b) X-Ray Observations of the Warm Absorber in NGC 3783. ApJ419:127–+, DOI 10.1086/173466
252. Turner TJ, George IM, Nandra K, Mushotzky RF (1997) ASCA Observations of Type 2 Seyfert Galaxies. I. Data Analysis Results. ApJS113:23–+, DOI 10.1086/313053
253. Turner TJ, George IM, Nandra K, Turcan D (1999) On X-Ray Variability in Seyfert Galaxies. ApJ524:667–673, DOI 10.1086/307834, `arXiv:astro-ph/9906050`
254. Turner TJ, Mushotzky RF, Yaqoob T, George IM, Snowden SL, Netzer H, Kraemer SB, Nandra K, Chelouche D (2002) Narrow Components within the Fe Kα Profile of NGC 3516: Evidence of the Importance of General Relativistic Effects? ApJ574:L123–L127, DOI 10.1086/342504, `arXiv:astro-ph/0206223`
255. Turner TJ, Kraemer SB, Reeves JN (2004b) Transient Relativistically Shifted Lines as a Probe of Black Hole Systems. ApJ603:62–66, DOI 10.1086/381312, `arXiv:astro-ph/0310885`
256. Turner TJ, Kraemer SB, George IM, Reeves JN, Bottorff MC (2005) Complex X-Ray Absorption and the Fe Kα Profile in NGC 3516. ApJ618:155–166, DOI 10.1086/425961, `arXiv:astro-ph/0409091`
257. Turner TJ, Miller L, George IM, Reeves JN (2006) Evidence for orbital motion of material close to the central black hole of Mrk 766. A&A445:59–67, DOI 10.1051/0004-6361:20053042, `arXiv:astro-ph/0506223`
258. Turner TJ, Miller L, Reeves JN, Kraemer SB (2007) The variable X-ray spectrum of Markarian 766. II. Time-resolved spectroscopy. A&A475:121–131, DOI 10.1051/0004-6361:20077947, `0708.1338`
259. Turner TJ, Reeves JN, Kraemer SB, Miller L (2008) Tracing a disk wind in NGC 3516. A&A483:161–169, DOI 10.1051/0004-6361:20078808, `0803.0080`
260. Urry CM, Padovani P (1995) Unified Schemes for Radio-Loud Active Galactic Nuclei. PASP107:803–+, `arXiv:astro-ph/9506063`
261. Vaughan S, Fabian AC (2004) A long hard look at MCG-6-30-15 with XMM-Newton- II. Detailed EPIC analysis and modelling. MNRAS348:1415–1438, DOI 10.1111/j.1365-2966.

2004.07456.x, `arXiv:astro-ph/0311473`

262. Vaughan S, Uttley P (2008) On the evidence for narrow, relativistically shifted X-ray lines. ArXiv e-prints `0807.4806`
263. Walter R, Fink HH (1993) The Ultraviolet to Soft X-Ray Bump of SEYFERT-1 Type Active Galactic Nuclei. A&A274:105–+
264. Wandel A (2002) Black Holes of Active and Quiescent Galaxies. I. The Black Hole-Bulge Relation Revisited. ApJ565:762–772, DOI 10.1086/338134, `arXiv:astro-ph/0108461`
265. Wandel A, Peterson BM, Malkan MA (1999) Central Masses and Broad-Line Region Sizes of Active Galactic Nuclei. I. Comparing the Photoionization and Reverberation Techniques. ApJ526:579–591, DOI 10.1086/308017, `arXiv:astro-ph/9905224`
266. Wang JM, Qu JL, Xue SJ (2004) The Additional Line Component within the Iron Kα Profile in MCG -6-30-15: Evidence for Blob Ejection? ApJ609:107–112, DOI 10.1086/420892, `arXiv:astro-ph/0407124`
267. Ward M, Elvis M, Fabbiano G, Carleton NP, Willner SP, Lawrence A (1987) The continuum of type 1 Seyfert galaxies. I - A single form modified by the effects of dust. ApJ315:74–91, DOI 10.1086/165115
268. Warwick RS, Pounds KA, Turner TJ (1988) Variable low-energy absorption in the X-ray spectrum of ESO 103-G35. MNRAS231:1145–1152
269. Weaver KA, Mushotzky RF, Arnaud KA, Serlemitsos PJ, Marshall FE, Petre R, Jahoda KM, Smale AP, Netzer H (1994) The Complex Soft X-Ray Excess in NGC 4151. ApJ423:621–+, DOI 10.1086/173840
270. Weymann RJ, Morris SL, Foltz CB, Hewett PC (1991) Comparisons of the emission-line and continuum properties of broad absorption line and normal quasi-stellar objects. ApJ373:23–53, DOI 10.1086/170020
271. Wilkes BJ, Elvis M (1987) Quasar energy distributions. I - Soft X-ray spectra of quasars. ApJ323:243–262, DOI 10.1086/165822
272. Wilms J, Reynolds CS, Begelman MC, Reeves J, Molendi S, Staubert R, Kendziorra E (2001) XMM-EPIC observation of MCG-6-30-15: direct evidence for the extraction of energy from a spinning black hole? MNRAS328:L27–L31, DOI 10.1046/j.1365-8711.2001.05066.x, `arXiv:astro-ph/0110520`
273. Woo JH, Urry CM (2002) Active Galactic Nucleus Black Hole Masses and Bolometric Luminosities. ApJ579:530–544, DOI 10.1086/342878, `arXiv:astro-ph/0207249`
274. Wu XB, Liu FK (2004) Black Hole Mass and Accretion Rate of Active Galactic Nuclei with Double-peaked Broad Emission Lines. ApJ614:91–100, DOI 10.1086/423446, `arXiv:astro-ph/0406415`
275. Yaqoob T, Padmanabhan U (2004) The Cores of the Fe K Lines in Seyfert 1 Galaxies Observed by the Chandra High Energy Grating. ApJ604:63–73, DOI 10.1086/381731, `arXiv:astro-ph/0311551`
276. Yaqoob T, Serlemitsos P (2005) Iron K Features in the Quasar E1821+643: Evidence for Gravitationally Redshifted Absorption? ApJ623:112–122, DOI 10.1086/428432, `arXiv:astro-ph/0502128`
277. Yaqoob T, Warwick RS, Pounds KA (1989) Variable X-ray absorption in NGC 4151. MNRAS236:153–170
278. Yaqoob T, Serlemitsos P, Mushotzky R, Madejski G, Turner TJ, Kunieda H (1994) X-ray spectrum and variability of the quasar PG 1211+143. PASJ46:L173–L177
279. Yaqoob T, George IM, Nandra K, Turner TJ, Serlemitsos PJ, Mushotzky RF (2001) Physical Diagnostics from a Narrow Fe Kα Emission Line Detected by Chandra in the Seyfert 1 Galaxy NGC 5548. ApJ546:759–768, DOI 10.1086/318315, `arXiv:astro-ph/0008471`
280. Yaqoob T, George IM, Kallman TR, Padmanabhan U, Weaver KA, Turner TJ (2003) Fe XXV and Fe XXVI Diagnostics of the Black Hole and Accretion Disk in Active Galaxies: Chandra Time-resolved Grating Spectroscopy of NGC 7314. ApJ596:85–104, DOI 10.1086/377687, `arXiv:astro-ph/0306428`
281. Young AJ, Lee JC, Fabian AC, Reynolds CS, Gibson RR, Canizares CR (2005) A Chandra HETGS Spectral Study of the Iron K Bandpass in MCG -6-30-15: A Narrow View of the Broad Iron Line. ApJ631:733–740, DOI 10.1086/432607, `arXiv:astro-ph/0506082`
282. Yu Q, Tremaine S (2002) Observational constraints on growth of massive black holes. MNRAS335:965–976, DOI 10.1046/j.1365-8711.2002.05532.x, `arXiv:astro-ph/0203082`
283. Zamorani G, Henry JP, Maccacaro T, Tananbaum H, Soltan A, Avni Y, Liebert J, Stocke J, Strittmatter PA, Weymann RJ, Smith MG, Condon JJ (1981) X-ray studies of quasars with the Einstein Observatory. II. ApJ245:357–374, DOI 10.1086/158815

284. Zdziarski AA, Fabian AC, Nandra K, Celotti A, Rees MJ, Done C, Coppi PS, Madejski GM (1994) Physical Processes in the X-Ray / Gamma-Ray Source of IC4329A. MNRAS269:L55+

285. Życki PT (2004) Modelling the variability of the Fe Kα line in accreting black holes. MNRAS351:1180–1186, DOI 10.1111/j.1365-2966.2004.07852.x, `arXiv:astro-ph/0403442`